AUTOPHOSPHORYLATION OF THE RESPONSE REGULATOR PHOB

Rachel Lea Creager-Allen

A dissertation submitted to the faculty of the University of North Carolina at Chapel Hill in partial fulfillment of the requirements for the degree of Doctor of Philosophy in the Department of Biochemistry and Biophysics.

Chapel Hill
2013

Approved by:

Robert Bourret

Edward Collins

Peggy Cotter

Andrew Lee

Richard Wolfenden

Abstract

RACHEL LEA CREAGER-ALLEN: Autophosphorylation of the Response Regulator PhoB
(Under the direction of Robert Bourret and Ruth Silversmith)

Two-component signal transduction systems are prevalent signal transduction systems in microorganisms. The essential elements of two-component systems are the sensor kinase and the response regulator. Response regulators typically receive a phosphoryl group *in vivo* from a sensor kinase, leading to a conformational change in the response regulator and a downstream effect. However, response regulators can also catalyze their own autophosphorylation with small-molecule phosphodonors. Using autophosphorylation to probe interactions between response regulators and small molecules might give insights potentially applicable to development of small molecule antibiotics.

Prior to the work presented here, CheY was the only response regulator for which extensively characterized autophosphorylation kinetics had been published. The relationship between accumulation of phosphorylated CheY and small-molecule phosphodonor concentration remains linear up to the highest concentrations of phosphodonor tested, indicating very weak substrate binding.

Here we describe extensive kinetic characterization of autophosphorylation of the *Escherichia coli* response regulator PhoB. Autophosphorylation kinetics differed greatly between PhoB and CheY. Specifically, the apparent rate constant for accumulation of PhoB-P appeared sigmoidal (Hill coefficient ~2) with respect to small-molecule phosphodonor concentration and to approach saturation. The data are consistent with a model in which PhoB-P forms a heterodimer with an unphosphorylated PhoB monomer,

which then autophosphorylates at an enhanced rate. Potential physiological implications of PhoB heterodimers are discussed. Substitutions of nonconserved residues in the PhoB active site appeared to change the autophosphorylation reaction rate but not substrate binding. Further investigation of the link between PhoB dimerization and autophosphorylation using biolayer interferometry is proposed.

“The most rewarding things in life are often the ones that look like they cannot be done.”

-Arnold Palmer

Acknowledgements

I would like to express my sincere gratitude to my mentors Bob Bourret and Ruth Silversmith. Bob and Ruth have always been supportive, patient, and enthusiastic when guiding me through this process. Their support has helped shape me into the scientist I am today. I would also like to thank my fellow Bourret lab members for their support and friendship.

I am grateful for my amazing family and friends for putting up with me through this whole process. Specifically, I would like to thank my husband, Matt, and my stepson, Cameron, for their love and support. The journey has been long and they have been there with me every step of the way. I would also like to thank my parents for instilling in me the drive and determination to push through until the end. Finally, I would like to thank my amazing friends for helping me remember that there is life outside of grad school.

Table of Contents

List of Tables

List of Figures

Abbreviations

°C	degree Celsius
µg	microgram
µL	microliter
µM	micromolar
^{32}P	radioactive isotope of phosphorus
AcP	acetyl phosphate
ADP	adenosine diphosphate
Ala, A	alanine
Arg, R	arginine
Asn, N	asparagine
Asp, D	aspartate
ATP	adenosine triphosphate
$BeCl_2$	beryllium chloride
BeF_3^-	beryllium trifluoride
BLI	biolayer interferometry
Ca^{2+}	calcium ion
Cd^{2+}	cadmium ion
CheY-P	phosphorylated CheY
cm	centimeter
Co^{2+}	cobalt ion
D	conserved aspartate in response regulator active site, site of phosphorylation
D+2	two residues C-terminal to the conserved Asp

D+3	three residues C-terminal to the conserved Asp
DD	two conserved acidic residues in response regulator active site
DD+1	one residue C-terminal to the two conserved acidic residues
DNA	deoxyribonucleic acid
DPI	diphosphoimidazole
DTT	dithiothreitol
Glu, E	glutamate
Gly, G	glycine
HAD	haloacid dehalogenase superfamily of enzymes
His, H	histidine
het	heterodimer
hom	homodimer
I	fluorescence intensity at a given concentration of ligand
I_0	fluorescence intensity with no added ligand
IPTG	isopropyl β-D-1-thiogalactopyranoside
K	conserved lysine in response regulator active site
$K_{1/2}$	concentration of ligand to reach mid-point of dose-response curve
k_{agg}	aggregation rate constant
k_{app}	apparent rate constant
KCl	potassium chloride
K_{conf}	conformational equilibrium constant for PhoB in the active conformation
k_{dephos}	autodephosphorylation rate constant
K_{dimer}	dimerization constant

$K_{dimer,act}$	associative dimerization constant of PhoB in the active conformation
$K_{dimer,link}$	apparent dimerization constant for heterodimer formation
k_{max}	maximum change in apparent rate constant
k_{min}	minimum apparent rate constant
KNF	Koshland-Nemethy-Filmer model
k_{obs}	observed rate constant
k_{phos}	autophosphorylation rate constant
K_S	dissociation constant
LB	lysogeny broth
Leu, L	leucine
Lys, K	lysine
M^{-1}	per molar
m	monomer
Met, M	methionine
Mg^{2+}	magnesium ion
$MgCl_2$	magnesium chloride
mL	milliliter
mM	millimolar
Mn^{2+}	manganese ion
$MnCl_2$	manganese chloride
MPI	monophosphoimidazole
MWC	Monod-Wyman-Changeux model
n	Hill coefficient

NaCl	sodium chloride
NaF	sodium fluoride
nm	nanometer
NMR	nuclear magnetic resonance
PAM	phosphoramidate
PCR	polymerase chain reaction
PAGE	polyacrylamide gel electrophoresis
Phe, F	phenylalanine
PhoBa	PhoB aggregate
$PhoB_F$	full-length PhoB (residues 1-256)
$PhoB_N$	N-terminal receiver domain of PhoB (residues 1-127)
PhoB-P	phosphorylated PhoB
PhoB:PhoB-P	PhoB heterodimer
PhoB-P:PhoB-P	PhoB homodimer
PhoR-P	phosphorylated PhoR
P_i	inorganic phosphate
RFI	relative fluorescence intensity
s^{-1}	per second
SDS	sodium dodecyl sulfate
Ser, S	serine
SPR	surface plasmon resonance
T	conserved threonine in response regulator active site
T-1	one residue N-terminal to the conserved Thr

T+1	one residue C-terminal to the conserved Thr
T+2	two residues C-terminal to the conserved Thr
Thr, T	threonine
Tyr, Y	tyrosine
v/v	volume per volume
Zn^{2+}	zinc ion

Chapter 1: Introduction

1.1 Signal transduction in bacteria

Signal transduction is the conversion of an environmental stimulus (changes in either the extracellular or intracellular conditions) into a functional change within the cell, typically a change in the behavior of the cell or the level of gene transcription. All organisms must be able to adapt to changes in both the internal and external environments to adequately tune proteins and enzymes to complete the life cycle; therefore, signal transduction is essential for life and occurs in all types of living organisms. Typically, signal transduction occurs via a series of sequential events (for instance ligand binding to a protein, leading to a protein modification [e.g. phosphorylation, conformational change], followed by a downstream response). In order to respond to a complex diversity of stimuli, signal transduction in bacteria is very diverse (1) and the number of signaling systems typically varies with genome size and the complexity of the extracellular environment occupied by a particular microbial species (2-4).

1.1.1 Two-component signal transduction systems

One of the most prevalent signal transduction systems in bacteria is the two-component signal transduction system. The essential components of two component systems are the sensor kinase and the response regulator (Figure 1.1). The sensor kinase

contains a variable input domain and a conserved histidine kinase domain, whereas the response regulator contains a conserved receiver domain and a variable output domain. Signal transduction typically commences upon detection of an environmental stimulus by the input domain of the sensor kinase (Figure 1.1). Upon detection, the sensor kinase typically uses ATP to autophosphorylate on a conserved histidine residue in the histidine kinase domain. The signal continues through the system when the phosphoryl group is transferred from the sensor kinase to a conserved aspartate residue in the receiver domain of the response regulator. To terminate the signal, the phosphorylated response regulator is dephosphorylated through autodephosphorylation (5), phosphatase-enhanced dephosphorylation (6,7), or reverse phosphotransfer (8). A divalent cation is required for both phosphorylation and dephosphorylation of the response regulator (9). Due to the great diversity of input and output domains, two-component systems are able to regulate many processes (1,10).

1.1.2 Two-component signal transduction systems in the context of other signaling systems

Though two-component systems are some of the best characterized signaling systems in bacteria, they are not the only mode of signal transduction (Figure 1.2). Prokaryotes contain a signal transduction system that is simpler in design than the two-component system, called the one-component system (Figure 1.2A). One-component signal transduction systems are widespread among both bacteria and archaea (1) and are highly represented in bacterial genomes (3,11), suggesting one-component systems are a dominant form of signal transduction in prokaryotes. The one-component system consists of a single protein containing both the stimulus sensing input domain and the output

domain that affects a downstream response (1,3). It is predicted that one-component systems bind ligand at the input domain, undergo a conformational change, and directly generate a response (11). Because the input and output domain of one-component systems are part of the same protein and the common predicted effect of one-component systems is transcription regulation (3,11), one-component systems are predicted to only respond to stimulus molecules within the cytosol.

Two-component systems (Figure 1.2B) likely evolved from one-component systems by the addition of the phosphoryl transfer domains [histidine kinase domain in sensor kinase and receiver domain in response regulator] (11). This adaptation allowed for the output domain (contained within the response regulator) to be physically separated from the input domain (contained within the sensor kinase) and for the incorporation of a transmembrane sensor that can respond to events in the extracellular or periplasmic environment (1,3,11). Because a single sensor kinase can autophosphorylate and transfer phosphoryl groups to many response regulators, the separation of stimulus sensing and response in two-component systems also allowed for signal amplification. Linking of the input and output domains by a phosphotransfer reaction allows for signal integration (multiple stimuli yield a single cellular response), distribution (one stimulus yields multiple cellular responses), or any combination in between. Separation of the input and output domains further allowed for further evolution of more complex signaling cascades (termed phosphorelay systems) to occur by addition of additional phospho-acceptor and phospho-donor proteins (Figure 1.2C).

Che-like signaling systems [Che systems control chemotaxis, Che-like systems control transcription] (Figure 1.2D) are a modified form of two-component systems (11-

13) and, at a minimum, contain a modified sensor kinase lacking an input domain, a response regulator lacking an output domain, a transmembrane receptor, and a scaffold protein that docks the receptor to the sensor kinase (11,12). Ligand interaction with transmembrane receptors affects autophosphorylation of the sensor kinase and subsequently the flow of phosphoryl groups from the sensor kinase to the response regulator. Bacteria are able to adapt to the extracellular environment through methylation and demethylation of the transmembrane receptor by auxiliary proteins, allowing cells to "forget" a constant environmental stimulus and to return to pre-stimulus activity levels. Because chemotaxis usually occurs via a biased random walk, Che-like signaling allowed bacteria to transition from passive sensing to active exploration of the environment (11,12). Che-like signaling systems also allowed for different ligands to affect the same cellular response. In *E. coli*, multiple transmembrane receptors respond to varying ligands (Tar responds to aspartate and maltose, Tsr responds to serine, Trg responds to galactose and ribose, and Tap responds to dipeptides) and interact with the sensor kinase CheA (14).

1.1.3 The potential benefits of understanding two-component systems

Two-component signal transduction systems are prevalent signaling systems in bacteria and there are multiple reasons to seek better understanding of the chemistry of the proteins involved. First, because chemical modification (especially phosphorylation) of proteins is widely employed by signaling proteins, understanding signaling by two-component systems would give better understanding to signal transduction in general (10). Second, understanding how bacteria respond to the presence of specific molecules in the environment may allow for a better manipulation of many bacterial processes [e.g.

engineering biosensors, enhancing environmental remediation] (10). Third, two-component systems are found in many eukaryotic and prokaryotic microorganisms as well as plants but are not found in higher eukaryotes (2). The lack of two-component systems in humans and animals makes two-component systems a potential target for antibiotics against microbial pathogens (10,15,16).

Because both prokaryotic and eukaryotic signal transduction pathways participate in many important cellular processes, signaling systems may be potential targets for therapeutic agents (16). Many targeted cancer therapies work on proteins that are involved in human signal transduction pathways that regulate cell growth, cell division and response to external stimuli (17,18). Two major targets for anti-cancer therapeutics are the Ras/Raf/MEK/ERK signaling pathway (17) and the estrogen receptor signaling pathway (18). In both cases, disruption of the signaling pathway either through inhibition of a protein kinase or a hormone receptor leads to treatment of certain types of cancer. Although there are currently no approved therapeutics that inhibit bacterial signal transduction pathways, previous success at targeting human signaling systems suggests that bacterial signaling pathways might be potential targets for antibiotics. Recently, there have been some advances made in targeting two-component signal transduction systems using small molecule inhibitors. The PhoQ/PhoP two-component system is thought to regulate the ability of *Salmonella enterica* to infect epithelial cells and to live within phagocytic cells (19). The response regulator PhoP must dimerize in order to interact with DNA to regulate transcription. Eight small molecule inhibitors have been shown to interrupt PhoP dimerization and thus DNA binding (20). Another example of targeting two-component systems involves the QseC/QseB two-component system, which plays a

role in virulence of at least 25 plant and animal pathogens, including Enterohemorrhagic *E. coli* (21). The sensor kinase QseC is a receptor for autoinducer-3 produced by the gastrointestinal microbial flora or host epinephrine and norephinephrine; detection of the stimuli leads to induction of transcription of virulence factors. A small molecule inhibitor prevents ligand binding and autophosphorylation of QseC, stopping expression of virulence factors and markedly inhibiting virulence of several pathogens in animal models (22).

1.2. Signaling by response regulator phosphorylation is due to conformational changes

Two-component systems are able to regulate a very diverse set of cellular processes from simple metabolism to complex cellular development (1,10). How are two-component signal transductions systems able to regulate such diverse cellular processes? To be able to understand regulation we must first discuss the conserved receiver domain structure of response regulators. The receiver domain (Figure 1.3) contains a conserved tertiary fold and approximately 25% amino acid sequence identity (10,15,23). The defining feature of the receiver domain is the $(\beta\alpha)_5$ topology with an active site containing both the site of phosphorylation and the divalent cation binding site (24,25). The receiver domain contains five invariable active site residues (Figure 1.3): the aspartate that is the site of phosphorylation, two acidic residues that coordinate the required divalent cation, and a threonine/serine and a lysine that form noncovalent bonds with the phosphoryl group.

The conserved receiver domain undergoes a conserved conformational change (15,26,27) [Figure 1.4]. Analysis of structures of numerous receiver domains shows that phosphorylation or binding of a phosphoryl group analog to the active site Asp leads to conformational rearrangements on the α4-β5-α5 surface (10,24,28). These conformational shifts occur via a conserved mechanism of allosteric communication between the site of phosphorylation and the functionally relevant α4-β5-α5 surface. Activation leads to reorientation of the two switch residues (the conserved threonine/serine in β4 and a tyrosine/phenylalanine in β5) towards the active site [Figure 1.4B] (10,15). In the inactive conformation, the switch residues are outward facing with the tyrosine/phenylalanine exposed on the domain surface (10). In the inactive solvent-exposed conformation, the tyrosine/phenylalanine sterically hinders interaction between the receiver domain and other proteins or domains of the same protein (28). In the active conformation, the threonine/serine rotates into the active site and forms a hydrogen bond with a phosphoryl group oxygen. The repositioning of the threonine/serine allows for movement of the β4α4 loop and stabilization of the tyrosine/phenylalanine side chain within a hydrophobic core (25). The conformational change leads to packing of other residues that stabilizes the active state, though the main changes between the inactive and active conformation are at the tyrosine/phenylalanine and in the β4α4 loop (15,28).

Though it is typically said that the receiver domain is in equilibrium between an inactive and an active conformation, the conformational change is not a simple two-state process. Studying the μs-ms timescale motions of CheY using NMR showed that CheY does not undergo a concerted mechanism between two states (26). Because proteins are dynamic by nature, movement within the protein between two predominant states implies

that there are also intermediate states. Intermediate conformational states of CheY have been demonstrated crystallographically both in the presence (29,30) and absence (31) of effector protein. Similarly, molecular dynamic simulations of the conformational change of CheY show that rotation of the tyrosine/phenylalanine and the formation of the hydrogen bond between the threonine/serine and the phosphoryl group are independent (32).

In the absence of phosphorylation, there is an intrinsic conformational equilibrium predominantly between the inactive and the active conformations, with the equilibrium greatly shifted towards the inactive conformation (Figure 1.5A). Upon phosphorylation, this conformational equilibrium is shifted primarily towards the active conformation, exposing the α4-β5-α5 interface. In single domain response regulators, the conformational change typically results in an interaction between the α4-β5-α5 interface and an effector protein (Figure 1.5B). In dimerizing response regulators (33-35), this conformational change is thought to allow two phosphorylated monomers to dimerize along the α4-β5-α5 surface (24) [Figure 1.5C]. As is true for all allosteric proteins, there are two popular models for how the link between phosphorylation and conformational change might work: the Koshland-Nemethy-Filmer (KNF) model and the Monod-Wyman-Changeux (MWC) model (36). In the KNF model, phosphorylation of the response regulator induces a conformational change from the inactive to the active conformation. In the MWC model, the response regulator exists in multiple conformational states, with the equilibrium greatly shifted towards the inactive conformation. Phosphorylation preferentially occurs in and stabilizes the subpopulation of response regulators that are in the active conformation. It is currently thought that the

MWC model descibes what occurs with response regulator phosphorylation based on the following evidence (15,26): 1) Unphosphorylated response regulators have some ability to regulate downstream effects (37,38), indicating the presence of some response regulator in the active conformation. 2) Crystal structure of CheY that is not bound to a phosphoryl group analog includes tyrosine occupying both the active and the inactive rotomers (39). 3) The coupling of phosphorylation and conformational change within the receiver domain occurs in both directions. Just as phosphorylation of response regulators promotes the active conformation, increasing the population of response regulator in the active conformation (e.g. binding target ligand) increases the rate of autophosphorylation (40,41). 4) NMR shows the unphosphorylated receiver domain of NtrC is in equilibrium between the inactive and active conformation with the equilibrium skewed towards the inactive conformation (27).

1.3 Response regulators self-catalyze phosphorylation and dephosphorylation chemistry

Response regulators typically receive a phosphoryl group *in vivo* from a sensor kinase, leading to a conformational change in the receiver domain. The five conserved residues in the receiver domain (see above) catalyze both phosphorylation and dephosphorylation of the response regulator (24,25). In addition to catalyzing phosphotransfer from the sensor kinase, response regulators can also catalyze their own autophosphorylation with small-molecule phosphodonors [Table 1.1] (42-46). The mechanisms of autophosphorylation and phosphotransfer likely occur via the same substitution chemistry, so understanding autophosphorylation can give insight into the

more complex phosphotransfer reaction (25,46) without the complication of purifying the transmembrane sensor kinase (10). Furthermore, understanding autophosphorylation with small-molecule phosphodonors containing an N-P bond (PAM, MPI, DPI) may help distinguish between the contributions of the phosphorylated histidine and the remainder of the sensor kinase. Also, because autophosphorylation involves interaction between the response regulator and a small molecule, understanding interaction between the two might give insight into potential small molecule antibiotics.

Table 1.1. Structures of small molecule phosphodonors

Small molecule phosphodonor	Structure at pH 7
Acetyl phosphate (AcP)	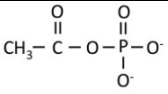
Carbamoyl phosphate	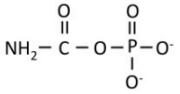
Phosphoramidate (PAM)	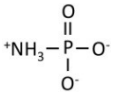
Monophosphoimidazole (MPI)	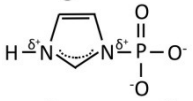
Diphosphoimidazole (DPI)	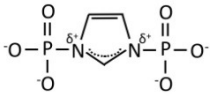

1.3.1 Autophosphorylation of the response regulator CheY is nonsaturable with respect to small molecule phosphodonor concentration

Prior to the work presented in this dissertation, CheY was the only response regulator for which extensively characterized autophosphorylation kinetics had been published (40,42,44,46). CheY (Figure 1.3) is a single domain response regulator that participates in transmission of chemotaxis signals from transmembrane chemoreceptors to flagellar motor proteins. Phosphorylated CheY binds to FliM at the flagellar motor,

inducing a change in the direction of flagellar rotation. The model of CheY autophosphorylation kinetics [in scheme 1.1 with the phosphodonor PAM (43)] involves initial binding of phosphodonor to CheY to form a noncovalent complex (dissociation constant K_S), followed by phosphorylation (rate constant k_{phos}) and subsequent autodephosphorylation (rate constant k_{dephos}).

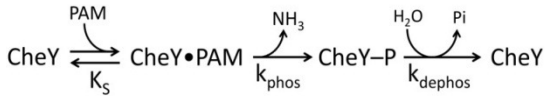

Scheme 1.1. Kinetic model of autophosphorylation of the response regulator CheY.

CheY contains a tryptophan in the active site that can be used as a fluorescent probe to monitor the pre-steady state kinetics of autophosphorylation. Specifically, the tryptophan follows the accumulation of phosphorylated CheY (CheY-P) from scheme 1.1. The observed rate constant for the accumulation of CheY-P (k_{obs}) is described by equation 1.1, using terms from scheme 1.1 (43). In reactions that exhibit saturable kinetics, the concentration of small-molecule phosphodonor exceeds the dissociation constant for substrate binding ([PAM] > K_S). As the concentration of small-molecule phosphodonor is increased, the observed rate of formation approaches a maximal value. Subsequent additions of small molecule will not result in an appreciable increase in the observed rate of accumulation. From a graph of the observed rate constant (k_{obs}) versus small molecule concentration (Figure 1.6A), it is possible to determine K_S and k_{phos}. For CheY, though, the relationship remains linear up to the highest concentrations of phosphodonor tested (100 mM), indicating very weak substrate binding (K_S > 500 mM) (40,42,46). For reactions where K_S is unattainable experimentally, it is not possible to separate binding

from catalysis; it is only possible to measure the apparent bimolecular rate constant, k_{phos}/K_S (Figure 1.6B). For CheY, k_{phos}/K_S is ~10 M^{-1} s^{-1} for autophosphorylation with either acetyl phosphate or PAM at 25°C and 230 mM ionic strength (40,42,44,46). Amino acid substitutions were made to nonconserved active site residues of CheY thought to interact with the small-molecule phosphodonor leaving group; however, the relationship between k_{obs} and phosphodonor concentration remained linear, even for mutants with a 10^3-fold rate enhancement (46) (Immormino, R.M, & Bourret, R.B., unpublished).

$$k_{obs} = \frac{k_{phos}[PAM]}{K_S + [PAM]} + k_{dephos} \qquad 1.1$$

However, CheY is not a typical response regulator in several respects. CheY consists only of a receiver domain and thus does not contain a variable output domain. Also, CheY does not act as a transcriptional regulator and does not dimerize upon phosphorylation.

1.4 Inorganic phosphate signaling in *E. coli*

In this dissertation, we sought to further explore response regulator autophosphorylation kinetics by characterizing a response regulator that is more typical than CheY. PhoB is a member of the largest class of response regulators, termed the OmpR/PhoB family, which contains ~30% of annotated response regulators (47). The PhoR/PhoB system is a very well-characterized two-component signal transduction system that regulates the large number of genes in the *pho* regulon in *E. coli* (48). The *pho* regulon is required for the incorporation of a variety of phosphorus sources from the environment, with inorganic phosphate (P_i) being the preferred phosphorus source (49).

Signal transduction by P_i requires seven proteins (48-50): inner membrane sensor kinase PhoR, response regulator PhoB, four components of the ABC transporter for high-affinity capture of P_i and low-velocity transport into cytosol (PstS, PstC, PstA, PstB), and the chaperone-like PhoR inhibitor PhoU. The likely *in vivo* mechanism for P_i signaling is (48): P_i binds to the transmembrane Pst complex when in excess and PhoU acts as a chaperone by interacting with both Pst and PhoR; PhoR is turned off and PhoB is not phosphorylated. When P_i is limiting, P_i is no longer bound to the Pst complex and PhoU dissociates from PhoR; PhoR autophosphorylates and PhoB is subsequently phosphorylated and thus regulates transcription. When P_i is in excess again, Pst, PhoU and PhoR interact and PhoB is dephosphorylated and dissociates from DNA.

Like many response regulators, PhoB dimerizes through its receiver domain, allowing two output domains to come together and bind to a DNA-binding site on the promoter to activate transcription (50,51). PhoB binds to the repeats as a head-to-tail dimer (52), allowing for recruitment of the σ^{70} subunit (specifically by binding of the σ_4 domain) of *E. coli* RNA polymerase (53). There are a large number of PhoB binding sites on the *E. coli* genome, though only 31 genes have been shown to be directly controlled by the PhoR/PhoB two-component system (48). Nearly all of the genes regulated by PhoB play a role in the assimilation of P_i or alternative phosphorus sources, with the most strongly activated promoter being the *pst* operon that encodes the four Pst components and PhoU. The *phoR* and *phoB* genes are also regulated by PhoB; under P_i limitation, PhoB and PhoR concentrations increase over 100-fold (49). PhoB binds to a sequence on the DNA called a *pho* box: an 11 base pair repeat that replaces the -35 promoter sequence (53,54).

1.5 Characterization of PhoB autophosphorylation yields insights not inferred from CheY autophosphorylation

Here, we present kinetic characterization of autophosphorylation of the *E. coli* response regulator PhoB. We found that the relationship between accumulation of PhoB-P and the concentration of small-molecule phosphodonor appeared sigmoidal and to approach saturation (Chapter 2). Mathematical modeling and biochemical evidence suggest a link between PhoB dimerization and autophosphorylation. Substitutions made within the nonconserved residues in the active site of PhoB resulted in several with autophosphorylation kinetics that varied from wild type (Chapter 3). Any effects on autophosphorylation kinetics appear to be due to changes to the rates of phosphorylation as opposed to changes in substrate binding to PhoB. Further investigation of the formation of PhoB heterodimers (formed between one phosphorylated and one unphosphorylated monomer) is proposed (Chapter 4). The link between autophosphorylation and dimerization of the response regulator PhoB is related to the fields of autophosphorylation and two-component signaling in general (Chapter 5).

1.6 Figures

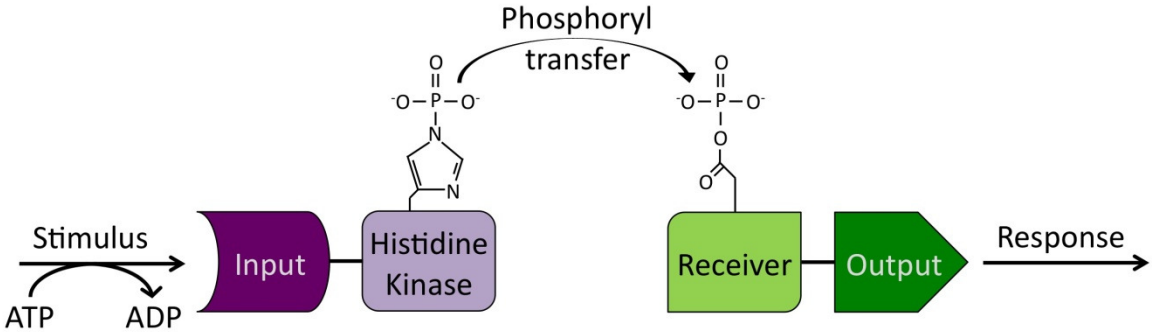

Figure 1.1. Schematic representation of two-component signal transduction system. Two-component signal transduction systems are composed of a sensor kinase (purple) and a response regulator (green). Upon stimulus, the sensor kinase autophosphorylates on a conserved histidine. The phosphoryl group is transferred to a conserved aspartate in the response regulator. The phosphorylated response regulator can exert its downstream effects.

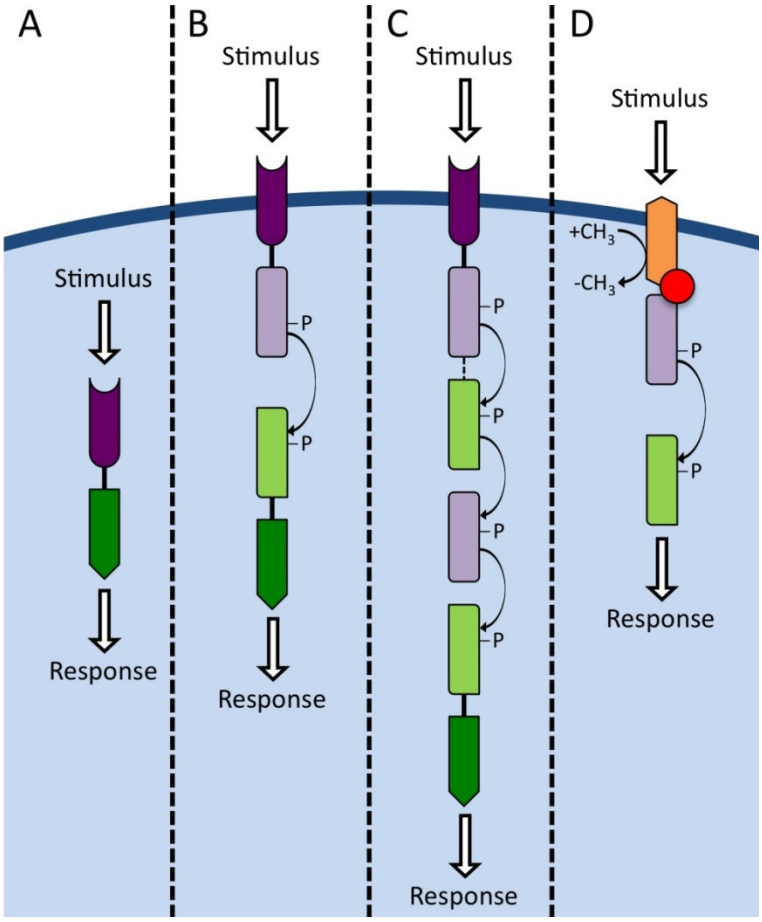

Figure 1.2. Four classes of prokaryotic signal transduction systems. (A) One-component signal transduction. Covalently linked stimulus sensing input domain (dark purple) and output domain (dark green) that affects a downstream response. **(B)** Two-component signal transduction. Sensor kinase (variable input domain, conserved histidine kinase domain [light green]) and response regulator (conversed receiver domain [light purple], variable output domain) signal via phosphoryl transfer. **(C)** Phosphorelay system. At a minimum, a sensor kinase, a receiver domain (attached to sensor kinase or stand-alone), a histidine phosphotransferase, and a terminal response regulator. **(D)** Che-like signaling system. At a minimum, a modified sensor kinase lacking an input domain, a response regulator lacking an output domain, a transmembrane receptor (orange), and a scaffold protein (red circle) that docks the receptor to the sensor kinase.

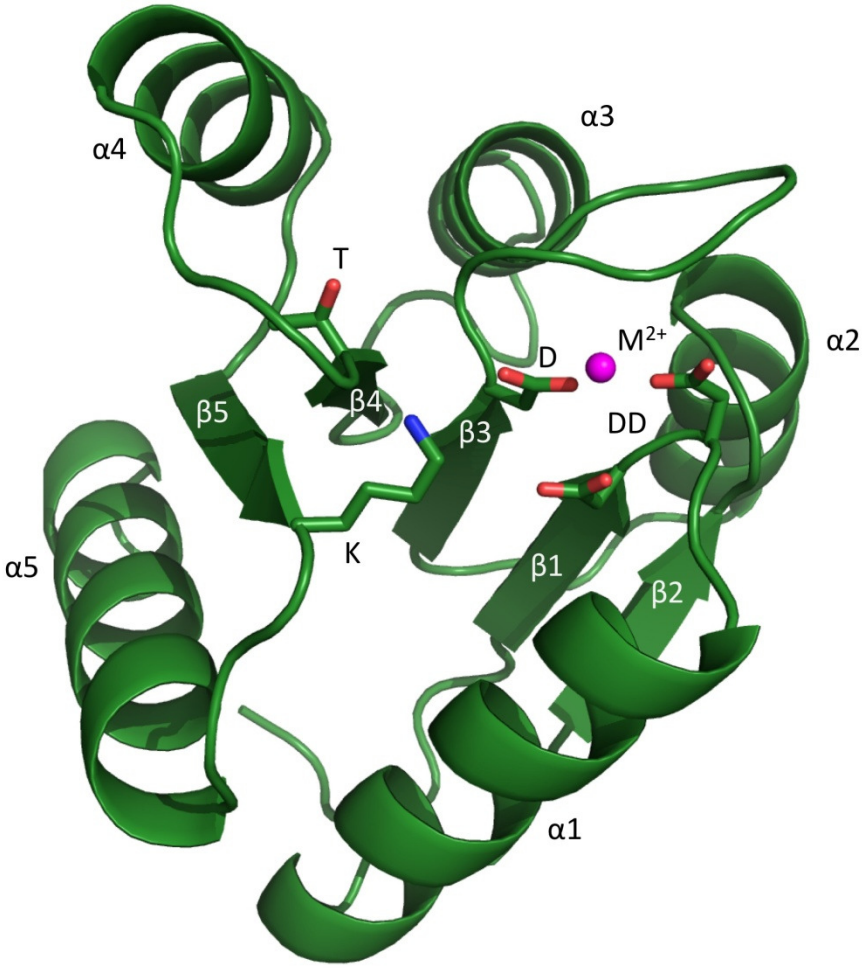

Figure 1.3. Ribbon representation of conserved receiver domain structure. The crystal structure shown is of *E. coli* CheY (PDBid 2CHE) as an example of the conserved tertiary structure and catalytically functional residues of receiver domains. Side chains for the following conserved active site residues are shown as sticks: Asp 57 ('D'), Asp 12 & Asp 13 ('DD'), Thr 87 ('T'), and Lys 109 ('K'). Also shown is the active site magnesium ion (magenta sphere).

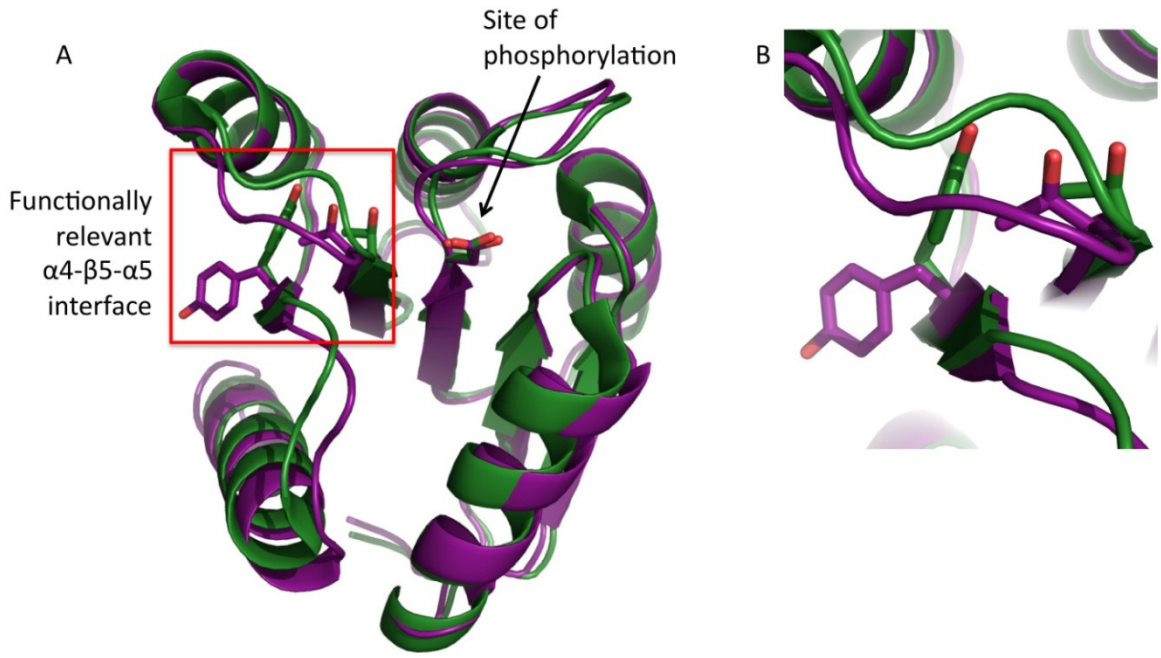

Figure 1.4. Phosphorylation-linked conformational of receiver domain. (A) Overlay of inactive (purple, PDBid 2CHE) and active (green, PDBid 1FQW) receiver domain conformations with the side chains of the switch residues (Thr 87 and Tyr 106) and site of phosphorylation (Asp 57) shown. **(B)** Magnified view of switch residues in red box from **(A)**.

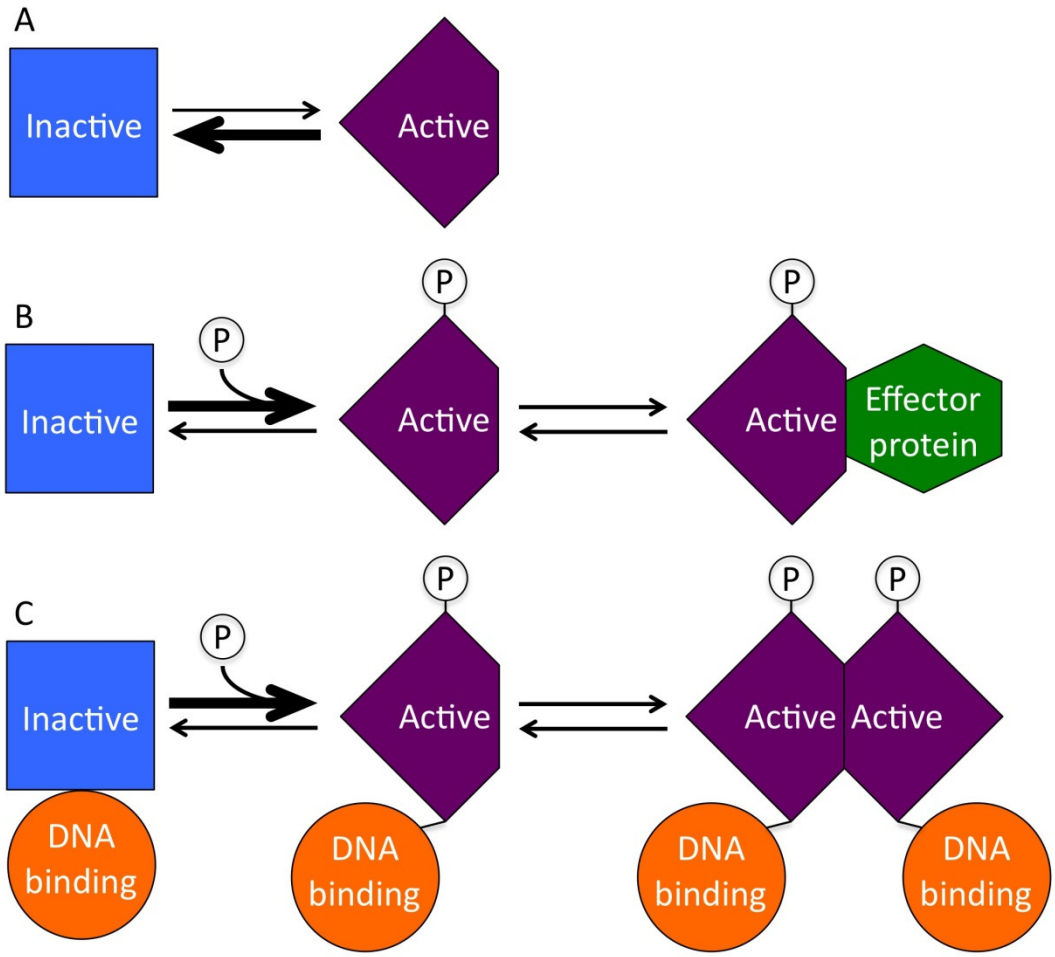

Figure 1.5. Conformational equilibria of response regulators. In the absence of phosphorylation, the conformational equilibrium of the receiver domain is greatly shifted towards the inactive conformation **(A)**. Phosphorylation shifts the conformational equilibrium greatly towards the active conformation. In single domain response regulators, this conformational change exposes the α4-β5-α5 interface that typically allows for interaction between the response regulator and an effector protein **(B)**. In dimerizing response regulators, this conformational change is thought to allow two phosphorylated monomers to dimerize along the α4-β5-α5 interface in the receiver domain **(C)**.

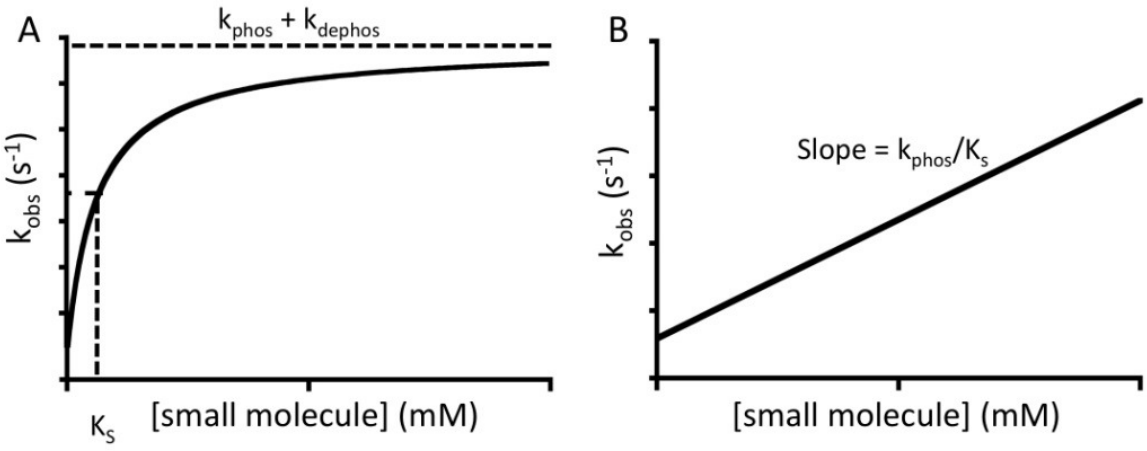

Figure 1.6. Plots of kobs versus small molecule concentration. **(A)** Observed rate versus substrate concentration for a reaction exhibiting saturable kinetics. **(B)** Observed rate versus substrate concentration for a reaction exhibiting nonsaturable kinetics.

Chapter 2: A link between dimerization and autophosphorylation of the response regulator PhoB[1]

2.1 Summary

Response regulator proteins within two-component signal transduction systems are activated by phosphorylation and can catalyze their own covalent phosphorylation using small-molecule phosphodonors. To date, comprehensive kinetic characterization of response regulator autophosphorylation is limited to CheY, which follows a simple model of phosphodonor binding followed by phosphorylation. We characterized autophosphorylation of the response regulator PhoB, known to dimerize upon phosphorylation. In contrast to CheY, PhoB time traces exhibited an initial lag phase and gave apparent pseudo-first order rate constants that increased with protein concentration. Furthermore, plots of the apparent autophosphorylation rate constant versus phosphodonor concentration were sigmoidal, as were PhoB binding isotherms for the phosphoryl group analog BeF_3^-. Successful mathematical modeling of the kinetic data necessitated inclusion of the formation of a PhoB heterodimer (one phosphorylated and one unphosphorylated monomer) with an enhanced rate of phosphorylation. Specifically,

[1] The material in this chapter is from: Creager-Allen, R.L., Silversmith, R.E., Bourret, R.B. (2013) A link between dimerization and autophosphorylation of the response regulator PhoB. *J. Biol. Chem.* **288**, 21755-21769.
(Creager-Allen, Silversmith, and Bourret designed research; Creager-Allen performed research; Creager-Allen, Silversmith, and Bourret analyzed data; Creager-Allen, Silversmith, and Bourret wrote the paper.)

dimerization constants for the PhoB heterodimer and homodimer (two phosphorylated monomers) were similar, but the rate constant for heterodimer phosphorylation was ~10-fold higher than for the monomer. In a test of the model, disruption of the known $PhoB_N$ dimerization interface by mutation led to markedly slower and non-cooperative autophosphorylation kinetics. Furthermore, phosphotransfer from the sensor kinase PhoR was enhanced by dimer formation. Phosphorylation-mediated dimerization allows many response regulators to bind to tandem DNA binding sites and regulate transcription. Our data challenge the notion that response regulator dimers primarily form between two phosphorylated monomers, and raise the possibility that response regulator heterodimers containing one phosphoryl group may participate in gene regulation.

2.2 Introduction

Two-component signal transduction systems, present in both eukaryotic and prokaryotic microorganisms as well as plants, are nearly ubiquitous in bacteria with tens of thousands of two-component system proteins currently annotated in sequence databanks (2,55). The essential components of any two-component system are a sensor kinase and a partner response regulator. Detection of an environmental stimulus regulates the sensor kinase, often leading to autophosphorylation of a conserved histidine. The phosphoryl group is subsequently transferred to a conserved aspartate residue on the partner response regulator. Phosphorylation switches the response regulator to an active conformation (10), allowing the response regulator to exert its downstream effects. Many response regulators control transcription (47), typically by dimerization and binding to a symmetric DNA-binding site (24). To terminate the signal, response regulators

dephosphorylate through autodephosphorylation (5), phosphatase-enhanced dephosphorylation (6,7), or reverse phosphotransfer (8).

All response regulators contain a conserved receiver domain and most also contain one or more variable output domains. The receiver domain (Fig. 2.1) has a conserved $(\beta\alpha)_5$ tertiary structure and contains the dimerization interface for many response regulators as well as the conserved active site that catalyzes both phosphorylation and dephosphorylation (24,25). The five invariable residues that compose the active site include a conserved aspartate that is the site of phosphorylation, two acidic residues that coordinate a divalent cation required for catalysis, a threonine/serine, and a lysine. In addition to catalyzing phosphotransfer from the sensor kinase, response regulators can also catalyze their own autophosphorylation with small-molecule phosphodonors including phosphoramidate ($H_3N^+–PO_3^{2-}$, PAM[1]), acetyl phosphate, and monophosphoimidazole (42-46).

Although autophosphorylation has been qualitatively demonstrated for many response regulators, CheY is the only response regulator for which extensively characterized autophosphorylation kinetics have been published (40,42,44,46). The model of CheY autophosphorylation kinetics [in scheme 1 with the phosphodonor PAM (43)] involves initial binding of phosphodonor to CheY to form a noncovalent complex (dissociation constant K_S), followed by phosphorylation (rate constant k_{phos}) and subsequent autodephosphorylation (rate constant k_{dephos}).

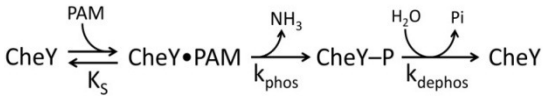

Scheme 1. Kinetic model of autophosphorylation of the response regulator CheY.

For CheY, the pre-steady state pseudo-first order rate constant for the accumulation of phosphorylated CheY (CheY-P) upon mixing CheY with phosphodonor remains linear with respect to PAM or acetyl phosphate concentration up to the highest concentrations of phosphodonor tested (100 mM), indicating very weak binding (K_S > 500 mM) (40,42,46). Thus for CheY, it is only possible to measure the apparent bimolecular rate constant, k_{phos}/K_S, for accumulation of CheY-P, which is ~10 M^{-1} s^{-1} for autophosphorylation with either acetyl phosphate or PAM (40,42,44,46). However, CheY is not a typical response regulator in several respects. CheY consists only of a receiver domain and thus does not contain a variable output domain. Also, CheY does not act as a transcriptional regulator and does not dimerize upon phosphorylation.

To further explore response regulator autophosphorylation kinetics, we sought to characterize a more typical response regulator. PhoB is a member of the largest class of response regulators, termed the OmpR/PhoB family, which contains ~30% of annotated response regulators (47). Like many response regulators, PhoB dimerizes through its receiver domain, allowing two output domains to come together and bind to a DNA-binding site on the promoter to regulate transcription (51). PhoB can autophosphorylate with acetyl phosphate or PAM (35,56-58) and contains an active site tryptophan (Fig. 2.1) that can be used as a fluorescent probe for both metal binding and autophosphorylation (35).

Analysis of structures of numerous receiver domains shows that phosphorylation or binding of a phosphoryl group analog to the active site Asp leads to conformational rearrangements on the α4-β5-α5 surface (10,24,28). These conformational shifts occur via a conserved mechanism of allosteric communication between the site of

phosphorylation and the functionally relevant α4-β5-α5 surface. In dimerizing response regulators like PhoB (33-35), this conformational change allows two monomers to dimerize along the α4-β5-α5 surface (24) [Fig. 1.5]. The coupling of phosphorylation and conformational change within the receiver domain occurs in both directions. Just as phosphorylation of response regulators promotes the active conformation, increasing the population of response regulator in the active conformation (e.g. binding target ligand) increases the rate of autophosphorylation (40,41).

The PhoB receiver domain ($PhoB_N$) has been demonstrated to form two different types of dimers. The two $PhoB_N$ dimers have been extensively characterized both structurally and biochemically (59-62). As expected, a dimer along the α4-β5-α5 surface (here termed dimer 1) forms in the presence of a phosphoryl group analog (62) and represents the functional, phosphorylation-mediated dimer. Unexpectedly, metal binding alone supports a modified version of dimer 1 (60). Phosphorylated full-length PhoB ($PhoB_F$) dimer (dimer 1) has a dimerization constant of 5.1 μM (61) measured by analytical ultracentrifugation. A second $PhoB_N$ dimer, here termed dimer 2, forms along the α1-β5α5 loop-α5 surface (Fig. 1.5) and has been observed under crystallographic conditions in either the absence of metal and phosphorylation (59) or in the presence of just metal [single crystallographic conditions resulted in $PhoB_N$ monomers in both dimer 1 and dimer 2 within the asymmetric unit (60)]. Dimer 2 may not be physiologically relevant due to a dimerization constant [>350 μM (61)] that is substantially higher than the *in vivo* concentration of PhoB (63).

Here, we present kinetic characterization of autophosphorylation of the *E. coli* response regulator PhoB with the phosphodonor PAM. PhoB autophosphorylation

exhibited several kinetic features that were fundamentally different from those of CheY. In contrast to the linear relationship between the pseudo-first order rate constant for accumulation of CheY-P and PAM concentration, this relationship for PhoB appeared sigmoidal and to approach saturation. Furthermore, unlike CheY, apparent pseudo-first order rate constants for PhoB autophosphorylation showed a protein concentration dependence. Additional biochemical evidence, supported by mathematical modeling, indicated a link between formation of PhoB dimer 1 and autophosphorylation kinetics. We propose that a heterodimer formed between a phosphorylated monomer and an unphosphorylated monomer of PhoB plays a role in PhoB autophosphorylation kinetics.

2.3 Experimental Procedures

2.3.1 Cloning and site directed mutagenesis

Genes encoding *E. coli* full-length PhoB ($PhoB_F$, residues 1-256) and the N-terminal receiver domain of PhoB ($PhoB_N$, residues 1-127) were amplified using standard PCR methods from the pENTR-b0399 (*phoB*) plasmid (64), provided by Dr. Michael Laub (Massachusetts Institute of Technology). The gene encoding *E. coli* CheY was amplified using standard PCR methods from pRS3 (65). PCR products were inserted into the pET28a vector (Novagen) to generate constructs ($PhoB_F$, pET28a·$phoB_F$; $PhoB_N$, pET28a·$phoB_N$; CheY, pKC1) that encode proteins with a thrombin cleavable His_6-tag at the N-terminus. After thrombin cleavage, the resultant proteins contain an additional Gly-Ser-His at the N-terminus. Addition of the three small residues is unlikely to affect the activity of the PhoB constructs because the N-terminus is on the opposite side of the protein from the site of phosphorylation and is in a portion of PhoB that does not undergo

a conformational change between the inactive and the active conformation. The presence of the same three residues in CheY did not affect the rates of autophosphorylation by PAM (data not shown) or autodephosphorylation (66). Site directed mutagenesis was performed using Quikchange technology (Agilent Technologies). Wild type and mutagenized plasmids were transformed into *E. coli* strain BL21(DE3) for protein expression and purification.

The Gateway Entry vector for *phoR* [pENTR-b0400 (64) encoding the soluble portion of *E. coli* PhoR (residues 193-431, throughout referred to as PhoR)] and the Gateway Destination vector (pML375) were provided by Dr. Michael Laub (Massachusetts Institute of Technology).The gene encoding PhoR was transferred from the entry vector into the destination vector using standard Gateway protocols (Invitrogen) to generate a construct (pDEST·phoR) that encodes a protein with a thrombin cleavable His_6-tag at the N-terminus.

2.3.2 Synthesis of phosphoramidate

The potassium salt of phosphoramidate (PAM) was synthesized as described (67).

2.3.3 Protein overexpression and purification

For the purification of CheY, $PhoB_F$, $PhoB_N$, $PhoB_N$ F20D, and PhoR, one liter of LB (+30 μg/mL kanamycin) was inoculated with 2.5 mL of an overnight culture of the appropriate expression strain and grown at 37°C to an optical density at 600 nm of 0.4. The culture was then transferred to room temperature, induced with 0.5 mM IPTG and grown 8-10 hours. Cells were collected by centrifugation and resuspended in lysis buffer (50 mM Hepes, pH 7.0, 300 mM NaCl, 10 mM imidazole). The cells were lysed by sonication and cellular debris was removed by ultracentrifugation (45 minutes, 4°C,

37,000xg). The supernatant was passed over a Nickel-NTA agarose (Qiagen) column and the column was subsequently washed with wash buffer (50 mM Hepes, pH 7.0, 300 mM NaCl, 20 mM imidazole). Protein was eluted with elution buffer (50 mM Hepes, pH 7.0, 300 mM NaCl, 150 mM imidazole). All eluted proteins except PhoR were incubated with human alpha-thrombin (1 unit/mL sample, *Haematologic Technologies, Inc*) overnight at 4°C, followed by gel filtration over a Superdex 75 16/60 column in 50 mM Hepes, pH 7.0, 100 mM KCl, 2 mM DTT, 10% (v/v) glycerol to remove the thrombin and cleaved His_6-tag (for CheY, DTT was omitted from the gel filtration buffer). PhoR was further purified using a Superose 12 gel filtration column in 50 mM Tris, pH 7.5, 500 mM NaCl, and 10% (v/v) glucose. Aliquots of purified proteins were flash frozen in dry ice/ethanol and stored at -80°C.

$PhoB_N$ R115D was expressed and purified similarly to the above procedure with slight modifications based on a published purification protocol (61). One liter of LB (+30 μg/mL kanamycin) with 1 M sorbitol and 10 mM betaine was inoculated with 2.5 mL of an overnight culture in LB and grown at 37°C to an optical density at 600 nm of 0.4. The culture was transferred to room temperature, induced with 0.25 mM IPTG, and grown for 17-20 hours. The cell pellet was resuspended in lysis buffer containing 140 μg Halt protease inhibitor cocktail (Thermo Scientific) followed by sonication, Nickel-NTA chromatography and thrombin cleavage as above. The Superdex 75 gel filtration buffer contained 50 mM Hepes, pH 7.0, 2 mM DTT, and 10% (v/v) glycerol.

2.3.4 Fluorescence measurements

All fluorescence measurements were made using a Perkin-Elmer LS-50B fluorimeter equipped with a magnetic stirring device and FLWinLab software.

Tryptophan fluorescence was measured at an excitation wavelength of 295 nm and an emission wavelength of 346 nm. Sample temperature was held at 25 ± 0.5°C by a circulating water bath.

2.3.5 Equilibrium fluorescence measurements

Tryptophan fluorescence was used to monitor binding of divalent cation (Mn^{2+} or Mg^{2+}) or beryllium trifluoride (BeF_3^-) to various $PhoB_N$ constructs. All ligand binding assays were performed in triplicate in a 1-cm x 1-cm quartz cuvette at an initial volume of 1.5 mL.

Divalent cation binding was assayed similarly to a published protocol (68). $PhoB_N$ (5 µM) or $PhoB_N$ F20D (5 µM) in 100 mM Hepes, pH 7.0, was allowed to come to temperature equilibrium with constant magnetic stirring and the initial fluorescence emission measured. Then, small volumes of a concentrated stock of $MnCl_2$ or $MgCl_2$ were incrementally added to the solution. After each addition, the solution was incubated for two minutes to ensure a homogenous mixture. Ten fluorescence measurements were taken (1 measurement/s) and the values averaged and corrected for dilution. Altogether, fluorescence was measured for fifteen concentrations of divalent cation ranging between 5-1000 µM $MnCl_2$ and between 0.25-5 mM $MgCl_2$.

For BeF_3^- binding, $PhoB_N$ (5 µM) or $PhoB_N$ F20D (5 µM) was incubated in 100 mM Hepes, pH 7.0, 3 mM $MnCl_2$, and 10 mM NaF with constant stirring to reach temperature equilibrium. Small volumes of a concentrated stock of $BeCl_2$ were incrementally added to give concentrations between 1 and 100 µM. After each addition of $BeCl_2$, the solution was incubated for two minutes. $BeCl_2$ reacts with NaF to form a series of beryllium fluoride adducts, which should be dominated by BeF_3^- at 10 mM NaF

(69). Thus, the concentration of BeF_3^- is assumed to be equal to the concentration of $BeCl_2$. Ten independent fluorescence measurements were taken (1 measurement/s) for each concentration of $BeCl_2$ and the values averaged and corrected for dilution. To correct for non-specific interactions between $PhoB_N$ and $BeCl_2$, titrations were also performed in the absence of NaF. There was a small increase in fluorescence upon the first addition of $BeCl_2$, which was subtracted from the fluorescence intensity for the titrations that contained 10 mM NaF.

The above protocols were modified slightly for measurements of ligand binding to $PhoB_N$ R115D. $PhoB_N$ R115D exhibited a modest time-dependent quench in fluorescence, which stabilized within 15 minutes, in response to changes in solution ionic strength. The initial solutions containing 5 μM $PhoB_N$ R115D in buffer were thus allowed to incubate for 30 minutes at 25°C. An additional control titration was carried out with KCl (0-15 mM) in lieu of Mn^{2+}, Mg^{2+}, or BeF_3^- to quantify the ionic strength response. For all titrations, solutions were incubated for 15 minutes after addition of ligand and before fluorescence measurements were taken. The changes in fluorescence due to changes in ionic strength as determined by KCl titration were subtracted from the fluorescence intensity at each concentration of ligand. For divalent metal and BeF_3^- binding, the changes in fluorescence due to changes in ionic strength were less than 5% of the total change in fluorescence.

For both divalent cation and BeF_3^- binding, plots of (I_0-I) versus ligand concentration were constructed, where I_0 is the fluorescence intensity with no added ligand and I is the fluorescence intensity at a given concentration of ligand. Plots of BeF_3^- binding to $PhoB_N$ and $PhoB_N$ F20D were sigmoidal and data were fit to equation 2.1

(GraphPad Prism) to determine n, the Hill coefficient, and $K_{1/2}$, the concentration of $BeCl_2$ required to acquire half (I_0-I_{max}).

$$(I_0 - I) = \frac{(I_0 - I_{max}) \text{ x } [ligand]^n}{{K_{1/2}}^n + [ligand]^n} \quad [2.1]$$

For determining all other ligand binding constants, a standard one-site binding equation was used.

2.3.6 Fluorescence measurements of reaction kinetics

Tryptophan fluorescence was used to continuously monitor autophosphorylation of both CheY and various PhoB constructs with PAM. Observed rate constants for autophosphorylation of CheY at a given concentration of PAM decrease with increasing ionic strength of the solution (44). Thus, all reactions were performed at a constant ionic strength of 400 mM, which includes the concentration of buffer, divalent cation, PAM, and KCl.

Fluorescence measurement of CheY autophosphorylation was similar to previous reports (40,43,46). Briefly, a rapid mixing device (Applied Photophysics RX2000) was used to mix equal volumes of 10 µM CheY (in 6 mM $MnCl_2$ and 100 mM Hepes, pH 7.0) and PAM (20-300 mM in 100 mM Hepes, pH 7.0). Both CheY and PAM solutions were supplemented with KCl to give a final ionic strength of 400 mM. Because CheY and PAM solutions were mixed at a one-to-one (v/v) ratio, the concentrations of CheY, $MnCl_2$ and PAM were decreased by half in the final reaction. Fluorescence was continuously monitored and time points recorded every twenty milliseconds. Reactions were performed in duplicate for each experimental condition.

Autophosphorylation reactions for $PhoB_F$, $PhoB_N$, and $PhoB_N$ F20D were carried out in a 1-cm x 0.4-cm quartz cuvette with manual mixing to initiate the reaction. The beginnings of the time traces were identical when measured using a stopped flow apparatus or the standard cuvette. However, the ends of the time traces showed variability when measured using the stopped flow apparatus, likely due to diffusion over the longer period of time required to achieve steady state for PhoB (up to 35 minutes). $PhoB_F$ (5 μM), $PhoB_N$ (2.5-20 μM), or $PhoB_N$ F20D (5 μM) were incubated in 100 mM Hepes, pH 7.0, 3 mM $MnCl_2$, and varying concentrations of KCl to reach a constant ionic strength of 400 mM (after PAM addition) with magnetic stirring to reach temperature equilibrium. The autophosphorylation reaction was initiated by addition of PAM (10-150 mM final concentration) to bring the final volume to 750 μL, followed by repetitive pipeting to mix (< 5 s), and fluorescence was continuously monitored. Time points were recorded every twenty or one hundred milliseconds. Reactions were performed in triplicate for each experimental condition.

Autophosphorylation time traces of $PhoB_N$ R115D were measured in a 1-cm x 1-cm quartz cuvette at a final volume of 1.5 mL. $PhoB_N$ R115D (10 μM) was incubated in 6 mM $MnCl_2$, 100 mM Hepes, pH 7.0, and 282 mM KCl at a volume of 750 μL for 30 minutes with magnetic stirring. Due to the effect of ionic strength on $PhoB_N$ R115D fluorescence (see above), it was necessary to keep the ionic strength of the whole system at 400 mM throughout the experiment. For that reason, the autophosphorylation reaction was initiated by addition of an equal volume of PAM (20-300 mM) in 100 mM Hepes, pH 7.0, and varying concentrations of KCl to maintain a constant ionic strength of 400 mM, followed by mixing by repetitive pipeting (< 5 s), and fluorescence was

continuously monitored. Because $PhoB_N$ R115D and PAM solutions were mixed at a one-to-one ratio, the concentrations of $PhoB_N$ R115D, $MnCl_2$ and PAM were decreased by half. Time points were recorded every 0.5 s. Reactions were performed in triplicate for each experimental condition.

2.3.7 Analysis of kinetic data

Autophosphorylation reactions were performed under pseudo-first order conditions, with a large molar excess of PAM over protein. Fluorescence time traces reflected a continually changing reaction rate, as the amount of unreacted CheY or PhoB decreased while PAM concentration was essentially unchanged. All time traces were normalized by dividing the fluorescence intensities by the initial fluorescence intensity (I_0) to generate relative fluorescence intensity (RFI). Replicate time courses for the same protein or PAM concentration were averaged. The averaged, normalized fluorescence intensities are referred to as 'time traces' for the rest of this document. Initial curve fits were made to a single exponential decay (GraphPad Prism). For CheY and $PhoB_N$ R115D, the time traces gave excellent fits to a single exponential and the resulting pseudo-first order rate constants were termed observed rate constants (k_{obs}). For $PhoB_F$, $PhoB_N$, and $PhoB_N$ F20D, there were modest but systematic deviations from a single exponential decay. Therefore, we also tried fitting these data to a two-phase exponential decay, but the fits were indistinguishable from a single exponential. As described in Results, there was utility in using the single exponential fits for initial data analysis, so the rate constants derived from imperfect single exponential fits were termed apparent rate constants (k_{app}). The simple kinetic model shown in scheme 1 implicates the relationship between the pseudo-first order rate constant k_{obs} and individual kinetic

parameters, shown in equation 2.2 (43). For CheY·Mn^{2+}, plots of k_{obs} versus PAM concentration were linear, consistent with results obtained with CheY·Mg^{2+} (40,42,46). This result indicates that the dissociation constant between CheY·Mn^{2+} and PAM is much larger than the highest concentration of PAM used in the experiment (K_S >> [PAM]), reducing equation 2.2 to equation 2.3. Thus the slope of the line is equal to the apparent bimolecular rate constant (k_{phos}/K_S). For $PhoB_N$ R115D, plots of k_{obs} versus the concentration of PAM were also linear, and the slope was similarly used to determine k_{phos}/K_S. Plots of the pseudo-first order rate constant k_{app} versus the concentration of PAM for $PhoB_F$, $PhoB_N$, and $PhoB_N$ F20D appeared sigmoidal and were thus fit using a modified Hill equation (Graph Pad Prism), equation 2.4, where k_{max} is the maximum change in apparent rate constant, $K_{1/2}$ is the PAM concentration required to reach the mid-point of the dose-response curve, n is the Hill coefficient, and k_{min} is the minimum apparent rate constant.

$$k_{obs} = \frac{k_{phos} \text{ x } [PAM]}{K_S + [PAM]} + k_{dephos} \quad [2.2]$$

$$k_{obs} = \frac{k_{phos}}{K_S} \text{ x } [PAM] + k_{dephos} \quad [2.3]$$

$$k_{app} = \frac{k_{max} \text{ x } [PAM]^n}{K_{1/2}{}^n + [PAM]^n} + k_{min} \quad [2.4]$$

2.3.8 Mathematical modeling of $PhoB_N$ autophosphorylation time traces

Mathematical modeling of $PhoB_N$ autophosphorylation time traces was performed using Dynafit software (70) to potentially explain several features of the kinetic data, including an apparent lag at the beginning of the $PhoB_N$ autophosphorylation time traces and the observation that protein concentration affected the apparent pseudo-first order rate constant for autophosphorylation. As described in Results, numerous models of increasing complexity were tried before choosing the model described below. In particular, the protein concentration dependence of normalized $PhoB_N$ time traces constrained the model significantly because it necessitated the inclusion of a reaction step whereby multiple molecules of $PhoB_N$ interact to give reaction species with altered phosphorylation kinetics. Thus, based on a large body of evidence documenting the dimerization of $PhoB_F$ and $PhoB_N$ (33-35,59-62), a comprehensive model of autophosphorylation kinetics of PhoB that included multiple versions of PhoB dimer 1 with the possibility of differing autophosphorylation kinetics was considered (Scheme 2). In the model, a monomer (m) of PhoB can bind to a molecule of PAM with dissociation constant K_S (m) and then phosphorylate with rate constant k_{phos} (m), analogous to the first two steps in scheme 1 for CheY. A phosphorylated PhoB monomer can then interact with either another phosphorylated PhoB monomer to form a homodimer (PhoB-P:PhoB-P), or with an unphosphorylated PhoB monomer to form a heterodimer (PhoB:PhoB-P), with dimerization constants K_{dimer} (hom) and K_{dimer} (het), respectively. The heterodimer can then bind to a molecule of PAM with dissociation constant K_S (het) and phosphorylate with rate constant k_{phos} (het). All three phosphorylated species of PhoB can also dephosphorylate, with rate constants k_{dephos} (hom), k_{dephos} (het), and k_{dephos} (m).

Dimerization of two unphosphorylated PhoB monomers (dimer 2) was excluded from the model due to a measured dimerization constant [378 μM (61)] that was much greater than the highest concentration of PhoB used in our experiments.

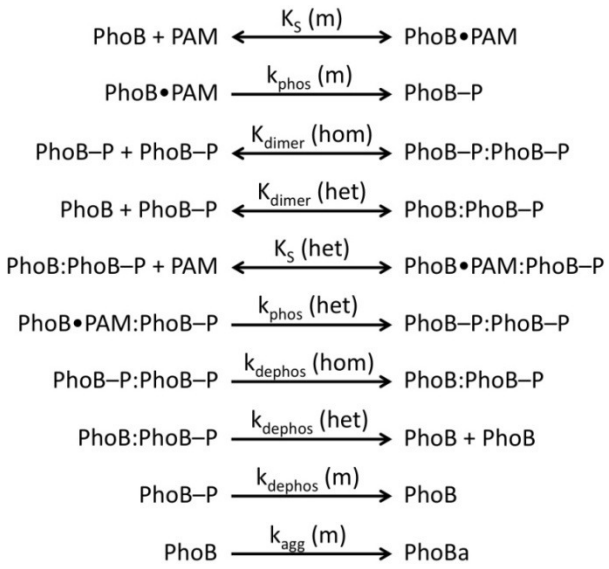

Scheme 2. Reactions included in mathematical model of PhoB autophosphorylation.

To fit the kinetic data to the model, the normalized fluorescence intensities for $PhoB_N$ autophosphorylation time traces were first multiplied by the protein concentration used in the experiment. Dynafit requires a conversion factor that translates the concentration of different PhoB species to the measured fluorescence responses. We established conversion factors based on the assumption that tryptophan fluorescence was quenched solely as a result of the conformational change that occurs upon PhoB phosphorylation or formation of the heterodimer, but not by PAM binding. Thus the species that are not primarily in the active conformation (PhoB and PhoB·PAM) were assigned a conversion factor equal to the initial fluorescence intensity divided by the

protein concentration. The species that are primarily in the active conformation (PhoB–P, PhoB:PhoB–P, PhoB·PAM:PhoB–P, and PhoB–P:PhoB–P) were assigned a conversion factor equal to the minimum fluorescence intensity for autophosphorylation of 5 μM $PhoB_N$ with 150 mM PAM (i.e. the time trace with the maximum quench in fluorescence intensity) divided by the protein concentration. The described assumptions for the conversion factors gave good fits. Alternative assumptions were also tested (e.g. PAM binding to $PhoB_N$ resulted in quenched tryptophan fluorescence). However, alternative conversion factors could not by themselves account for fundamental features of the kinetics, such as the lag phase observed in the time traces or the protein concentration dependence of the apparent pseudo-first order rate constant.

An initial model composed of the nine reactions described above gave good fits for ten of the twelve autophosphorylation time traces representing different concentrations of protein or PAM. However, there were systematic deviations for the two experimental conditions with the slowest timescales for autophosphorylation (10 mM and 20 mM PAM). Specifically, the rate and equilibrium constants predicted by Dynafit gave modeled time traces that had the expected initial lag phases; however, the modeled plateaus at long reaction times were up to 30% below the experimental data. Slow formation of a PhoB aggregate (PhoBa) was added to the model with a rate constant of k_{agg} (m). To compensate for the higher plateau observed in the experimental time traces, the conversion factor for PhoBa was set to three times the initial fluorescence intensity divided by the protein concentration. This larger conversion factor is consistent with light scattering due to formation of a soluble aggregate.

Next, we set the following four parameters to experimentally measured values. K_{dimer} (hom) was set to the published value of 5.1 μM (61). [For all equilibrium constants, we assumed rapid equilibrium and set the k_{on} rate constant equal to $1x10^6$ M^{-1} s^{-1} (71).] The three autodephosphorylation rate constants were determined by monitoring the disappearance of [^{32}P]$PhoB_N$-P or [^{32}P]$PhoB_N$ R115D-P over time (see Experimental Procedures below, data not shown). The rate constant k_{dephos} (hom) was set equal to the rate constant determined for [^{32}P]$PhoB_N$-P (0.0003 s^{-1}). Because $PhoB_N$ R115D cannot form dimer 1, k_{dephos} (m) was set equal to the rate constant determined for [^{32}P]$PhoB_N$ R115D-P (0.0002 s^{-1}). Because the model does not include formation of the unphosphorylated PhoB dimer, autodephosphorylation of the heterodimer is equivalent to dimer dissociation followed by monomer dephosphorylation. For that reason, k_{dephos} (het) was also set equal to the rate constant determined for [^{32}P]$PhoB_N$ R115D-P. Note that the measured k_{dephos} values for $PhoB_N$ are in close agreement with previously reported values for k_{dephos} for $PhoB_F$ (63,68,72).

The remaining six rate and equilibrium constants [K_S (m), k_{phos} (m), K_{dimer} (het), K_S (het), k_{phos} (het), k_{agg} (m)] were then manually varied until the modeled time traces were similar to the raw time traces for autophosphorylation of 5 μM $PhoB_N$ with 60 mM PAM. These modeled values were then used as initial constants for global analysis of all of the time traces for $PhoB_N$ autophosphorylation (i.e. 2.5-20 μM $PhoB_N$ with 60 mM PAM and 5 μM $PhoB_N$ with 10-150 mM PAM). Nonlinear least-square regressions were performed to simultaneously fit the six adjustable rate and equilibrium constants: K_S (m), k_{phos} (m), K_{dimer} (het), K_S (het), k_{phos} (het), k_{agg} (m). Perturbing the initial values for the rate and equilibrium constants did not affect the resultant output. The residuals that were

output by Dynafit were divided by protein concentration to allow for comparison between protein concentrations.

2.3.9 Radiolabeling of PhoR using [γ-^{32}P]ATP

His_6-tagged PhoR (230 μg) was reacted with 1 mM [γ-^{32}P]ATP (18 Ci/mmol) in 35 mM Tris, pH 8.0, 35 mM KCl, and 3.5 mM $MgCl_2$ in a total volume of 200 μL for 30 minutes at room temperature. The sample was passed over 100 μL prewashed nickel·NTA resin in a small centrifugal 0.22 μm filtration device and washed ten times with 400 μL wash buffer (50 mM Hepes, pH 7.0, 300 mM NaCl, 20 mM imidazole) to remove excess [γ-^{32}P]ATP. The [^{32}P]PhoR-P was eluted with 3x 400 μL elution buffer (50 mM Hepes, pH 7.0, 300 mM NaCl, 150 mM imidazole) and concentrated. The concentration of [^{32}P]PhoR-P was determined using a Bradford assay with BSA standards. Purified aliquots of [^{32}P]PhoR-P were stored at -20°C.

2.3.10 Phosphotransfer from [^{32}P]PhoR-P to $PhoB_N$

[^{32}P]PhoR-P was thawed and diluted into 35 mM Tris, pH 8.0, 35 mM KCl and 3 mM $MnCl_2$ to give a final protein concentration of 1 μM and a final volume of 120 μL. A 7.5 μL aliquot was removed and added to 7.5 μL 2x-SDS PAGE buffer for a zero time point. Either $PhoB_N$ or $PhoB_N$ R115D was added at a ten-fold molar excess (10 μM), mixed, and a series of 7.5 μL time points up to ten minutes were removed and immediately combined with 2x-SDS PAGE buffer. Samples were electrophoresed on 18% polyacrylamide gels and the gels were subsequently dried. The amount of [^{32}P]PhoR-P at each time point was determined by phosphorimaging. The percentage of [^{32}P]PhoR-P remaining was plotted against time and then fit to a one-phase exponential decay to determine the rate constant for phosphotransfer.

2.3.11 Rate constants for [^{32}P]PhoB-P autodephosphorylation

His_6-tagged PhoR (6 μM) was reacted with 1 mM [γ-^{32}P]ATP (18 Ci/mmol) in 35 mM Tris, pH 8.0, 35 mM KCl, and 3 mM $MnCl_2$ in a total volume of 50 μL for 15 minutes at room temperature. The sample was passed over 100 μL prewashed nickel·NTA resin in a small centrifugal 0.22 μm filtration device to bind His_6-tagged PhoR and washed ten times with 400 μL of buffer containing 35 mM Tris, pH 8.0, 35 mM KCl, and 3 mM $MnCl_2$ to remove excess [γ-^{32}P]ATP. A 100 μL sample of either $PhoB_N$ (30 μM) or $PhoB_N$ R115D (30 μM) in 35 mM Tris, pH 8.0, 35 mM KCl, and 3 mM $MnCl_2$ was added to the column and incubated for five minutes at room temperature. The sample was allowed to filter over the nickel·NTA resin and the non-bound material was collected. 7.5 μL samples were removed and added to an equal volume of 2x SDS-PAGE buffer at the following time points: 5 min, 10 min, 15 min, 30 min, 45 min, 60 min, 90 min and 120 min. Samples were electrophoresed on 18% polyacrylamide gels. The gels were dried and the amount of [^{32}P]$PhoB_N$-P at each time point was determined by phosphorimaging. The percentage of [^{32}P]$PhoB_N$-P remaining was plotted against time and then fit to a one-phase exponential decay to determine the rate constant for autodephosphorylation.

2.4 Results

2.4.1 Optimization of PhoB autophosphorylation reaction conditions

A divalent cation bound in the receiver domain active site is essential for catalysis of both response regulator phosphorylation and dephosphorylation (9,43). Therefore, as a prerequisite for measuring PhoB autophosphorylation kinetics, it was necessary to

characterize the metal binding properties of the various PhoB proteins [full-length PhoB ($PhoB_F$), the N-terminal receiver domain ($PhoB_N$), $PhoB_N$ F20D, and $PhoB_N$ R115D] so that the occupancy of the metal binding site was known for subsequent autophosphorylation experiments. Tryptophan fluorescence measurements indicated that binding between Mg^{2+} and $PhoB_N$ occurred with a dissociation constant (K_D) of 1.6 ± 0.2 mM, in agreement with the reported K_D for $PhoB_F$ Mg^{2+} binding of 2.0 ± 0.5 mM (68). However, the concentration of Mg^{2+} required to reach high levels of metal-bound PhoB (> 95%) led to visible precipitation of both $PhoB_N$ and $PhoB_F$ within the timescale of the autophosphorylation reactions.

To avoid complications associated with precipitation, we searched for another metal ion that bound to PhoB and could support autophosphorylation. Although Mg^{2+} is most likely the divalent cation utilized by PhoB *in vivo*, Mg^{2+} and Mn^{2+} have similar size and preferred coordination number, geometry, and ligand type (73). Furthermore, Mn^{2+} supports autophosphorylation of the response regulator Spo0F with PAM (74), autophosphorylation of several sensor kinases, and phosphotransfer from a sensor kinase to a response regulator *in vitro* (75-77). Binding of Mn^{2+} to both $PhoB_F$ and $PhoB_N$ was much tighter than Mg^{2+}, with a K_D of 82 ± 6 μM and 70 ± 4 μM, respectively. Mn^{2+} bound to $PhoB_N$ F20D and $PhoB_N$ R115D with similar affinities (K_D of 51 ± 5 μM and 20 ± 8 μM, respectively). Furthermore, Mn^{2+} was highly capable of mediating $PhoB_N$ autophosphorylation and the concentration of Mn^{2+} required for > 95% occupancy of the metal binding site (3 mM $MnCl_2$) did not lead to visible precipitation. Thus, the standard conditions for all autophosphorylation reactions in this study included 3 mM $MnCl_2$ to ensure high occupancy of the metal binding site. Autophosphorylation of CheY was also

readily catalyzed by 3 mM Mn^{2+} (see below); thus, all autophosphorylation experiments were done in parallel for PhoB and CheY to rule out the possibility that any novel characteristics of PhoB autophosphorylation were due to the use of Mn^{2+} as opposed to Mg^{2+}.

The visible precipitation that occurred between Mg^{2+} and PhoB was more severe for $PhoB_F$ than for $PhoB_N$. Though no visible precipitation occurred in solutions containing Mn^{2+} and either $PhoB_F$ or $PhoB_N$, we wanted to take every measure to minimize formation of aggregates during autophosphorylation experiments. For that reason, the majority of the autophosphorylation reactions were performed using the highly soluble $PhoB_N$. As expected from previous work (78), the removal of the DNA-binding domain did not affect autophosphorylation of PhoB (see below).

2.4.2 Normalized autophosphorylation time traces for $PhoB_N$ displayed a visible lag phase and a protein concentration dependence

Autophosphorylation of both $PhoB_N$ and CheY at various PAM and protein concentrations were monitored by continuous measurement of tryptophan fluorescence. In all cases, PAM concentration exceeded protein concentration by at least three orders of magnitude, so the reactions occurred under pseudo-first order conditions. For both CheY and $PhoB_N$, autophosphorylation was initiated by the addition of PAM, which resulted in a time-dependent quench in fluorescence that eventually leveled out (Fig. 2.2A-D). The fluorescence intensity is a relative measure of the process of the reaction from all unphosphorylated CheY or $PhoB_N$ (intensity at zero time) to a steady state level of phosphorylated CheY or $PhoB_N$ (intensity after steady state is achieved). Achievement of steady state indicates equal rates of autophosphorylation and autodephosphorylation.

Because the absolute magnitude of the initial fluorescence intensity varied for individual reactions (especially for different protein concentrations), time traces (Fig. 2.2) were normalized by dividing by the initial fluorescence intensities and are reported as relative fluorescence intensities (RFI).

As expected, the time traces for CheY·Mn^{2+} autophosphorylation (Fig. 2.2A) displayed similar properties as those reported for CheY·Mg^{2+} (42,44). The shapes of the time traces for CheY·Mn^{2+} autophosphorylation were the same as for CheY·Mg^{2+} and occurred on a similar time scale (20-100 s). Also, the maximum quench in fluorescence due to autophosphorylation was ~50% for both CheY·Mn^{2+} and CheY·Mg^{2+}. Because of the pseudo-first order reaction conditions employed ([PAM] >> [CheY]) and the fact that fluorescence is a measure of the relative progress of the reaction, increasing the concentration of PAM resulted in a shift of the time traces to shorter reaction times (Fig. 2.2A) but varying the concentration of CheY did not affect the time frame of the normalized time traces (Fig. 2.2C).

However, comparison of autophosphorylation time traces for CheY (Fig. 2.2A) and $PhoB_N$ (Fig. 2.2B) revealed three evident differences. First, autophosphorylation of $PhoB_N$ was markedly slower than autophosphorylation of CheY, although the $PhoB_N$ time traces were still dependent on PAM concentration. For example, at 60 mM PAM, it took approximately 500 s for autophosphorylation of $PhoB_N$ to reach steady state, while it only took approximately 35 s for CheY. Second, the $PhoB_N$ autophosphorylation time traces displayed a visible lag phase (Fig. 2.2B – inset) that was not present in time traces for CheY autophosphorylation (Fig. 2.2A – inset). This lag was most evident during the first 100 seconds of the autophosphorylation time traces for 40 mM and 60 mM PAM.

Finally, the half-life of the normalized autophosphorylation time traces of $PhoB_N$ clearly decreased with increasing protein concentration (2.5-20 μM) (Fig. 2.2D); however, CheY autophosphorylation time traces did not show a protein concentration dependence (Fig. 2.2C).

Both the lag and the protein concentration dependence of normalized time traces suggested that $PhoB_N$ autophosphorylation occurred with a more complex kinetic mechanism than CheY. Protein concentration dependence was inconsistent with a reaction in which a single molecule of $PhoB_N$ participates, but was consistent with a reaction that involves interactions between two or more $PhoB_N$ molecules. The $PhoB_N$ protein concentration dependence, in particular, suggested that interactions between $PhoB_N$ monomers play a role in the kinetic mechanism of $PhoB_N$ autophosphorylation.

2.4.3 Initial analysis of $PhoB_N$ autophosphorylation suggested positive cooperativity with respect to PAM

To analyze the kinetics of autophosphorylation more quantitatively, we fit the autophosphorylation time traces to a one-phase exponential decay and plotted the resultant rate constants against PAM concentration. For CheY, the time traces fit extremely well to a one-phase exponential decay (Fig. 2.3A), with low residuals [difference between data and curve fitting] (< ±0.25%) that displayed no obvious pattern. The CheY rate constants from these fits were termed k_{obs}. For CheY·Mn^{2+}, the plot of k_{obs} versus PAM concentration was linear, consistent with results obtained with CheY·Mg^{2+} (40,42,46), and the slope of the plot was equal to k_{phos}/K_S. The k_{phos}/K_S for reaction of CheY·Mn^{2+} with PAM was 2.2 ± 0.04 M^{-1} s^{-1}, which was 1/2 to 1/3 the k_{phos}/K_S of 6.1 M^{-1} s^{-1} for reaction of CheY·Mg^{2+} [after corrections for ionic strength (46)].

In contrast to CheY and consistent with the visible lag, the $PhoB_N$ autophosphorylation time traces exhibited systematic deviations from a one-phase exponential decay (Fig. 2.3B). The residuals for $PhoB_N$ followed a pattern and were 4-52x larger than for CheY throughout the entire time course (Fig. 2.3A and 2.3B – lower panel). Despite the systematic deviations from a single exponential decay, R^2 values for fitting $PhoB_N$ autophosphorylation time traces with a one-phase exponential decay were greater than 0.98. Rate constants obtained from the single exponential fits were used to estimate the overall rate of acquisition of steady state; however, due to the systematic deviations, we labeled these apparent rate constants k_{app} and used these values as an initial tool for analyzing the data.

A plot of k_{app} versus PAM concentration for $PhoB_N$ (Fig. 2.3D) differed from the plot of k_{obs} versus PAM concentration for CheY (Fig. 2.3C) in two ways. First, the plot of k_{app} versus PAM concentration for $PhoB_N$ fit to a sigmoidal dose-response curve with a Hill coefficient of 2.1 ± 0.2, which suggested that autophosphorylation of $PhoB_N$ exhibited some sort of positive cooperativity. The apparent positive cooperativity indicated communication between $PhoB_N$ active sites, such that autophosphorylation of one active site led to enhanced autophosphorylation kinetics at other sites, another suggestion that multimerization affects the rate of autophosphorylation of $PhoB_N$. Second, in contrast to k_{obs} for CheY, which showed no signs of saturating at the PAM concentrations used, k_{app} for $PhoB_N$ appeared to saturate at high PAM concentrations.

Previous work on PhoB autophosphorylation showed that removal of the DNA-binding domain did not affect the rate of PhoB autophosphorylation with 20 mM PAM (78). As expected, $PhoB_F$ autophosphorylation time traces with multiple PAM

concentrations also showed a visible lag (Fig. 2.4A) and protein concentration dependence (data not shown) similar to $PhoB_N$. Also, plots of k_{app} versus PAM concentration for $PhoB_F$ (Fig. 2.4B) were nearly superimposable on $PhoB_N$ (Fig. 2.3D, Hill coefficient of 2.1 ± 0.3) and also appeared saturable. Thus, the kinetic properties exhibited by $PhoB_N$ were not due to removal of the DNA-binding domain.

2.4.4 Beryllium trifluoride binding to $PhoB_N$ displayed positive cooperativity

The plot of k_{app} versus PAM concentration for $PhoB_N$ (Fig. 2.3D) used rate constants derived from curve fits that systematically deviated from a single exponential decay. Thus, we sought an alternate method of assessing communication between $PhoB_N$ active sites by examining binding of a phosphoryl group analog. BeF_3^- binds to the active site of response regulators and mimics the Asp-phosphate linkage of phosphorylated response regulators (28,62,79). A plot of the quench in $PhoB_N$ tryptophan fluorescence versus BeF_3^- concentration (Fig. 2.5) was also sigmoidal with a Hill coefficient of 1.8 ± 0.2. The positive cooperativity exhibited in BeF_3^- binding lends credibility to the apparent cooperativity of $PhoB_N$ autophosphorylation kinetics (Fig. 2.3D). Also, with a $K_{1/2}$ for BeF_3^- binding to $PhoB_N$ in the low micromolar range (44 ± 4 μM), the concentrations of BeF_3^- required to reach saturation were approximately three orders of magnitude lower than PAM concentrations needed, further reducing the possibility that a small amount of invisible aggregation could be affecting the $PhoB_N$ fluorescence signal.

2.4.5 Mathematical modeling supported a link between dimerization and autophosphorylation of $PhoB_N$

In an attempt to account for the lag in the time traces and the protein concentration dependence of $PhoB_N$ autophosphorylation, we utilized mathematical

modeling software to construct a model of autophosphorylation. We began with a model that was similar to the kinetic model of CheY autophosphorylation (scheme 1) and included PAM binding, phosphorylation and dephosphorylation of $PhoB_N$. This model was unable to account for either the lag of the autophosphorylation time traces or the protein concentration dependence, even when slow PAM binding or a variety of fluorescence intensity conversion factors were considered, suggesting a more complex kinetic mechanism of $PhoB_N$ autophosphorylation. The protein concentration dependence of $PhoB_N$ autophosphorylation, the visible lag in the $PhoB_N$ autophosphorylation time traces, the cooperative relationship between k_{app} and PAM concentration, and the sigmoidicity of BeF_3^- binding to $PhoB_N$ all suggested that there was a relationship between multimerization and autophosphorylation of $PhoB_N$. Specifically, the protein concentration dependence of autophosphorylation rate constants demanded that multiple $PhoB_N$ molecules participated in the autophosphorylation reaction and the lag suggested the existence of an step early in the reactions that, once completed, resulted in faster autophosphorylation. PhoB is known to dimerize when phosphorylated, so we next included formation of a homodimer ($PhoB_N$-P:$PhoB_N$-P) in the model. This too was unable to account for the protein concentration dependence of autophosphorylation and the lag in the $PhoB_N$ autophosphorylation time traces, suggesting an even more complex mechanism.

To account for all aspects of the autophosphorylation data, formation of a $PhoB_N$ heterodimer ($PhoB_N$-P:$PhoB_N$) was fundamental to the model. The resultant ten-step kinetic model (Scheme 2, Fig. 2.6, see Experimental Procedures for extensive details) included the formation of both the $PhoB_N$ homodimer ($PhoB_N$-P:$PhoB_N$-P) and the

$PhoB_N$ heterodimer ($PhoB_N$-P:$PhoB_N$) and the possibility of differing autophosphorylation kinetics (K_S and k_{phos}) for the $PhoB_N$ monomer and the $PhoB_N$ heterodimer. Four out of the ten kinetic parameters were set to constants obtained experimentally to limit the number of variables that were subject to change by Dynafit software.

All twelve time traces for autophosphorylation [i.e. 5 μM $PhoB_N$ with 10-150 mM PAM (Fig. 2.2B) and 2.5-20 μM $PhoB_N$ with 60 mM PAM (Fig. 2.2D)] were simultaneously fit to the model by global analysis using Dynafit software (Fig. 2.7). The global analysis of the $PhoB_N$ autophosphorylation time traces succeeded in fitting all data and a single set of predicted kinetic constants (Fig. 2.6) gave simulated time traces that overlaid well with all twelve of the $PhoB_N$ autophosphorylation time traces. Formation of the PhoB aggregate was an extremely slow process with a rate constant [k_{agg} (m)] at least two orders of magnitude slower than either the rate constant for phosphorylation of the monomer [k_{phos} (m)] or the heterodimer [k_{phos} (het)]. Furthermore, excluding aggregation from the model did not greatly affect ten of the twelve autophosphorylation time traces. This was consistent with slow formation of a very small amount of soluble aggregate.

The rate and equilibrium constants generated by computer modeling were consistent with a link between $PhoB_N$ dimerization and autophosphorylation. Specifically, formation of a $PhoB_N$ heterodimer ($PhoB_N$-P:$PhoB_N$) and different autophosphorylation properties of the heterodimer compared to the monomer were fundamental to the model. Not only was inclusion of the heterodimer essential to fit the data, it was essential that the dimerization constant for the heterodimer [K_{dimer} (het)] had to be in the low micromolar range, similar to the dimerization constant for formation of

the homodimer [K_{dimer} (hom), 5.1 μM]. In addition, k_{phos} (het) had to be at least ten-fold faster than k_{phos} (m). Dimerization constants in the same range as the protein concentration used in the experiments account for the protein concentration dependence of k_{app}. The difference between k_{phos} (m) and k_{phos} (het) accounts for the lag in the autophosphorylation time traces. Even modest modifications (± 50%) to the rate and equilibrium constants predicted by Dynafit led to poor fits to the autophosphorylation data.

2.4.6 Disruption of the physiologically relevant dimer 1 interface of $PhoB_N$ impeded autophosphorylation

Crystallographic evidence shows that $PhoB_N$ is able to dimerize at two different dimerization interfaces (59,60,62), the α4-β5-α5 surface (dimer 1) and the α1-β5α5 loop-α5 surface (dimer 2) [Fig. 2.1]. To more directly test the potential link between dimer formation and autophosphorylation of $PhoB_N$, we characterized autophosphorylation kinetics of $PhoB_N$ variants containing previously characterized amino acid substitutions known to disrupt dimer formation (61). Replacement of Arg 115 with Asp ($PhoB_N$ R115D) disrupted the electrostatic interaction between residues Arg 115 and Asp 101 in the dimer 1 interface. Replacement of Phe 20 with Asp ($PhoB_N$ F20D) disrupted the hydrophobic dimerization interface of dimer 2.

Autophosphorylation of $PhoB_N$ F20D (dimer 2 mutant) with varying PAM concentrations displayed kinetics similar to wild type $PhoB_N$. The autophosphorylation time traces exhibited a visible lag at the beginning of the time traces similar to wild type $PhoB_N$ (Fig. 2.4A). A plot of k_{app} versus PAM concentration for $PhoB_N$ F20D also fit to a sigmoidal curve with a Hill coefficient of 1.8 ± 0.2 (Fig. 2.4B), implying positive

cooperativity of autophosphorylation similar to wild type $PhoB_N$. Therefore, the cooperativity of autophosphorylation of wild type $PhoB_N$ was not likely due to formation of a dimer along the non-physiological dimer 2 interface.

In contrast, autophosphorylation of $PhoB_N$ R115D (dimer 1 mutant) with PAM occurred over a much longer timescale than wild type $PhoB_N$ and did not exhibit a visible lag at the beginning of the time traces (Fig. 2.4A-inset). The plot of k_{obs} versus PAM concentration for $PhoB_N$ R115D (Fig. 2.4B) showed no signs of sigmoidicity and fit to a linear regression. Thus, disruption of the physiologically relevant $PhoB_N$ dimer 1 interface resulted in slow autophosphorylation kinetics that were not cooperative. This result supported the link between dimerization and autophosphorylation of $PhoB_N$ and, furthermore, identifies the dimer 1 interface as the functionally relevant dimerization surface in autophosphorylation. Putting the mutant results together with previous observations and modeling, we propose that autophosphorylation kinetics of wild type $PhoB_N$ reflect the formation of a heterodimer along the dimer 1 interface, which leads to an enhanced rate constant for phosphorylation of the $PhoB_N$ heterodimer compared to the $PhoB_N$ monomer.

2.4.7 Beryllium trifluoride binding to the physiologically relevant dimer 1 mutant PhoBN R115D was not cooperative

To further investigate the role of dimer formation on the cooperativity of wild type $PhoB_N$ kinetics, we characterized the BeF_3^- binding properties of $PhoB_N$ R115D and $PhoB_N$ F20D. Binding of BeF_3^- to $PhoB_N$ F20D was cooperative with a Hill coefficient (2.0 ± 0.1) and binding constant (51 ± 3 μM) similar to wild type $PhoB_N$ (Fig. 2.5). In contrast, binding of BeF_3^- to $PhoB_N$ R115D was not cooperative and displayed a much

weaker binding constant than wild type $PhoB_N$ (Fig. 2.5). Because disruption of dimer 1 eliminated the cooperativity of BeF_3^- binding to $PhoB_N$, the cooperativity of BeF_3^- binding to wild type $PhoB_N$ was likely due to the formation of a dimer along the dimer 1 interface.

2.4.8 Phosphotransfer from [^{32}P]PhoR-P to wild type $PhoB_N$ was faster than to $PhoB_N$ R115D

To determine if there was a link between the formation of the $PhoB_N$ dimer and phosphotransfer from the histidine kinase PhoR, the rate constants for phosphotransfer from [^{32}P]PhoR-P to wild type $PhoB_N$ and $PhoB_N$ R115D were determined by monitoring the time-dependent disappearance of [^{32}P]PhoR-P in the presence of ten-fold molar excess $PhoB_N$ (Fig. 2.8). Phosphotransfer from [^{32}P]PhoR-P to wild type $PhoB_N$ was approximately five-times faster than phosphotransfer from [^{32}P]PhoR-P to $PhoB_N$ R115D, with bimolecular rate constants of 77,000 ± 5,000 M^{-1} s^{-1} and 16,000 ± 1,000 M^{-1} s^{-1}, respectively. Therefore, both $PhoB_N$ autophosphorylation with PAM and phosphotransfer from [^{32}P]PhoR-P to $PhoB_N$ were enhanced by the formation of dimer 1. Furthermore, accumulation of radiolabeled phosphoryl group on $PhoB_N$ R115D occurred in a time dependent manner to a similar extent as wild type $PhoB_N$ (Fig. 2.8) indicating functional $PhoB_N$ R115D protein.

2.5 Discussion

A central observation here was that in contrast to CheY, $PhoB_N$ and $PhoB_F$ autophosphorylation kinetics exhibited properties indicative of communication between active sites from different monomers. Numerous lines of evidence supported the notion

that association of PhoB monomers to form heterodimers (one phosphorylated and one unphosphorylated monomer) affected autophosphorylation kinetics, including the protein concentration dependence of the normalized autophosphorylation time traces (Fig. 2.2D), the systematic deviation of the autophosphorylation time traces from a one-phase exponential (Fig. 2.3B), and the sigmoidicity of the plot of k_{app} versus PAM concentration (Fig. 2.3D). Binding of the phosphoryl group analog BeF_3^- to $PhoB_N$ was sigmoidally dependent on BeF_3^- concentration (Fig. 2.5) also indicating communication between $PhoB_N$ active sites. As predicted by a reaction scheme in which heterodimers play a role in autophosphorylation kinetics, disruption of the dimer 1 dimerization interface by the previously characterized R115D amino acid substitution (61) greatly reduced the rate of $PhoB_N$ autophosphorylation (Fig. 2.4B) and eliminated cooperativity in both autophosphorylation and BeF_3^- binding (Fig. 2.5).

2.5.1 Successful mathematical modeling of autophosphorylation data provided insights into the PhoB reaction mechanism

After testing multiple models of increasing complexity, we developed a scheme that linked autophosphorylation and dimerization of $PhoB_N$ (Fig. 2.6). A mathematical model based on this scheme and utilizing a single set of kinetic and equilibrium constants (some experimentally determined, some computationally inferred) was able to faithfully reproduce all the experimentally observed effects of changing either $PhoB_N$ or PAM concentration (Fig. 2.7).

First, the difference between k_{phos} (m) and k_{phos} (het) accounted for the lag in the autophosphorylation time traces and deviation from a single phase exponential. Specifically, PhoB autophosphorylation kinetics were initially dominated by monomers

[k_{phos} (m)] and hence slow. After creation of phosphorylated monomers facilitated heterodimer formation with an excess of unphosphorylated PhoB monomers, faster autophosphorylation kinetics [k_{phos} (het)] became evident. The model predicted that under the experimental conditions employed, there was a flux from monomers through heterodimers to homodimers, but not necessarily a large accumulation of heterodimers. Second, a predicted dimerization constant [K_{dimer} (het)] for heterodimer formation in the same range as the protein concentration used in the experiments accounted for the protein concentration dependence of the normalized $PhoB_N$ time traces observed in Fig. 2.2D. Changing $PhoB_N$ concentration around K_{dimer} (het) altered heterodimer formation and hence the experimentally measured rate constants for the reaction. Additional insights gleaned from the mathematical model into the detailed mechanism of PhoB positive cooperativity are described in the next two sections.

2.5.2 Dimerization constant for the $PhoB_N$-P:$PhoB_N$ heterodimer was in the low micromolar range

A surprising prediction from the kinetic modeling was that the dimerization constant for formation of the $PhoB_N$-P:$PhoB_N$ heterodimer [K_{dimer} (het), 12 μM] was similar to that measured for formation of the $PhoB_N$-P:$PhoB_N$-P homodimer [K_{dimer} (hom), 5.1 μM (61)]. Receiver domain phosphorylation results in a conserved allosteric activating conformational change that includes changes in the α4-β5-α5 surface (10,24). For multiple response regulators in the OmpR/PhoB family, the changes in the α4-β5-α5 surface result in formation of a dimer (10,24,33-35). Thus, it might be expected that acquisition of the active conformation is a prerequisite for dimerization and that formation of a PhoB heterodimer would involve association of a phosphorylated PhoB

monomer with an unphosphorylated monomer that is in the active conformation. In such a circumstance, K_{dimer} (het) would be a composite of both the equilibrium constants for the conformational change and for dimerization [linked equilibria (80)], described by $K_{dimer,link}$ in equation 2.5, where $K_{dimer,link}$ is the apparent dimerization constant for heterodimer formation, K_{conf} is the conformational equilibrium constant for PhoB in the active conformation and $K_{dimer,act}$ is the associative dimerization constant of PhoB in the active conformation:

$$K_{dimer,link} = K_{conf} \cdot K_{dimer,act} \qquad [2.5]$$

Though it is difficult to measure the fraction of the response regulator population in the active conformation, it is estimated that no more than 10% of unphosphorylated response regulator molecules are in the active conformation (27,40). Therefore, if K_{conf} is less than 0.1, we would predict K_{dimer} (het) to be at least 10-fold larger than K_{dimer} (hom), which does not contain a significant conformational component because the phosphorylated monomers are predominantly in the active conformation. The similarity between the predicted K_{dimer} (het) and the measured K_{dimer} (hom) suggests that acquisition of the active conformation is not a prerequisite for PhoB heterodimer formation. Though there is no direct evidence for the formation of a $PhoB_N$ heterodimer, a modified version of dimer 1 has been crystallized in the absence of BeF_3^- (60). Both monomers in the structure were in the inactive conformation, implying that $PhoB_N$ dimer 1 formation does not require acquisition of the active conformation before association.

2.5.3 Accelerated autophosphorylation of the $PhoB_N$-P:$PhoB_N$ heterodimer

The second important prediction from the mathematical modeling of $PhoB_N$ autophosphorylation was that the rate constant for phosphorylation of the heterodimer [k_{phos} (het)] was approximately ten times higher than the rate constant for phosphorylation of the monomer [k_{phos} (m)], implying that formation of the heterodimer of $PhoB_N$ enhanced the rate of autophosphorylation. This result is consistent with other observations that have linked an activated conformation to faster autophosphorylation kinetics. Addition of FliM [a ligand that pushes CheY towards an active-like conformation (29)] to CheY greatly enhances the rate of autophosphorylation compared to when no ligand is present (40). Similarly, addition of DNA that binds to OmpR increases the rate of autophosphorylation compared to no ligand present (41). We propose that formation of the heterodimer of $PhoB_N$ pushes the conformational equilibrium of the unphosphorylated monomer in the heterodimer towards the active conformation, which results in a faster rate of autophosphorylation of the $PhoB_N$ heterodimer compared to the $PhoB_N$ monomer.

2.5.4 Physiological implications of cooperative kinetics

We have presented extensive yet indirect evidence for formation of a PhoB heterodimer. It is not presently known if other response regulators form heterodimers, and, if so, whether heterodimer formation leads to enhanced phosphorylation kinetics. However, there is at least one published observation consistent with heterodimer formation by another response regulator. An apparent heterodimer of ComE was trapped by cross-linking and separated from cross-linked homodimer by SDS-PAGE (81).

How the network properties of different two-component systems can result in different output behaviors, including all-or-none versus graded responses, is the focus of both theoretical and experimental studies (82,83). Response regulators that form heterodimers with enhanced phosphorylation kinetics may contribute to an all-or-none output response. Our data demonstrating that phosphotransfer from the sensor kinase PhoR to PhoB was enhanced by dimer 1 formation (Fig. 2.8) would predict a sigmoidal relationship between phosphorylated PhoR (PhoR-P) and phosphorylated PhoB (PhoB-P) (i.e. a sudden nonlinear output response over a small change in input). PhoB is an autoregulated response regulator, where PhoB-P regulates transcription of both *phoR* and *phoB*, leading to a positive feedback loop for *phoB* regulation (84). In combination, the positive cooperativity and auto-regulation could lead to a physiological response that acts as an on/off switch. At low concentrations of PhoR-P, there would be little PhoB-P and thus a low level of transcriptional activation within the cell. Eventually, a threshold concentration of PhoR-P will be reached and PhoB-P will abruptly accumulate, leading to an abrupt cellular response. There is precedent for such behavior in the all-or-none response of PhoB to phosphorylation by non-cognate histidine kinases (85). Because the PhoRB system regulates transcription of genes encoding proteins involved in phosphorus assimilation, the potential on/off switch may act as a way to dampen responses to minor fluctuations in the environmental concentration of phosphate.

Because formation of dimer 1 of PhoB orients the DNA-binding domains to interact with the symmetric DNA-binding sites (62), it is possible that a PhoB heterodimer would have similar affinity for DNA and thus could regulate transcription *in vivo*. A recent study that characterizes the relationship between unphosphorylated and

phosphorylated PhoB concentrations *in vivo* and transcriptional activity showed that, even at full transcriptional activity, the concentration of phosphorylated PhoB was less than the total concentration of PhoB (63). Although there are multiple explanations for this phenomenon, it could be due to a physiologically active heterodimer. If the heterodimer is active *in vivo*, there are many potential consequences. First, because the heterodimer only requires phosphorylation of a single monomer of PhoB, it will accumulate at lower concentrations of PhoB-P than the homodimer, leading to an increased sensitivity of response for the heterodimer. Second, some response regulators [e.g. OmpR (86), BvgA (87), NtrC (88)] bind to different promoters with different affinities, which allows step-wise responses to changing environmental circumstances. High affinity promoters are populated at low response regulator concentrations and promoters with low binding affinities are not populated until the concentration of response regulator is sufficiently high. The PhoB heterodimer and homodimer might exhibit different promoter binding affinities, which would facilitate a more complex regulatory scheme. Third, when the cellular signal is turned off, dephosphorylation of the PhoB homodimer may result in a functional heterodimer that can induce transcription for a longer timeframe than if no active heterodimer is formed.

2.5.5 Autophosphorylation of $PhoB_N$ was different than CheY

Positive cooperativity was not the only parameter that differed between CheY and PhoB. Although CheY autophosphorylation was 15-30 times faster than $PhoB_N$ autophosphorylation, $PhoB_N$ appeared to bind PAM slightly tighter than CheY. Based on our mathematical modeling, PAM binds to both the heterodimer and the monomer with binding constants [K_S (het), K_S (m)] of approximately 150 mM, whereas the PAM

binding affinity for CheY is estimated to be greater than 500 mM (40,42,46). These differences in rate and binding constants were noteworthy due to the similarities in tertiary structure, active site geometry, and divalent metal coordination of $PhoB_N$ and CheY. There must be other characteristics that differ between $PhoB_N$ and CheY that can explain the differences in rate and binding constants. One hypothesis based on work on CheY where positions near to the site of phosphorylation were substituted is that a more positive charge at the active site leads to faster autophosphorylation kinetics (46). We looked at the electrostatic surface potential of the Mg^{2+}-bound forms of $PhoB_N$ [PDB 2IYN (60)] and CheY [PDB 2CHE (89)] using Adaptive Poisson-Boltzman Solver software (90). The surface of CheY is more positively charged than $PhoB_N$ due to residues with varying charges in nonconserved positions structurally adjacent to the active site. Because the small-molecule phosphodonor is intrinsically negatively charged, the overall positive charge of the surface of CheY may lead to the faster rate of autophosphorylation compared to $PhoB_N$.

2.6 Figures

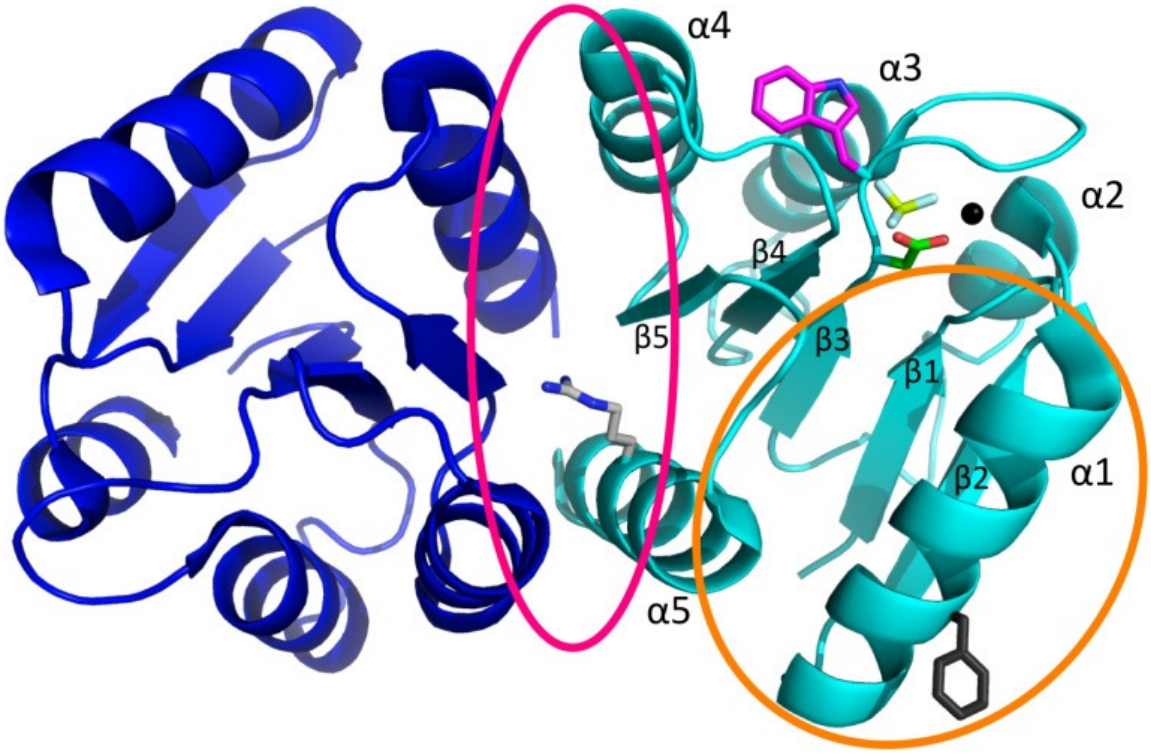

Figure 2.1. Ribbon representation of the physiologically relevant PhoBN dimer (dimer 1). The crystal structure shown is of $PhoB_N$ bound to the phosphoryl group analog BeF_3^- (PDBid 1ZES). The two $(\beta\alpha)_5$ monomers that comprise the dimer are colored blue (1ZES chain B) and cyan (1ZES chain C). Phosphoryl group analog BeF_3^- (yellow and white) is bound to Asp53 (green). Also shown are the active site magnesium ion (black sphere) and the side chain for the Trp54 fluorophore (magenta). The dimer 1 interface (pink circle) is comprised of residues on helix α4, strand β5, and helix α5 and includes Arg115 (light grey). The non-physiological dimer 2 interface (orange circle) is comprised of residues on helix α1, β5α5 loop, and helix α5 and includes Phe20 (dark grey).

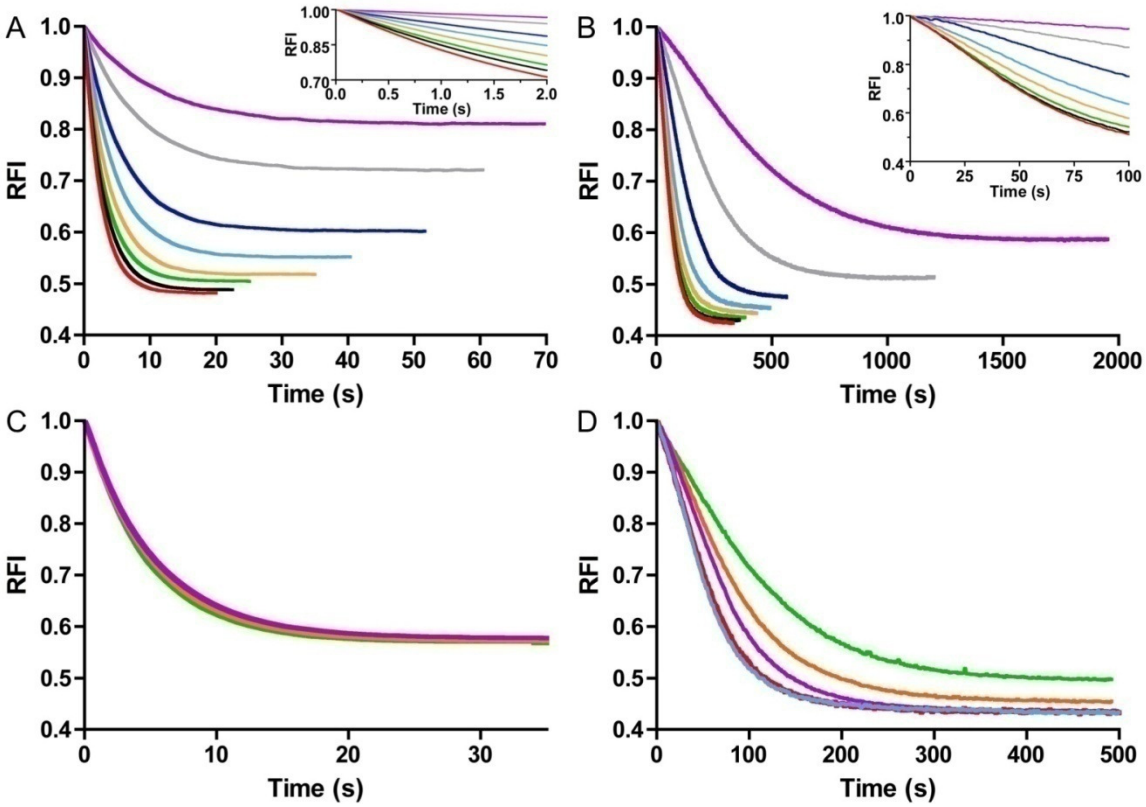

Figure 2.2. Normalized CheY and PhoBN autophosphorylation time traces at various substrate or protein concentrations. Fluorescence measurement of autophosphorylation of 5 μM CheY **(A)** and 5 μM $PhoB_N$ **(B)** at the following PAM concentrations: 10 mM (purple), 20 mM (grey), 40 mM (dark blue), 60 mM (light blue), 80 mM (orange), 100 mM (green), 125 mM (black), and 150 mM (red). Insets show a magnified view of the first portions of the autophosphorylation time traces. **(C)** Autophosphorylation of 2.5 μM (green), 5 μM (orange), and 10 μM (purple) CheY with 60 mM PAM. **(D)** Autophosphorylation of 2.5 μM (green), 5 μM (orange), 10 μM (purple), 15 μM (red), and 20 μM (blue) $PhoB_N$ with 60 mM PAM. RFI (relative fluorescence intensity) is obtained by dividing all fluorescence intensities by the initial fluorescence intensity. Reactions were carried out in duplicate for panels A and C and in triplicate for panels B and D. Time traces represent the mean of multiple reactions.

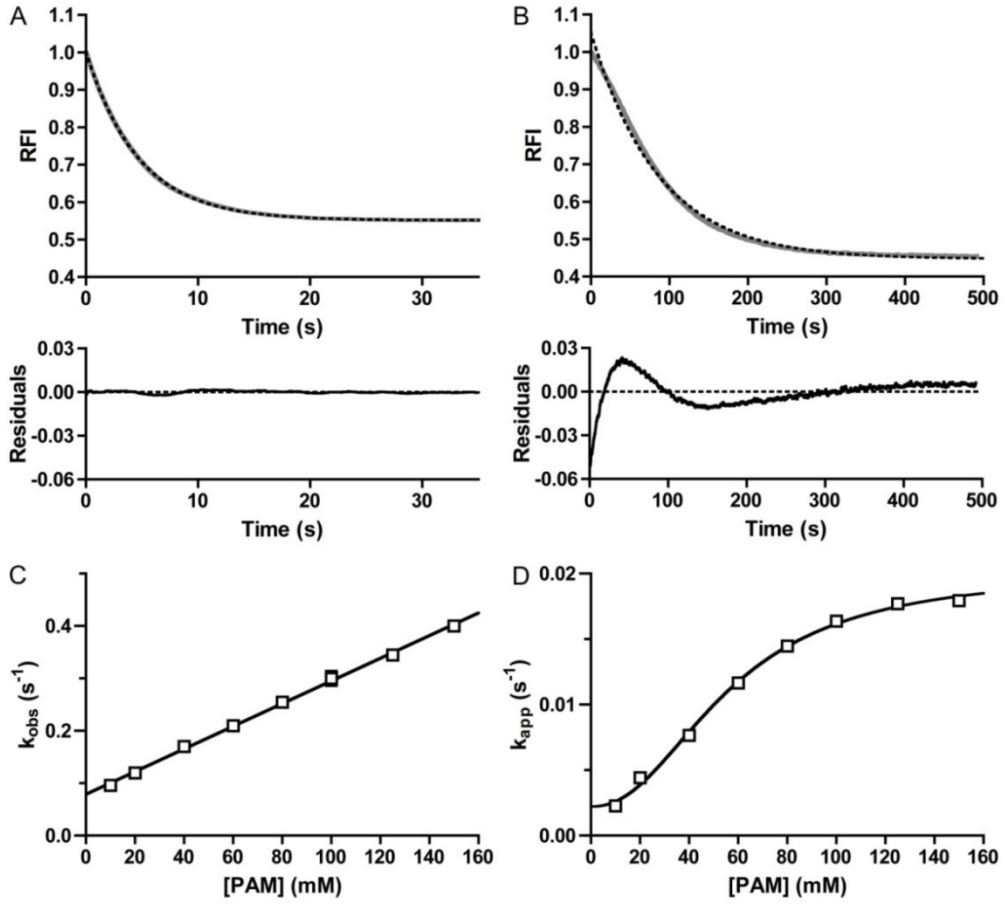

Figure 2.3. Analysis of CheY and $PhoB_N$ time traces by fitting to a single exponential decay. Autophosphorylation time traces for reaction of 5 µM CheY **(A)** or 5 µM $PhoB_N$ **(B)** with 60 mM PAM (grey) fit to a one-phase exponential decay (dashed black line). The rate constant from the fit is k_{obs} for CheY and k_{app} for $PhoB_N$. Residuals (the difference between the raw data and the fit) are shown below. Time traces represent the mean of multiple reactions. RFI is as defined in Figure 2.2. **(C)** Plot of k_{obs} versus PAM concentration for 5 µM CheY fit with linear regression (see equation 2.3). The slope of the line gave k_{phos}/K_S and the y-intercept gave k_{dephos}. Error bars represent standard deviation from duplicate experiments. **(D)** Plot of k_{app} versus PAM concentration for 5 µM $PhoB_N$ fit with sigmoidal dose response curve (see equation 2.4). Error bars represent standard deviation from triplicate experiments.

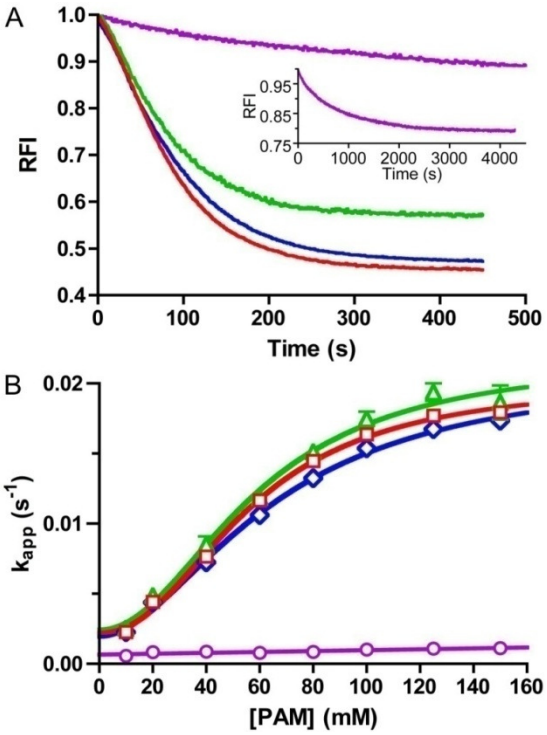

Figure 2.4. Autophosphorylation kinetics of wild type PhoB ($PhoB_F$ and $PhoB_N$) and $PhoB_N$ dimer interface mutants. (A) Autophosphorylation time traces for reaction of 5 µM $PhoB_F$ (green), 5 µM $PhoB_N$ F20D (blue), 5 µM $PhoB_N$ R115D (purple), or 5 µM $PhoB_N$ (red, from Figure 2.2B) with 60 mM PAM. Inset: expanded timescale to show the full autophosphorylation time trace for $PhoB_N$ R115D. $PhoB_F$ contains a tryptophan in the output domain that is not present in $PhoB_N$, leading to a smaller maximal quench in fluorescence for $PhoB_F$. Time traces represent the mean of three reactions, with standard deviations (not shown for clarity) that were less than 3% of the mean. RFI same as defined in Figure 2.2. **(B)** Plot of k_{app} versus PAM concentration for 5 µM $PhoB_F$ (green triangles), 5 µM $PhoB_N$ F20D (blue diamonds), 5 µM $PhoB_N$ R115D (purple circles), or 5 µM $PhoB_N$ (red squares, Figure 2.3D) fit with sigmoidal dose response curve (see equation 2.4) for $PhoB_F$ and $PhoB_N$ F20D or linear regression (see equation 2.3) for $PhoB_N$ R115D. Error bars represent standard deviation from triplicate experiments.

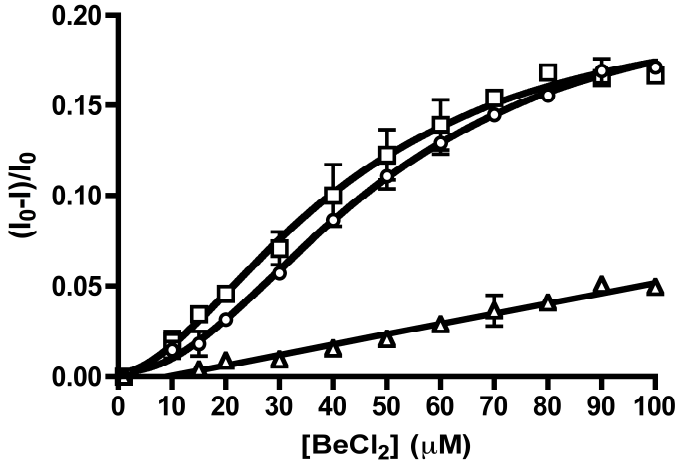

Figure 2.5. Beryllium trifluoride binding to PhoB constructs. Beryllium chloride titration with 5 μM $PhoB_N$ (square), 5 μM $PhoB_N$ F20D (circle), or 5 μM $PhoB_N$ R115D (triangle) measured by fluorescence. The buffer contains 10 mM NaF. Error bars represent standard deviation from triplicate experiments.

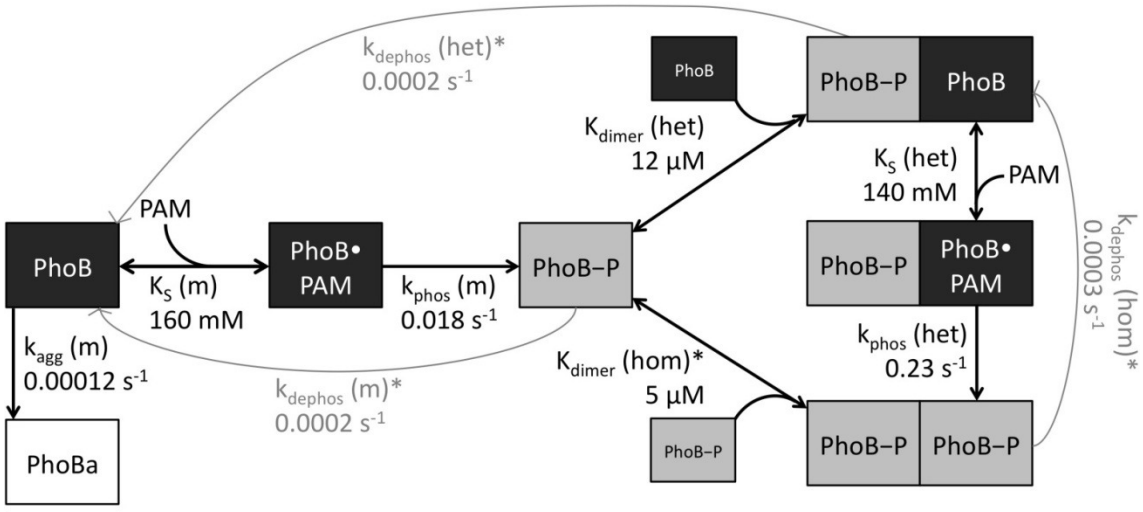

Figure 2.6. Model linking $PhoB_N$ heterodimer formation and autophosphorylation.

A monomer of $PhoB_N$ binds a small molecule phosphodonor (PhoB·PAM) and phosphorylates (PhoB–P). The phosphorylated monomer can bind another phosphorylated monomer to form a homodimer. The phosphorylated monomer can also bind an unphosphorylated monomer to form a heterodimer, which can then bind PAM and phosphorylate. All three phosphorylated species of $PhoB_N$ can autodephosphorylate. Rate and equilibrium constants predicted by mathematical modeling included by corresponding arrows. Kinetic constants marked with a star (*) were measured experimentally.

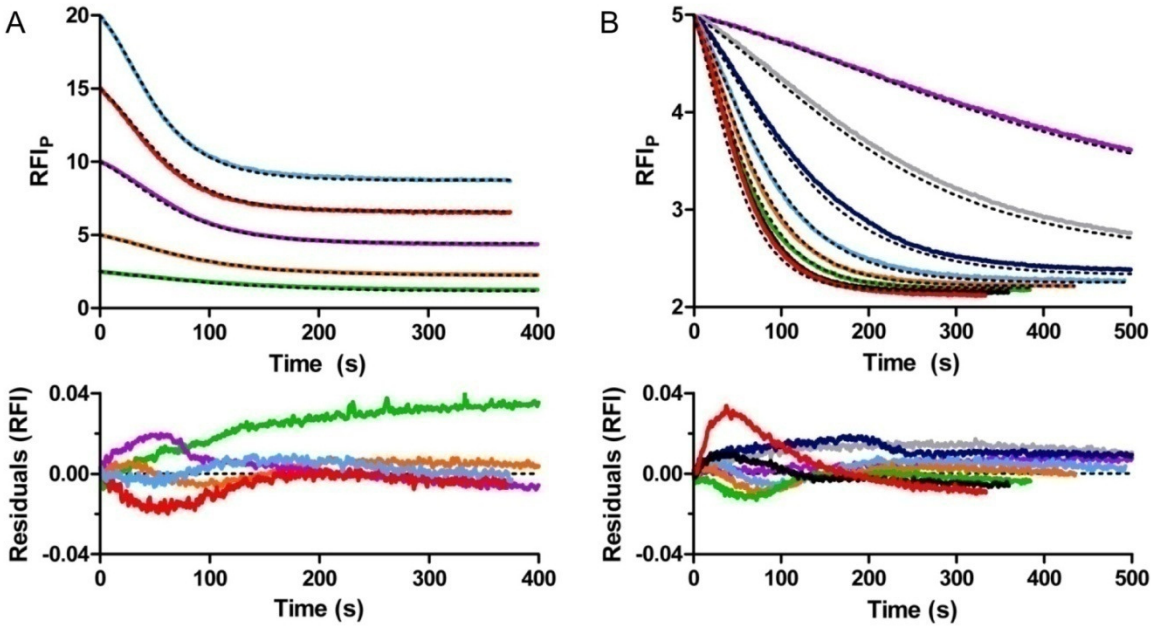

Figure 2.7. Mathematical modeling by global kinetic analysis of autophosphorylation of $PhoB_N$. Autophosphorylation time traces for reaction of 2.5-20 μM $PhoB_N$ with 60 mM PAM (**A**) and for reaction of 5 μM $PhoB_N$ with 10-150 mM PAM truncated to 500 s (**B**) with overlays of modeled fits from global kinetic analysis by Dynafit (black dashed lines) and residuals. Colors in panel A as described in Figure 2.2D. Colors in panel B as described in Figure 2.2B. RFI_P represents the normalized tryptophan fluorescence intensity obtained by dividing all fluorescence intensities by the initial fluorescence intensity then multiplying by the protein concentration. RFI in the residual plots is the same as defined in Figure 2.2.

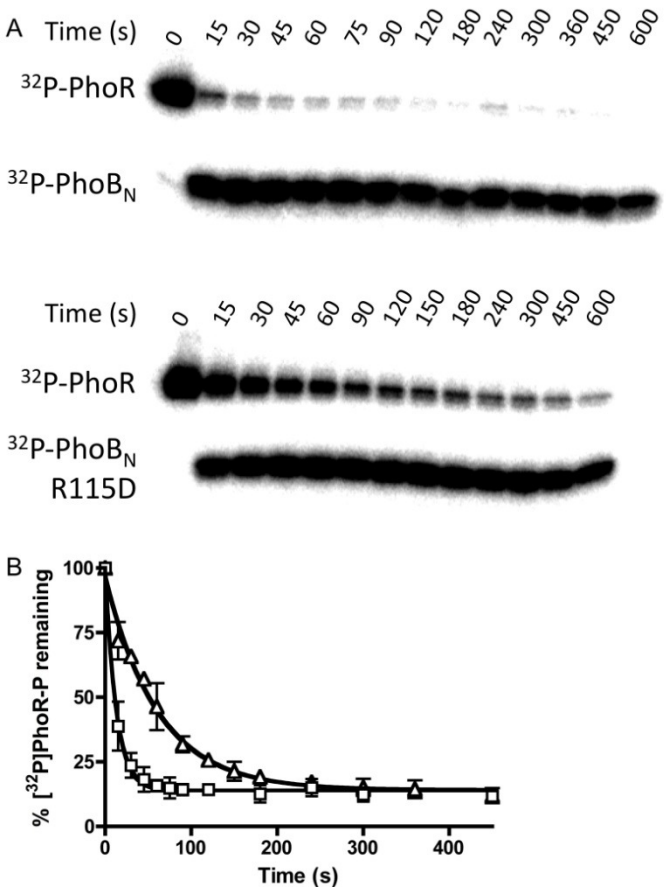

Figure 2.8. Phosphotransfer from [^{32}P]PhoR-P to either wild type PhoB$_N$ or PhoB$_N$ R115D. (A) Phosphorimage of SDS-PAGE gel analysis of phosphotransfer reactions. Each lane represents a different time point between 0-600 seconds as shown. **(B)** Quantitative analysis of the phosphorimage as shown in panel A for wild type PhoB$_N$ (squares) and PhoB$_N$ R115D (triangles), fit to a one-phase exponential decay. Each point represents the average and standard deviation of replicate experiments.

Chapter 3 – Substitutions at nonconserved active site residues affect the rates of $PhoB_N$ autophosphorylation

3.1 Introduction

As discussed in Chapters 1 and 2, response regulators can autophosphorylate with small-molecule phosphodonors. Because typical antibiotics are small-molecule inhibitors of proteins or enzymes, better understanding of the interaction between response regulators and small-molecule phosphodonors may inform the search for or design of compounds with enhanced affinity for response regulators. For CheY, the relationship between the observed rate of autophosphorylation and the concentration of small-molecule phosphodonor is linear up to the highest concentrations of phosphodonor tested (100 mM), indicating very weak substrate binding (K_S> 500 mM) (40,42,46). Four nonconserved residues are predicted to form the surface of the response regulator active site where the small-molecule phosphodonor approaches and docks to the response regulator. Amino acid substitutions made at these positions in CheY greatly affected the rate of autophosphorylation with different phosphodonors; however the relationship between k_{obs} and phosphodonor concentration remained linear, even for mutants with a 10^3-10^4-fold rate enhancement (46) (Immormino, R.M, & Bourret, R.B., unpublished). Because small-molecule inhibitors must bind tightly to target proteins, CheY is not a good model system for better understanding of small molecule binding to response

regulators. Autophosphorylation of the response regulator PhoB, however, appeared to saturate at high concentrations of PAM (see Chapter 2). Apparent saturation of autophosphorylation of PhoB implies measurable binding of small molecules to PhoB. PhoB potentially offers an opportunity not available with CheY to gain a better understanding of the factors that determine the specificity and affinity of small molecule binding to response regulators.

Here, we present kinetic characterization of autophosphorylation of mutants of the response regulator PhoB with the phosphodonors PAM and MPI. $PhoB_N$ substitutions were based on previously characterized substitutions in CheY as well as two previously uncharacterized positions inspired by small molecule docking into a crystal structure of $PhoB_N$. The mathematical model described in Chapter 2 was utilized to predict which kinetic constants in the autophosphorylation mechanism are affected by the $PhoB_N$ substitutions. It is predicted that the $PhoB_N$ substitutions only affected the rates of phosphorylation and had no affect on small molecule binding or dimerization.

3.2 Experimental Procedures

3.2.1 Docking of small-molecule phosphodonors into $PhoB_N$ crystal structure

The prodrg server (http://davapc1.bioch.dundee.ac.uk/prodrg/) was used to generate the atomic coordinates for MPI, PAM, and AcP. Water molecules were removed from the BeF_3^- and Mg^{2+}-bound $PhoB_N$ crystal structure (PDBid 1ZES). The Docking Wizard utility in the Pymol Molecular Graphics System (Schrodinger, LLC) was used to do a three-on-three point docking of each small-molecule phosphodonor onto the $PhoB_N$ crystal structure. The atoms used for docking were the three fluorine atoms of BeF_3^- and

the three oxygen atoms of the phosphoryl group of the small-molecule phosphodonor, with the small-molecule phosphodonor leaving group oriented towards the solvent. The torsional angles of MPI and AcP were manually rotated to dock all three potential rotamers. Hydrogen atoms were added to each of the resultant protein-small molecule structures using Reduce (91). Pymol was used to select residues within 4 Å of the small-molecule phosphodonor to identify residues that potentially interact with the small molecule.

3.2.2 Previously described experimental procedures

Cloning and site-directed mutagenesis of $PhoB_N$ was performed as described in Section 2.3.1 and resultant proteins were purified as in Section 2.3.3. The potassium salt of PAM was synthesized as described in Section 2.3.2. The sodium salt of MPI was synthesized as described (46,92). Autophosphorylation kinetics of $PhoB_N$ mutants with PAM (10-150 mM final concentration) and MPI (2.5-50 mM final concentration) were measured and processed as described in sections 2.3.6 and 2.3.7, respectively.

3.2.3 Modified mathematical modeling

Mathematical modeling of autophosphorylation kinetics of $PhoB_N$ mutants with PAM was performed as in Section 2.3.8 with the following modifications. As before, four parameters were fixed using experimentally determined values. The six remaining rate and equilibrium constants were set to the values determined in Chapter 2 for autophosphorylation of wild type $PhoB_N$. Nonlinear least-square regressions were performed to allow a subset of the rate and equilibrium constants to change: i) k_{phos} (m), k_{phos} (het), and k_{agg} (m), ii) K_S (m), K_S (het), and k_{agg} (m), iii) k_{phos} (m), k_{phos} (het), K_S

(m), K_S (het), and k_{agg} (m), iv) k_{phos} (m), k_{phos} (het), K_S (m), K_S (het), K_{dimer} (het), and k_{agg} (m).

3.3 Results

3.3.1 Substitutions at nonconserved active site residues

Docking of small-molecule phosphodonors into the crystal structure of BeF_3^--bound $PhoB_N$ identified six nonconserved active site residues that might interact with the phosphodonors: Glu 11 (one residue C-terminal to the two conserved acidic residues, DD+1), Met 55 (two residues C-terminal to the conserved Asp, D+2), Leu 56 (three residues C-terminal to the conserved Asp D+3), Leu 82 (one residue N-terminal to the conserved Thr, T-1), Ala 84 (one residue C-terminal to the conserved Thr, T+1), Arg 85 (two residues C-terminal to the conserved Thr, T+2) [Figure 3.1]. Nine substitutions were made at one or more of these six residues (Table 3.1) to determine if any of the residues affected small-molecule phosphodonor binding to $PhoB_N$. The effects of two of these residues on CheY autophosphorylation have not been previously characterized (D+3 and T-1); therefore, initial substitutions to Ala were made to determine if removal of the side chains affected autophosphorylation. The four remaining residues predicted to interact with the phosphodonor have been previously characterized in CheY (46), (Immormino, R.M, & Bourret, R.B., unpublished). Previous characterization of substitutions at DD+1 in CheY showed no effect on autophosphorylation kinetics (46). To determine if DD+1 had an effect on $PhoB_N$ autophosphorylation, this residue was substituted to Ala.

Table 3.1. $PhoB_N$ substitutions

Position	Wild type residue(s)	Substitution(s)	Nomenclature
11 (DD+1)	Glu	Ala	$PhoB_N$ 11EA
55 (D+2)	Met	Asp	$PhoB_N$ 55MD
	Met	Asn	$PhoB_N$ 55MN
56 (D+3)	Leu	Ala	$PhoB_N$ 56LA
82 (T-1)	Leu	Ala	$PhoB_N$ 82LA
84 (T+1)	Ala	Thr	$PhoB_N$ 84AT
55 (D+2) 85 (T+2)	Met Arg	Asn Glu	$PhoB_N$ NE
	Met Arg	Asn Tyr	$PhoB_N$ NY
	Met Arg	Lys Tyr	$PhoB_N$ KY

The six remaining $PhoB_N$ substitutions were based on previously characterized substitutions in CheY :

- A class of phosphatases within the haloacid dehalogenase superfamily of enzymes (HAD phosphatases) has a tertiary structure and active site that are highly similar to response regulators. HAD phosphatases catalyze the same phosphorylation and dephosphorylation chemistry as response regulators, but with rate constants ~10^3-10^4-fold greater than the rate constants for response regulators (93). Substitutions made in CheY to mimic the HAD phosphatase active site (Asp at D+2, Arg at T+2) resulted in greatly enhanced rates of autophosphorylation and autodephosphorylation (Immormino, R.M, Starbird, C., Silversmith, R.E., & Bourret, R.B., unpublished). Because $PhoB_N$ already has an Arg at T+2, a single substitution was made at D+2 to an Asp to mimic the HAD phosphatase active site. To test whether the Asp at D+2 acts through acid/base catalysis, D+2 was also substituted to an Asn, which contains an amide instead of a reactive carboxylic acid.
- Based on an analysis of response regulator amino acid sequences, T+1 is typically occupied by a small amino acid like Ala or Gly [~73%], though sometimes a Ser/Thr is found at the T+1 position [15%] (Immormino, R.M, & Bourret, R.B., unpublished).

In CheY, incorporation of the larger, branched Thr side chain partially occludes the site of phosphorylation from small-molecule phosphodonors (Immormino, R.M, & Bourret, R.B., unpublished), decreasing the rate of autophosphorylation. To determine if this result occurs in another response regulator, T+1 in $PhoB_N$ was substituted to a Thr.

- Finally, we made three double substitutions at D+2 and T+2. The first double mutant is a mimic of CheY with as Asn at D+2 and a Glu at T+2. The other two double mutants include the residues that resulted in the fastest autophosphorylation kinetics for CheY, Asn at D+2 and Tyr at T+2 or Lys at D+2 and Tyr at T+2 (46).

3.3.2 Initial characterization of autophosphorylation of $PhoB_N$ mutants with PAM

To begin characterizing autophosphorylation of the nine $PhoB_N$ mutants, we first monitored autophosphorylation at a single PAM concentration (60 mM) [Figure 3.2]. Any $PhoB_N$ mutants with obvious differences from wild type would be further characterized at multiple PAM and protein concentrations. Four of the substitutions ($PhoB_N$ 11EA, $PhoB_N$ 55MN, $PhoB_N$ NY, $PhoB_N$ KY) did not appear to affect autophosphorylation at 60 mM PAM, giving time traces that were similar to wild type $PhoB_N$. Two of the mutants ($PhoB_N$ 56LA, $PhoB_N$ NE) showed no change in fluorescence intensity upon addition of PAM, possibly due to a non-functioning protein or a rate of autodephosphorylation that is much larger than the rate of autophosphorylation, resulting in no accumulation of phosphoryl group on the protein. The rate of autodephosphorylation of $PhoB_N$ NE was 0.24 min^{-1} (Stephani Page, Pers. Comm.), which is 15-fold faster than wild type $PhoB_N$, suggesting that $PhoB_N$ NE was unable to accumulate phosphoryl groups. Three substitutions appeared to significantly affect the

apparent rate of $PhoB_N$ autophosphorylation. $PhoB_N$ 55MD exhibited a greatly enhanced apparent rate of $PhoB_N$ autophosphorylation in comparison to wild type $PhoB_N$, whereas $PhoB_N$ 82LA and $PhoB_N$ 84AT had reduced apparent rates of $PhoB_N$ autophosphorylation.

3.3.3 Full characterization of autophosphorylation of $PhoB_N$ mutants with PAM

In addition to the three mutants ($PhoB_N$ 55MD, $PhoB_N$ 82LA, $PhoB_N$ 84AT) that differed substantially from wildtype autophosphorylation at 60 mM PAM, we chose to further characterize $PhoB_N$ 55MN and $PhoB_N$ KY. $PhoB_N$ 55MN was examined for comparison to $PhoB_N$ 55MD and $PhoB_N$ KY was of interest due to the greatly enhanced rate of autophosphorylation for the same substitutions in CheY. For all five substitutions, we monitored autophosphorylation of 5 μM $PhoB_N$ with 10-150 mM PAM and 2.5-20 μM $PhoB_N$ with 60 mM PAM. Preliminary results showed that precipitation of $PhoB_N$ 82LA was an issue due to the length of time required to get a full time trace for autophosphorylation; therefore, it was not possible to obtain a full data set. Autophosphorylation of $PhoB_N$ 55MN and $PhoB_N$ KY resulted in time traces and plots of k_{app} versus PAM concentration that were very similar to wild type $PhoB_N$ (data not shown). Autophosphorylation of $PhoB_N$ 55MD gave normalized time traces that reached equilibrium much more quickly than wild type $PhoB_N$ for all PAM and protein concentrations (Figure 3.3AB). Autophosphorylation of $PhoB_N$ 84AT gave normalized time traces that reached equilibrium much more slowly than wild type $PhoB_N$ for all PAM and protein concentrations (Figure 3.4AB).

For both $PhoB_N$ 55MD and $PhoB_N$ 84AT, the autophosphorylation time traces exhibited a visible lag at the beginning of the time traces similar to wild type $PhoB_N$. For

both $PhoB_N$ 55MD (Figure 3.3C) and $PhoB_N$ 84AT (Figure 3.4C), plots of k_{app} versus PAM concentration fit to a sigmoidal curve with Hill coefficients of 1.6 ± 0.2 and 1.6 ± 0.3, respectively, implying positive cooperativity of autophosphorylation similar to wild type $PhoB_N$. However, the maximal apparent rate was much larger for $PhoB_N$ 55MD and much smaller for $PhoB_N$ 84AT than for wild type $PhoB_N$.

3.3.4 Mathematical modeling of $PhoB_N$ 55MD and $PhoB_N$ 84AT

In an attempt to understand the differences in autophosphorylation kinetics for $PhoB_N$ 55MD and $PhoB_N$ 84AT, we utilized the mathematical model described in Chapter 2 (Figure 2.5) to predict which kinetic parameters are affected by the substitutions. Four parameters were fixed to experimentally determined values and the six remaining rate and equilibrium constants were set to the values determined in Chapter 2 for autophosphorylation of wild type $PhoB_N$ (see Chapter 2, Table 3.2). Dynafit was used to modulate a subset of the kinetic parameters in an attempt to globally fit the mutant autophosphorylation kinetic data. It was possible to adequately fit the $PhoB_N$ 55MD autophosphorylation data by changing just k_{phos} (m), k_{phos} (het), and k_{agg} (m) [Figure 3.5A, Table 3.2]. In contrast, it was not possible to fit the $PhoB_N$ 55MD autophosphorylation data by changing just K_S (m), K_S (het) and k_{agg} (m) [Figure 3.5B, Table 3.2]. Allowing Dynafit to modulate other combinations of the parameters [e.g. k_{phos} (m), k_{phos} (het), K_S (m), K_S (het), and k_{agg} (m)] did not increase the goodness of fit compared to modulating just k_{phos} (m), k_{phos} (het), and k_{agg} (m) [data not shown]. Dynafit predicted that k_{phos} (m) and k_{phos} (het) for autophosphorylation of $PhoB_N$ 55MD with PAM were approximately 30-fold higher than for autophosphorylation of wild type

$PhoB_N$. Furthermore, k_{phos} (m) and k_{phos} (het) were changed to a similar extent and k_{phos} (het) remained approximately 10-fold higher than k_{phos} (m).

Table 3.2. Rate constants predicted by mathematical modeling for $PhoB_N$ 55MD and $PhoB_N$ 84AT.

	k_{phos} (m) [s^{-1}]	k_{phos} (het) [s^{-1}]	K_S (m) [mM]	K_S (het) [mM]	k_{agg} (m) [s^{-1}]
Wild type	0.018	0.14	160	140	$2.3x10^{-3}$
55MD: k_{phos}	0.53	4.9	---	---	$1.9x10^{-6}$
84AT: k_{phos}	0.0051	0.080	---	---	$5.6x10^{-4}$

Similarly, it was possible to satisfactorily fit the data for autophosphorylation of $PhoB_N$ 84AT by changing just k_{phos} (m), k_{phos} (het), and k_{agg} (m) [Figure 3.6, Table 3.2]. Dynafit predicted that k_{phos} (m) and k_{phos} (het) for autophosphorylation of $PhoB_N$ 84AT with PAM were approximately 1/2 to 1/3 of the value for wild type $PhoB_N$. Furthermore, k_{phos} (m) and k_{phos} (het) were changed to a similar extent and k_{phos} (het) was approximately 10-fold higher than k_{phos} (m). Because the mathematical model was able to account for the changes in the $PhoB_N$ 55MD and $PhoB_N$ 84AT autophosphorylation data compared to wild type by only changing k_{phos} (m), k_{phos} (het), and k_{agg} (m) [Figure 3.5A, Table 3.2], we predict that the 55MD and the 84AT substitutions greatly affected the rates of phosphorylation. However, it appears that neither the 55MD nor the 84AT substitution affected PAM binding.

In order to achieve a satisfactory global fit for all PAM autophosphorylation data with wild type $PhoB_N$, it was necessary to include a slow aggregation step in the mathematical model (see Section 2.3.8 of Chapter 2). In particular, the plateau RFI values observed in the two of 12 experimental conditions with the longest time traces were not as high as expected, a discrepancy attributed to light scattering by aggregates.

The values of k_{agg} predicted for $PhoB_N$ 55MD and $PhoB_N$ 84AT were substantially different than for wild type $PhoB_N$, presumably due to different experimental conditions. k_{agg} for $PhoB_N$ 55MD was three orders of magnitude smaller than for wild type $PhoB_N$, a difference consistent with the much faster autophosphorylation kinetics (and hence less opportunity for aggregate formation) of the mutant. We did not attempt to fit the $PhoB_N$ 55MD data without the aggregation step, but it may be possible to do so. In contrast, the $PhoB_N$ 84AT autophosphorylation reactions were slower than those of $PhoB_N$ conducted under analogous conditions. As a result, aggregation potentially affected many more experimental conditions for $PhoB_N$ 84AT than wild type $PhoB_N$ (cf. length of time courses in Figures 2.2BD and 3.4AB). Therefore, the k_{agg} value predicted from fitting the $PhoB_N$ data (~1/4 of the k_{agg} value predicted from wild type $PhoB_N$) may be more accurate than that derived from analysis of the wild type $PhoB_N$ data.

3.3.5 Optimization of $PhoB_N$ autophosphorylation with MPI

Mathematical modeling predicted that the 55MD and 84AT substitutions did not affect PAM binding to $PhoB_N$. However, the leaving group for PAM is just ammonia (Table 1.1), which does not offer much surface area for interaction with the side chains of nonconserved active site residues in $PhoB_N$. Therefore, we chose to monitor $PhoB_N$ autophosphorylation with MPI to see if a larger leaving group revealed changes in small molecule binding to $PhoB_N$. Initial characterization of autophosphorylation of wild type $PhoB_N$ with 1.5 mM $MnCl_2$ and MPI resulted in no quench in fluorescence intensity, suggesting that $PhoB_N$ cannot autophosphorylate with Mn^{2+} and MPI. However, Mg^{2+} was able to support autophosphorylation of $PhoB_N$ with MPI. Autophosphorylation of wild type and mutant CheY with MPI is faster than autophosphorylation with PAM

(45,46), so we anticipated that precipitation due to the presence of Mg^{2+} would not be an issue within the timescale of the $PhoB_N$ autophosphorylation reactions with MPI.

Autophosphorylation of $PhoB_N$ 55MD was measured with PAM and 20 mM $MgCl_2$ to determine whether changing the divalent cation from Mn^{2+} to Mg^{2+} affected autophosphorylation kinetics. It was not possible to measure autophosphorylation of wild type $PhoB_N$ with $MgCl_2$ and PAM due to precipitation issues; however, autophosphorylation of $PhoB_N$ 55MD occurred over a fast enough timescale to measure autophosphorylation prior to precipitation occurring. Because, for any given PAM concentration, k_{obs} was two- to three-fold faster for 20 mM $MgCl_2$ compared to 1.5 mM $MnCl_2$ (Figure 3.7), any large effects on $PhoB_N$ autophosphorylation with MPI and $MgCl_2$ should not be due to a change in the divalent cation.

3.3.6 Autophosphorylation of wild type $PhoB_N$ with MPI and Mg^{2+}

Autophosphorylation of wild type $PhoB_N$ was monitored with varying concentrations of MPI (2.5-50 mM) [Figure 3.8A]. It was not possible to measure autophosphorylation with higher concentrations of MPI due to precipitation. The autophosphorylation time traces exhibited a visible lag at the beginning of the time traces similar to autophosphorylation with PAM. A plot of k_{app} versus PAM concentration for autophosphorylation of wild type $PhoB_N$ with MPI also fit to a sigmoidal curve with a Hill coefficient of 1.6 ± 0.4 (Figure 3.8B), implying positive cooperativity of autophosphorylation with MPI similar to autophosphorylation with PAM. A plot of k_{app} versus phosphodonor concentration for wild type $PhoB_N$ with MPI was about two- to three-fold faster than with PAM (data not shown).

3.3.7 Initial characterization of autophosphorylation of $PhoB_N$ mutants with MPI

As we did with PAM, we began characterizing autophosphorylation of the nine $PhoB_N$ mutants by monitoring autophosphorylation at a single MPI concentration (30 mM) [Figure 3.9]. Again, the same four substitutions ($PhoB_N$ 11EA, $PhoB_N$ 55MN, $PhoB_N$ NY, $PhoB_N$ KY) did not appear to affect autophosphorylation at 30 mM MPI, and gave time traces that were similar to wild type $PhoB_N$. Also similar to autophosphorylation with PAM, addition of MPI to $PhoB_N$ 56LA or $PhoB_N$ NE did not result in a change in fluorescence intensity. The apparent rates of autophosphorylation of $PhoB_N$ 82LA and $PhoB_N$ 84AT were again reduced compared to wild type $PhoB_N$; however, $PhoB_N$ 84AT had a slower apparent rate of autophosphorylation than $PhoB_N$ 82LA. This was reversed from autophosphorylation with PAM, where $PhoB_N$ 82LA had a slower apparent rate of autophosphorylation than $PhoB_N$ 84AT.

The most surprising result from the initial characterization with 30 mM MPI was that $PhoB_N$ 55MD had an apparent rate of autophosphorylation that was similar to wild type $PhoB_N$. The normalized time trace for autophosphorylation of $PhoB_N$ 55MD with 30 mM MPI had a much smaller change in fluorescence intensity than autophosphorylation of $PhoB_N$ 55MD with PAM or wild type $PhoB_N$ with PAM or MPI. The rate of autodephosphorylation of $PhoB_N$ 55MD [k_{dephos} (55MD) = 0.036 s^{-1}] was much faster than wild type $PhoB_N$ [k_{dephos} (WT) = 0.0003 s^{-1}] (data not shown). If the apparent rates of autophosphorylation of wild type $PhoB_N$ and $PhoB_N$ 55MD are indeed similar as is suggested by autophosphorylation with 30 mM MPI, then the enhanced rate of autodephosphorylation would result in fewer phosphoryl groups accumulating on $PhoB_N$ 55MD, resulting in a smaller change in fluorescence intensity.

Full characterization of autophosphorylation of the PhoBN mutants was not possible at this time. Because autophosphorylation with MPI requires the use of Mg2+, precipitation was a major issue at high concentrations of MPI and for long reaction times. Furthermore, preparation of MPI involves a multi-step organic synthesis that requires removal of contaminating reactants and byproducts (e.g. PAM, DPI). Consecutive preparations of MPI were inconsistent and resulted in varying levels of remaining contaminant. Further work is required to optimize both the preparation of MPI and the protocol for PhoBN autophosphorylation with MPI.

3.4 Discussion

To date, response regulator autophosphorylation has been extensively characterized for only CheY and PhoB. Previous characterization of autophosphorylation of CheY mutants with varying small molecule phosphodonors resulted in apparent rate constants that varied linearly with respect to small molecule phosphodonor concentration (46) (Immormino, R.M, & Bourret, R.B., unpublished), indicating weak substrate binding. $PhoB_N$ autophosphorylation, on the other hand, appears to saturate at high PAM concentrations (see Chapter 2). We took advantage of this apparent saturability to determine if a set of substitutions within the $PhoB_N$ active site had an effect on small molecule phosphodonor binding to $PhoB_N$. None of the substitutions tested affected PAM binding to $PhoB_N$; however, further experiments are needed to determine if the substitutions have an effect on MPI binding.

3.4.1 Comparison of PhoB mutants and CheY mutants

Four of the six nonconserved active site positions substituted here in $PhoB_N$ were previously characterized in CheY (DD+1, D+2, T+1, T+2). To compare the effects of substitutions in $PhoB_N$ and CheY, the rate constants of the $PhoB_N$ mutants are compared to that of wild type $PhoB_N$, and the rate constants of the CheY mutants are compared to that of a CheY mutant that mimics the wild type $PhoB_N$ active site by containing the PhoB residues Asp at D+2, Ala at T+1, and Arg at T+2. All of the substitutions characterized here had similar effects in $PhoB_N$ and CheY. Though the same substitutions were not made in CheY and $PhoB_N$, all substitutions at DD+1 in $PhoB_N$ ($PhoB_N$ 11EA) [Figure 3.2] and CheY (46) had no effect on autophosphorylation kinetics with multiple small molecule phosphodonors. Substituting a Thr at T+1 for an Ala in both $PhoB_N$ ($PhoB_N$ 84AT) and CheY (46) gave slightly slower autophosphorylation with PAM (Figure 3.2) and much slower autophosphorylation with MPI (Figure 3.9) compared to wild type. It is predicted that the planar imidazole ring of MPI clashed with the branched Thr side chain at position T+1 (Immormino, R.M, & Bourret, R.B., unpublished), resulting in the greatly reduced autophosphorylation rate constant.

Substitutions at positions D+2 and T+2 resulted in similar changes in rate constants for autophosphorylation in $PhoB_N$ and CheY. The substitutions in CheY with the greatest enhancement in autophosphorylation with PAM contain an Asp at D+2 and an Arg at T+2 [CheY DR] (Immormino, R.M, Starbird, C., Silversmith, R.E., & Bourret, R.B., unpublished). The rate constant for autophosphorylation of CheY DR with PAM is 12-fold faster than for the CheY mutant containing wild type PhoB residues at D+2 and T+2 (CheY MR). Because $PhoB_N$ already contains an Arg at T+2, a single substitution

was made at position D+2 ($PhoB_N$ 55MD) to give the same pair of residues as CheY DR. Mathematical modeling predicted that $PhoB_N$ 55MD had rate constants for phosphorylation with PAM that were enhanced approximately 30-fold over wild type (Table 3.2). In contrast, the 55MD substitution did not appear to affect the apparent rate of autophosphorylation with 30 mM MPI compared to wild type $PhoB_N$ (Figure 3.9). Autophosphorylation of CheY DR with MPI has not been measured; however, docking of MPI into the crystal structure of CheY DR (Figure 3.10 A) predicts steric clashes between the Asp and Arg side chains and the imidazole ring of MPI that are not predicted with PAM (Figure 3.10 B).

Substituting D+2 with an Asn ($PhoB_N$ 55MN) gave apparent PAM autophosphorylation kinetics that were similar to wild type $PhoB_N$ (Figures 3.2, 3.9), suggesting that the carboxylic acid of Asp at D+2 affects the chemistry of autophosphorylation. The effects on $PhoB_N$ autophosphorylation of Asn versus Asp at D+2 results were similar to previous observations with CheY. In particular, CheY mutants bearing an Arg at T+2 and either an Asn (like $PhoB_N$ MN) or Met (like wild type $PhoB_N$) at D+2 exhibited similar rate constants for PAM autophosphorylation, and both values of k_{phos} were an order of magnitude smaller than for CheY DR (3).

The three $PhoB_N$ double mutants at positions D+2 and T+2 potentially had similar affects as were seen in CheY. The CheY mimic at positions D+2 and T+2 ($PhoB_N$ NE) showed no change in fluorescence upon addition of PAM (Figure 3.2) or MPI (Figure 3.10). Autophosphorylation of wild type CheY with PAM is slower than autophosphorylation of CheY MR (46) and autodephosphorylation of wild type CheY is faster than autodephosphorylation of CheY MR (94). Similarly, $PhoB_N$ NE has a much

faster rate of autodephosphorylation than wild type $PhoB_N$ (Stephani Page, Pers. Comm.). Therefore, if autophosphorylation of $PhoB_N$ NE is slower than autophosphorylation of wild type $PhoB_N$, we would expect any phosphoryl group that binds to $PhoB_N$ NE to be immediately removed, resulting in no accumulation of phosphoryl group and no change in fluorescence.

Finally, $PhoB_N$ NY and $PhoB_N$ KY both had autophosphorylation kinetics that were similar to wild type $PhoB_N$ with both PAM (Figure 3.2) and MPI (Figure 3.9). Although CheY NY and CheY KY had rate constants for autophosphorylation that were much larger than wild type CheY, CheY NY, CheY KY, and CheY MR all had autophosphorylation kinetics that varied only approximately five-fold (46). Based on docking of MPI into the crystal structure of CheY *KY, there are stabilizing pi-pi interactions between the imidazole ring and the T+2 Tyr side chain (46). Although Arg is not able to form as strong pi-pi interactions as the aromatic Tyr side chain, Arg is still able to form moderate pi-pi interactions, possibly explaining the moderate changes in autophosphorylation between wild type $PhoB_N$ and $PhoB_N$ NY/$PhoB_N$ KY.

3.4.2 Previously uncharacterized substitutions

Two substitutions presented here ($PhoB_N$ 56LA and $PhoB_N$ 82LA) have not been previously characterized in CheY. $PhoB_N$ 56LA showed no change in fluorescence upon addition of phosphodonor, suggesting that $PhoB_N$ 56LA was unable to accumulate phosphoryl groups (Figure 3.2, 3.9). $PhoB_N$ 82LA had slower apparent rates of autophosphorylation than wild type $PhoB_N$ (Figure 3.2, 3.9); however, $PhoB_N$ 82LA precipitated during autophosphorylation experiments. Further analysis of the small molecule phosphodonor docked $PhoB_N$ crystal structure (Figure 3.1) showed that the side

chains of positions 56 and 82 are not close to the site of phosphorylation and it is likely that the main chain was predicted to interact with the phosphodonor. $PhoB_N$ 56LA and $PhoB_N$ 82LA likely affected the stability of the protein as opposed to phosphorylation chemistry.

3.4.3 Small molecule phosphodonor binding to $PhoB_N$

Mathematical modeling was used to model the autophosphorylation kinetics of four of the $PhoB_N$ mutants, $PhoB_N$ 55MD (Figure 3.5), $PhoB_N$ 55MN (data not shown), $PhoB_N$ KY (data not shown), and $PhoB_N$ 84AT (Figure 3.6). Modeling of the autophosphorylation kinetics predicted that none of the substitutions tested affected small molecule binding to $PhoB_N$. However, full characterization of autophosphorylation kinetics of these mutants were with the phosphodonor PAM, which has a small side chain that likely does not interact with the side chains of the $PhoB_N$ active site residues. The larger leaving group of MPI might allow for more interaction between the small molecule phosphodonor and the side chains of $PhoB_N$. However, measuring autophosphorylation of $PhoB_N$ with MPI was complicated by inconsistent MPI preparations and precipitation due to the use of Mg^{2+}. Optimization of both the MPI preparation and the protocol for $PhoB_N$ autophosphorylation with MPI is feasible; however, it may be time intensive. If no effects on MPI binding to $PhoB_N$ are observed for this set of mutants, other residues could be manipulated to identify potential interfaces involved in small molecule phosphodonor binding.

3.5 Figures

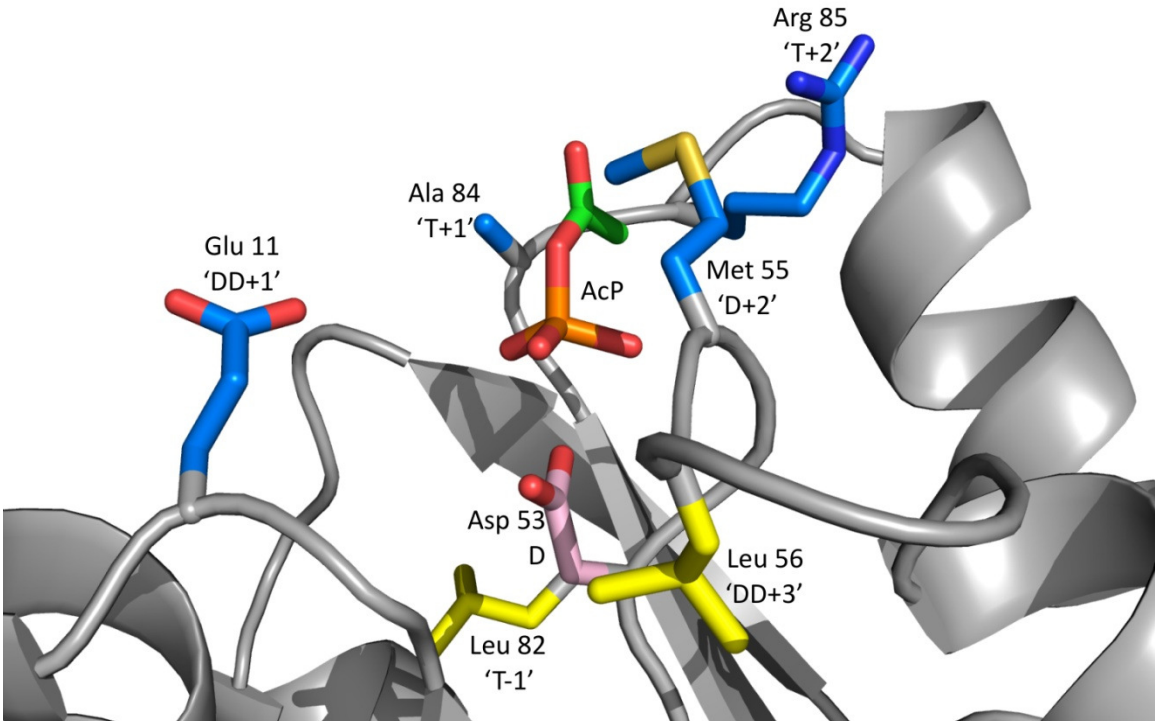

Figure 3.1. Model of AcP docked into the active site of $PhoB_N \cdot BeF_3^-$ structure (PDBid 1ZES). Small-molecule phosphodonor AcP (carbon – green, oxygen – red, phosphorus - red) is bound to Asp53 (pink). Residues previously characterized in CheY (46) (unpublished data) are shown in blue. Residues that have not been previously substituted in CheY are shown in yellow.

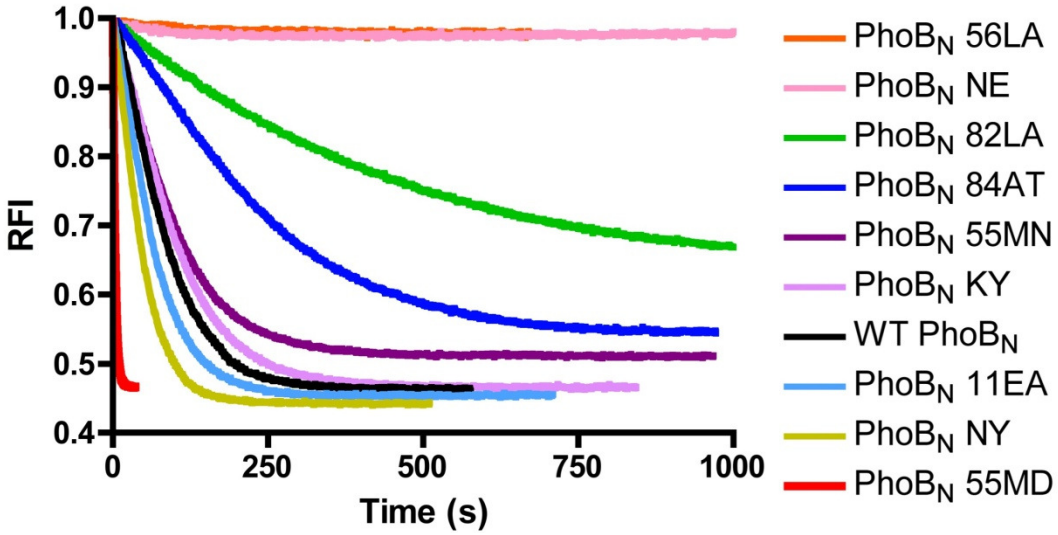

Figure 3.2. Autophosphorylation of nine PhoB$_N$ mutants with 60 mM PAM and 1.5 mM MnCl$_2$. Overlay of wild type PhoB$_N$ (WT PhoB$_N$) from Figure 2.2B shown for comparison.

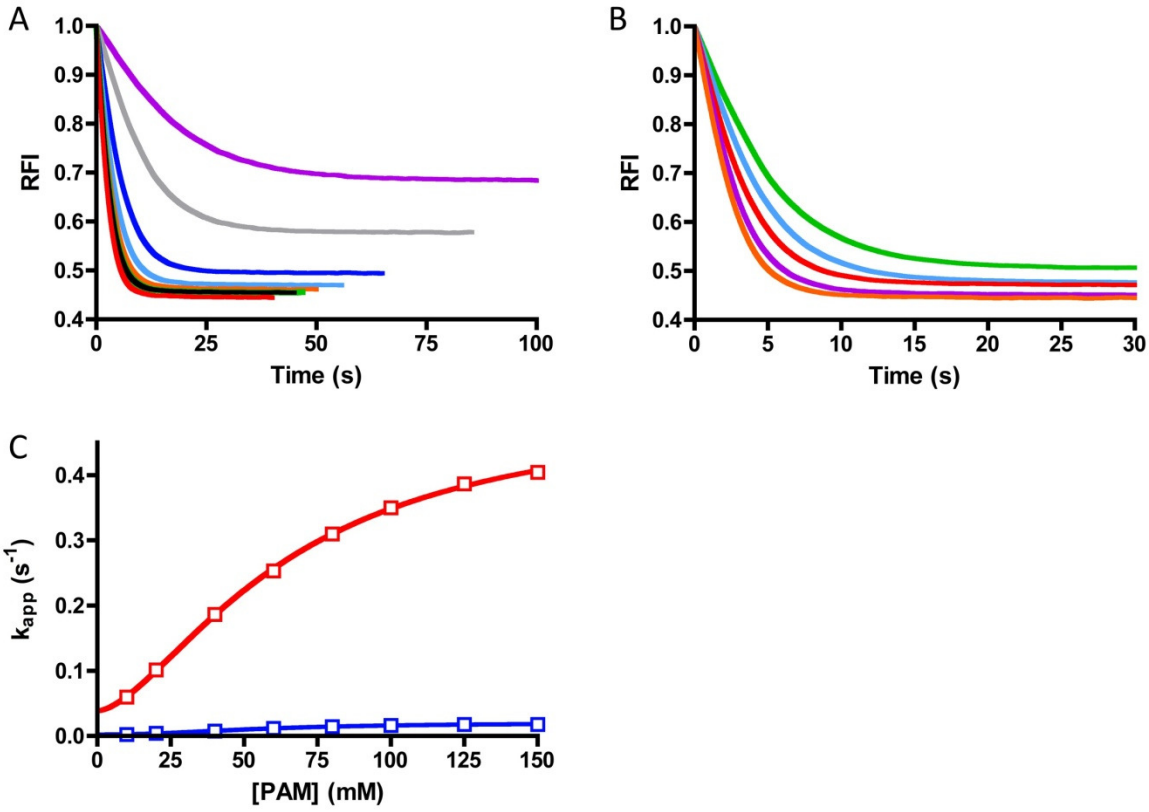

Figure 3.3. Characterization of PhoB$_N$ 55MD autophosphorylation. **(A)** Fluorescence measurement of autophosphorylation of 5 µM PhoB$_N$ 55MD with 10-150 mM PAM concentrations. Colors in panel A as described in Figure 2.2B. **(B)** Autophosphorylation of 2.5-20 µM PhoB$_N$ 55MD with 60 mM PAM. Colors in panel B as described in Figure 2.2D. Reactions in panels A and B were performed in duplicate. RFI is as defined in Figure 2.2. **(C)** Plot of k_{app} versus concentration of PAM for 5 µM PhoB$_N$ 55MD (red) and 5 µM PhoB$_N$ as shown in Figure 2.3D for comparison (blue) fit with sigmoidal dose response curve (equation 3.4). Error bars represent standard deviation from duplicate experiments. Most error bars in panels C and D were smaller than data points.

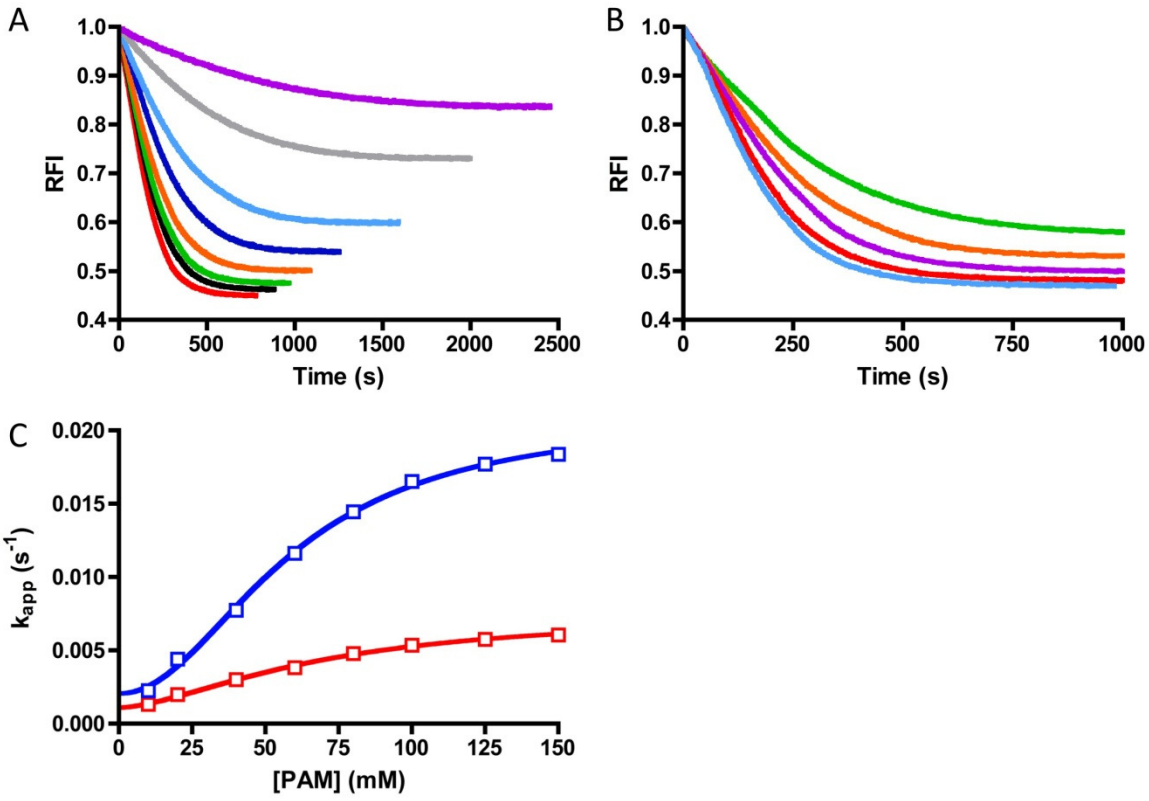

Figure 3.4. Characterization of PhoB$_N$ 84AT autophosphorylation. **(A)** Fluorescence measurement of autophosphorylation of 5 µM PhoB$_N$ 84AT with 10-150 mM PAM concentrations. Colors in panel A as described in Figure 2.2B. **(B)** Autophosphorylation of 2.5-20 µM PhoB$_N$ 84AT with 60 mM PAM. Colors in panel B as described in Figure 2.2D. Reactions in panels A and B were performed in duplicate. RFI is as defined in Figure 2.2. **(C)** Plot of k_{app} versus concentration of PAM for 5 µM PhoB$_N$ 84AT (red) and 5 µM PhoB$_N$ as shown in Figure 2.3D for comparison (blue) fit with sigmoidal dose response curve (equation 3.4). Error bars represent standard deviation from duplicate experiments. Most error bars in panels C and D were smaller than data points.

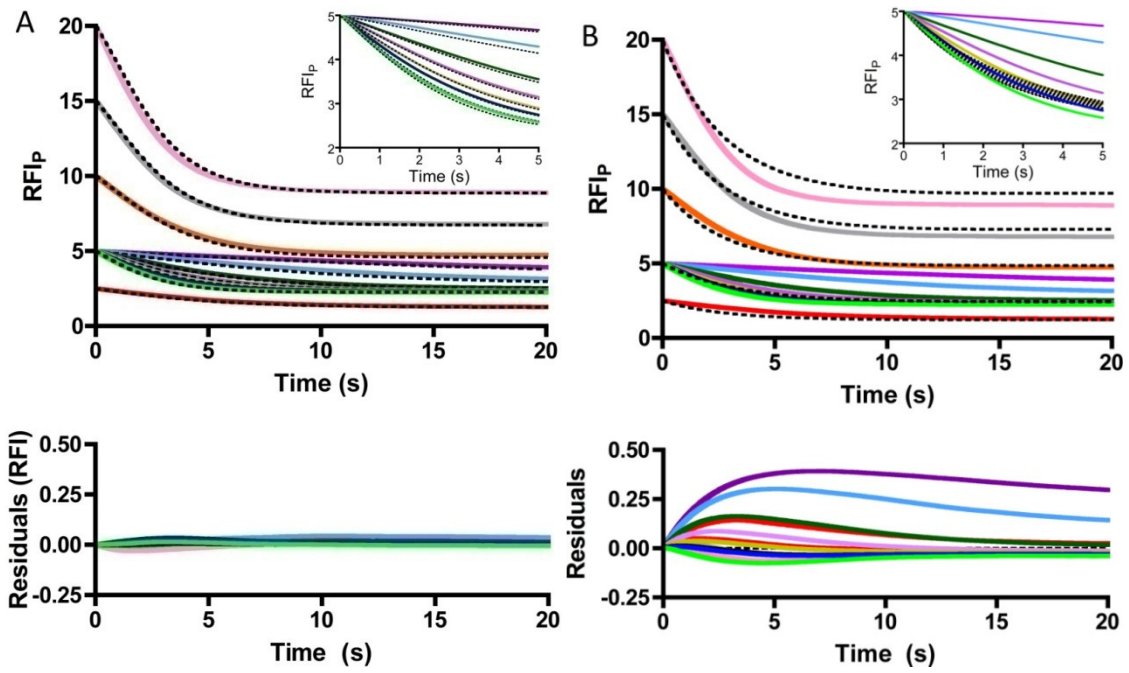

Figure 3.5. Mathematical modeling by global kinetic analysis of autophosphorylation of $PhoB_N$ 55MD. Autophosphorylation time traces for reaction of 20 µM (pink), 15 µM (grey), 10 µM (orange), and 2.5 µM (red) $PhoB_N$ 55MD with 60 mM PAM and for reaction of 5 µM $PhoB_N$ 55MD with 10 mM (dark purple), 20 mM (light blue), 40 mM (dark green), 60 mM (light purple), 80 mM (mustard), 100 mM (black), 125 mM (dark blue), and 150 mM (lime green) PAM truncated to 20 s. Insets of first 5 s of reactions of 5 µM $PhoB_N$ 55MD with varying concentrations of PAM. Overlays of modeled fits from global kinetic analysis by Dynafit (black dashed lines) and residuals for modulation of k_{phos} (m), k_{phos} (het), and k_{agg} (m) **[A]** or modulation of K_S (m), K_S (het), k_{agg} (m) **[B]**. RFI_P as described in Figure 2.7. RFI as defined in Figure 2.2.

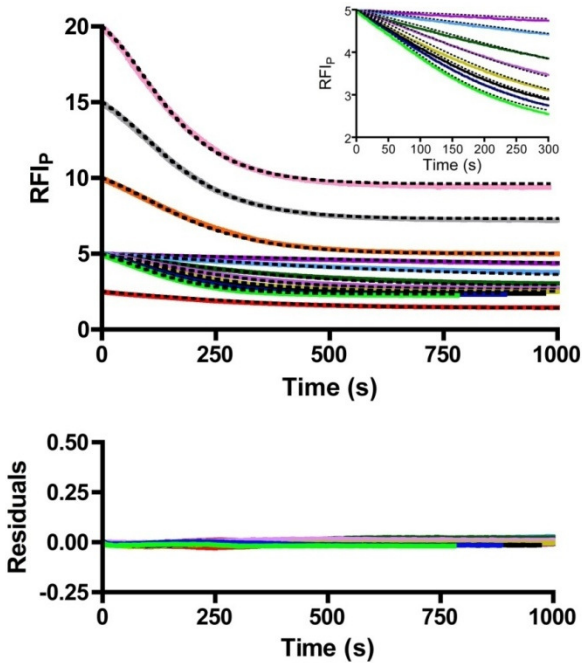

Figure 3.6. Mathematical modeling by global kinetic analysis of autophosphorylation of $PhoB_N$ 84AT. Autophosphorylation time traces for reaction of 2.5-20 $PhoB_N$ 84AT with 60 mM PAM and for reaction of 5 µM $PhoB_N$ 84AT with 10-150 mM PAM truncated to 1000 s. Colors as defined in Figure 3.5. Insets of first 300 s of reactions of 5 µM $PhoB_N$ 84AT with varying concentrations of PAM. Overlays of modeled fits from global kinetic analysis by Dynafit (black dashed lines) and residuals for modulation of k_{phos} (m), k_{phos} (het), and k_{agg} (m)**.** RFI_P as described in Figure 2.7. RFI as defined in Figure 2.2.

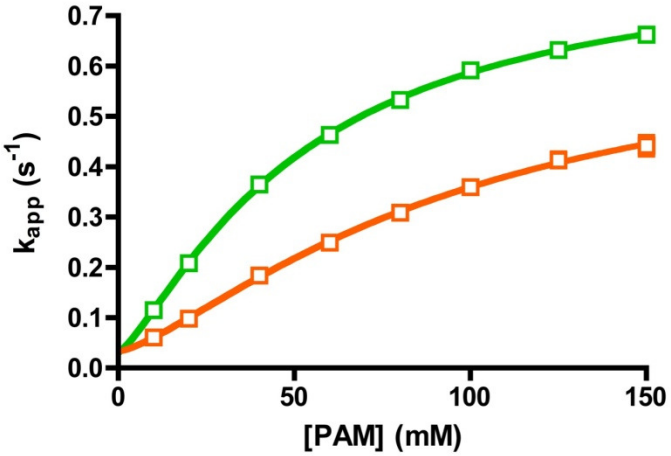

Figure 3.7. Autophosphorylation of $PhoB_N$ 55MD with Mn^{2+} or Mg^{2+}. Plot of k_{app} versus PAM concentration for 5 µM $PhoB_N$ 55MD with 1.5 mM $MnCl_2$ (orange) or 20 mM $MgCl_2$ (green) fit with sigmoidal dose response curve (equation 3.4). Error bars represent standard deviation from duplicate experiments.

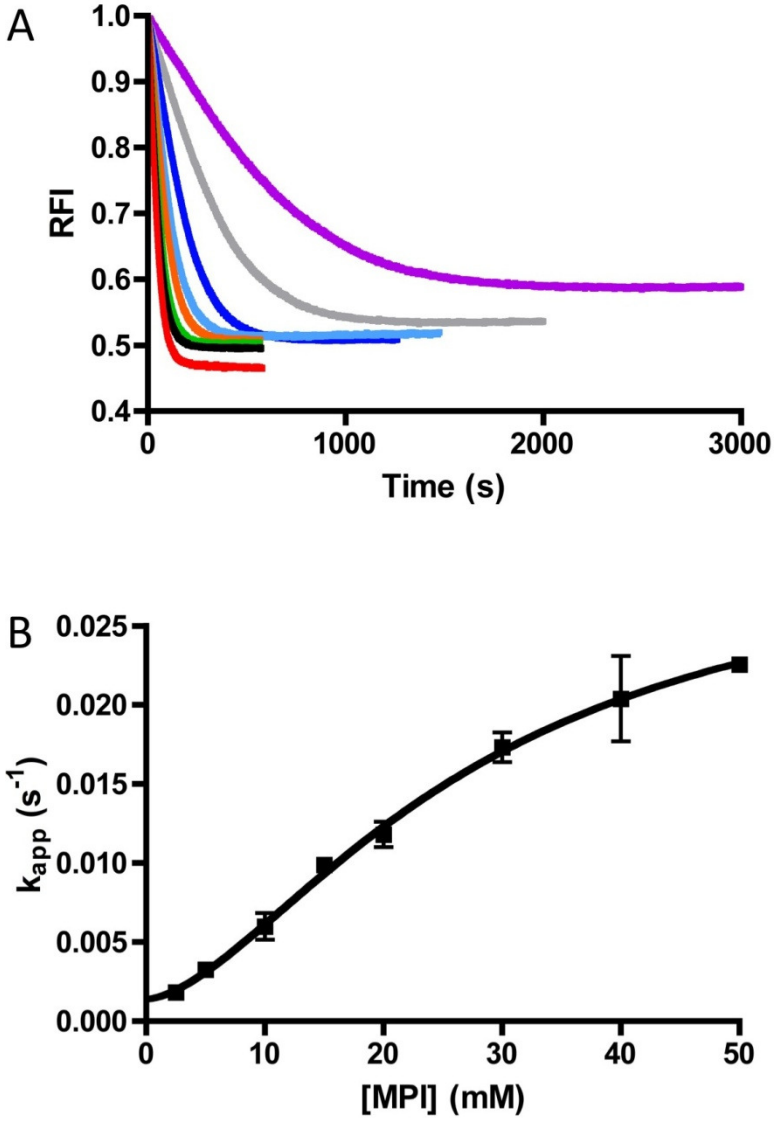

Figure 3.8. Autophosphorylation of wild type $PhoB_N$ with MPI. (A) Fluorescence measurement of autophosphorylation of 5 μM wild type $PhoB_N$ with 2.5 mM (purple), 5 mM (grey), 10 mM (dark blue), 15 mM (light blue), 20 mM (orange), 30 mM (green), 40 mM (black), and 50 mM (red) MPI. **(B)** Plot of k_{app} versus MPI concentration for 5 μM $PhoB_N$ fit with sigmoidal dose response curve (equation 3.4). Error bars represent standard deviation from duplicate experiments.

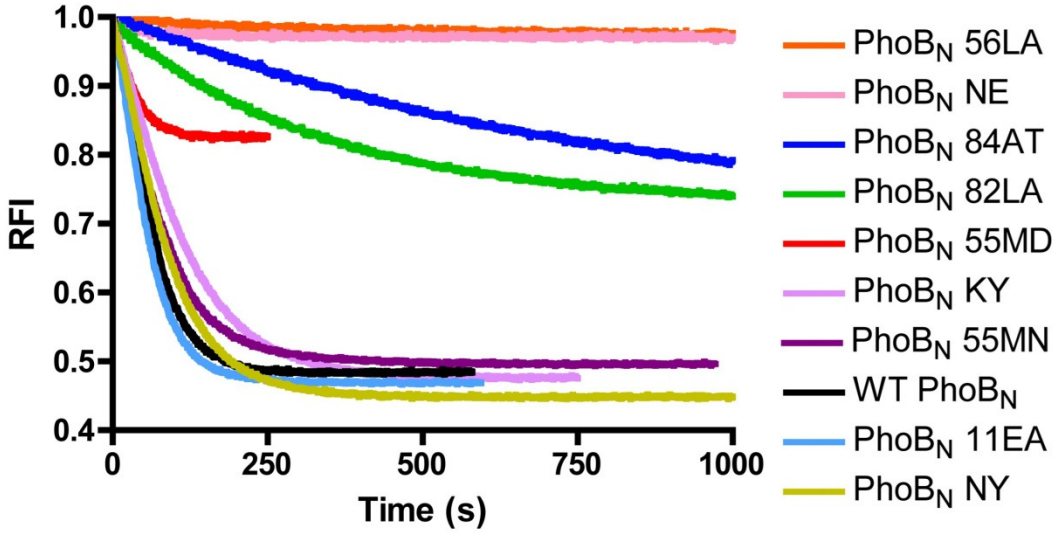

Figure 3.9. Autophosphorylation of nine PhoB$_N$ mutants with 30 mM MPI and 20 mM MgCl$_2$. Overlay of wild type PhoB$_N$ (WT) from Figure 3.8A shown for comparison.

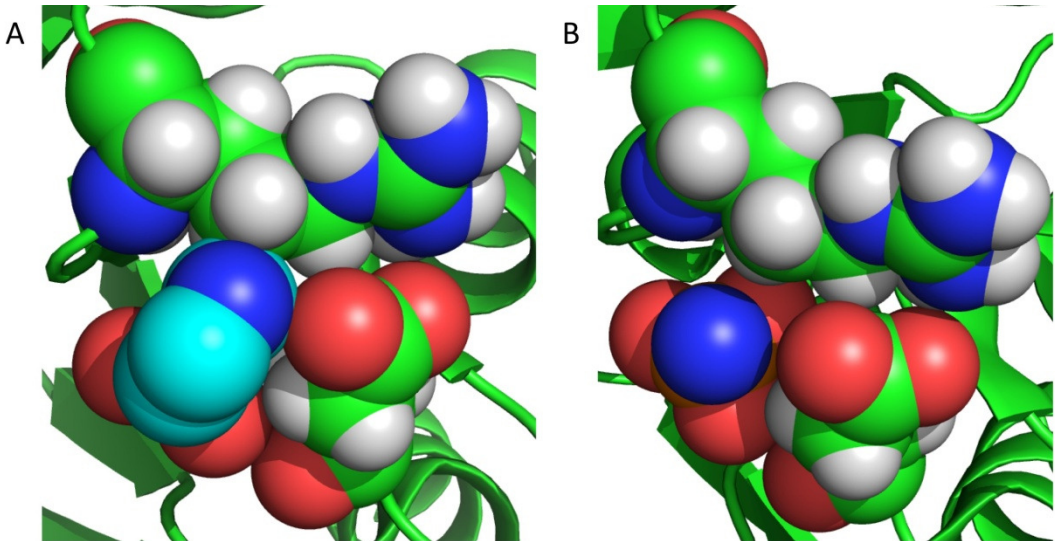

Figure 3.10. Model of phosphodonors docked into the active site of CheY DR·BeF_3^- structure (PDBid 3RVL). Small-molecule phosphodonor MPI **(A)** and PAM **(B)** and side chains of 59D and 89R shown as spheres.

Chapter 4 – Experimentally monitoring heterodimer formation

4.1 Mechanisms of PhoB phosphorylation and dimerization

As discussed in Chapter 2, there is an apparent link between dimerization and autophosphorylation of PhoB. There are at least four potential mechanisms linking autophosphorylation and dimerization [Figure 4.1]: i) two phosphorylated monomers dimerize to form a homodimer [Figure 4.1 A], ii) two unphosphorylated monomers dimerize to form an apo dimer and subsequently phosphorylate [Figure 4.1 B], iii) one phosphorylated monomer and one unphosphorylated monomer dimerize to form a heterodimer and the second monomer phosphorylates [Figure 4.1 C], iv) dimerization and phosphorylation occur simultaneously. It is possible that more than one mechanism occurs in nature, even within the same response regulator. The current dogma and widespread belief in the field is that phosphorylation occurs prior to dimerization [Figure 4.1 A] (95,96).

However, there are multiple pieces of evidence suggesting that $PhoB_N$ dimerization occurs via multiple mechanisms (see Chapter 2). Both nondimerizing response regulators (e.g. CheY) and a $PhoB_N$ mutant that is unable to dimerize ($PhoB_N$ R115D) are able to phosphorylate, indicating that dimerization is not a prerequisite for phosphorylation (Figure 4.1 B) and that phosphorylation and dimerization do not occur simultaneously. Mathematical modeling of $PhoB_N$ autophosphorylation suggests that

both the homodimer and the heterodimer form during autophosphorylation reactions. Furthermore, formation of the $PhoB_N$ heterodimer enhances the rate of phosphotransfer from the sensor kinase PhoR compared to the $PhoB_N$ monomer, further indicating that $PhoB_N$ dimerization can occur via a heterodimer. It is not presently known if other response regulators form heterodimers, and, if so, whether heterodimer formation leads to enhanced autophosphorylation kinetics similar to $PhoB_N$. However, an apparent heterodimer of the ComE response regulator was trapped by cross-linking and separated from cross-linked homodimer by SDS-PAGE (81).

The experiments described in Chapter 2 were not capable of directly observing $PhoB_N$ heterodimer formation. Experimental evidence of heterodimers might further elucidate mechanistic information about the link between response regulator phosphorylation and dimerization. Furthermore, experimentally measuring the dimerization constant for heterodimer formation [K_{dimer} (het)] would lead to even better understanding of response regulator heterodimers. To be able to experimentally observe heterodimers, it will be necessary to either separate the heterodimer and homodimer populations or to watch the formation of heterodimers by isolating phosphorylated monomers without formation of homodimers.

4.2 Strategies for experimentally monitoring heterodimer formation

4.2.1 Gel electrophoresis

Using gel electrophoresis to separate populations of proteins has the potential to separate heterodimers from homodimers. Cross-linking of proteins followed by SDS-PAGE is one example of using gel electrophoresis to experimentally observe

heterodimers. Because heterodimers readily phosphorylate and form homodimers in the presence of excess phosphodonor, it will be necessary to phosphorylate $PhoB_N$ with low phosphodonor concentrations for any subsequent experiments. Under these conditions, most of the protein will be present as an unphosphorylated monomer, but the low level of phosphorylation should allow for both heterodimer and homodimer formation. After $PhoB_N$ is incubated with phosphodonor, heterodimers and homodimers may be trapped using a chemical cross-linker and potentially separated using SDS-PAGE. In theory, SDS-PAGE should remove the charge differences between the homodimer and the heterodimer; however, it has been shown previously that the extra phosphoryl group may change the migration of the heterodimer and the homodimer, allowing for separation (81).

An advantage of using cross-linking and gel electrophoresis to distinguish between $PhoB_N$ dimers is that no special or expensive equipment is required. However, optimization of cross-linking (e.g. which reagent to use and what concentration of cross-linker is required) and phosphorylation (e.g. phosphodonor concentration and reaction time) reaction conditions could be very time intensive and difficult. Also, because SDS-PAGE separates proteins solely by size, it is only possible to determine the molecular weight of the proteins of interest and assumptions must be made about what phosphorylation states are being observed. Finally, because cross-linking only has the potential to separate the heterodimer from the homodimer, it is not possible to measure K_{dimer} (het).

It may be possible to overcome some of the complications of using chemical cross-linking and SDS-PAGE to separate the heterodimer from the homodimer by using a

gel that allows for separation of proteins based on the presence of phosphorylated residues. Phos-tag acrylamide (Wako Pure Chemical Industries, Inc.) forms a specific noncovalent complex with phosphomonoester dianions, leading to slower migration of phosphorylated proteins in the gel. Phos-tag acrylamide has been shown to interact with phosphorylated response regulators, including PhoB (56,63,78,95). Using Phos-tag acrylamide to separate heterodimers and homodimers would be better than using cross-linking because it does not require modification of the proteins. However, the technique is very finicky and out lab has not had success using Phos-tag acrylamide.

4.2.2 Surface plasmon resonance

Another way to experimentally monitor $PhoB_N$ heterodimer formation would be to isolate phosphorylated $PhoB_N$ monomer and then add unphosphorylated monomer. However, because phosphorylated monomers readily form homodimers, it would be necessary to isolate $PhoB_N$ monomers prior to phosphorylation and then allow for heterodimer formation. One technique that may be utilized to observe heterodimers and potentially measure K_{dimer} (het) is surface plasmon resonance [SPR] (97). SPR uses optics near a metal buffer interface to determine the interactions between a ligand and an analyte due to changes in the refractive index of the interface surface. A ligand is immobilized on a sensor chip (Figure 4.2 A) and a constant flow of buffer is passed over the chip. After a stable baseline is reached for the ligand alone, buffer containing the second binding partner is passed over the chip allowing for association of the analyte to the ligand (Figure 4.3 B). After the association phase, the initial buffer is passed over the chip to allow for dissociation of the analyte from the ligand. To monitor heterodimer formation, this protocol would need to be modified slightly: a monomer of $PhoB_N$ would

be bound to the chip and subsequently phosphorylated with a small-molecule phosphodonor, then nonphosphorylated $PhoB_N$ would be flowed over the chip, potentially allowing for heterodimer formation without competing formation of phosphorylated homodimers.

Using SPR to monitor $PhoB_N$ heterodimer formation has many advantages. First, because association of $PhoB_N$ monomers is measured in real time, it may be possible to measure K_{dimer} (het). Also, SPR does not require any special residue or protein modification so experiments can be performed with wild type protein. Because no special residues or protein modifications are required, SPR can potentially be used to monitor dimerization of any dimerizing response regulator. However, there are also many drawbacks to using SPR to monitor $PhoB_N$ heterodimer formation. The major limitation to SPR is due to the depletion of analyte molecules as they travel from one end of the sensor chip to the other, called mass transport. To accurately measure binding kinetics, all ligand molecules in the system should have a constant amount of analyte available for binding, which cannot occur if the analyte molecules are depleted due to reaction with the first few ligand molecules. Also, SPR is very expensive (with sensor chips costing hundreds of dollars apiece) and requires specialized equipment, although a BiaCore instrument is available at UNC.

4.2.3 Biolayer interferometry

Another technique that can potentially isolate $PhoB_N$ monomers prior to phosphorylation and potentially measure K_{dimer} (het) is biolayer interferometry [BLI] (98). BLI measures the interference pattern of white light reflected from two surfaces (Figure 4.3 A): an internal reference layer and the end of the sensor tip (e.g. immobilized

protein). Binding of ligand to the immobilized protein changes the interference pattern due to an increase in optical thickness on the sensor tip and is reported in units of wavelength nm shift (Figure 4.3 B). BLI can potentially be used similarly to SPR to monitor heterodimer formation: a monomer is bound to a sensor tip, phosphorylated, and then allowed to bind to nonphosphorylated monomer, potentially forming a heterodimer.

There are many advantages to using BLI to monitor heterodimer formation. First, the equipment (both the machine and the fiber optic biosensor tip) required is much less expensive than the equipment for SPR. Second, BLI is performed in a 96-well plate and it is possible to monitor eight interactions in parallel, reducing the time required for the experiments. Third, the sensor tip is moved into the analyte-containing solution, removing the potential for mass transport issues that are seen with SPR. Finally, large scale preparations can be performed to bind the ligand to the sensor tip away from the machine. However, there are two major disadvantages to using BLI to monitor heterodimer formation. First, BLI is a new technique and there are still issues with immobilization and sensitivity that need to be worked out in initial experiments. Also, the sensitivity of BLI is less than the sensitivity of SPR and BLI cannot be used to measure interactions of small ligands and analytes.

4.3 Preliminary experiments using BLI

We chose to try to monitor $PhoB_N$ heterodimer formation using BLI because BLI has the potential to monitor both heterodimer formation and measure K_{dimer} (het) and is less expensive and faster than SPR. We established a collaboration with Jonathan McMurry at Kennesaw State University in Kennesaw, GA to use his ForteBio Octet QK

biosensor using Nickel·NTA sensors. Because the protocol we plan to use to monitor heterodimer formation includes a chemistry step (autophosphorylation followed by washing the sensor tip to remove unreacted phosphodonor) and is different from published BLI protocols (99,100), I went to Kennesaw State University to optimize our protocol. I tried to bind purified His_6-tagged $PhoB_N$, His_6-tagged $PhoB_F$, His_6-tagged $PhoB_N$ F20D, and His_6-tagged $PhoB_N$ R115D to the Nickel·NTA sensors. I saw initial binding of protein to the sensor tips; however, the protein washed off of the tips. We are currently working on cloning the genes for the PhoB variants into vectors containing different affinity tags (e.g. biotin-tag to bind to streptavidin tips or GST-tag to bind to anti-GST tips) to potentially get higher affinity protein binding to sensor tips.

4.4 Potential outcomes from BLI experiments

4.4.1 – Implications of BLI experiments

The BLI experiments described above might allow for direct observation of $PhoB_N$ heterodimers; however, it may not be possible to monitor heterodimer formation using BLI. The inability of monitoring heterodimer formation using BLI may be due to flaws in the BLI experiments. Because the biocompatible surface on the biosensor tip is densely packed, the phosphorylated $PhoB_N$ monomers may be able to form homodimers on the tip. Also, because the sensitivity of BLI is less than the sensitivity of SPR, it may not be possible to monitor interactions between proteins as small as $PhoB_N$ (~14.5 kDa). An inability to monitor heterodimer formation may also be because our model accounting for the $PhoB_N$ autophosphorylation data is wrong and $PhoB_N$ may not be able to form heterodimers.

If it is possible to monitor heterodimer formation using BLI, it may also be possible to experimentally measure K_{dimer} (het). We will be able to compare the experimental value for K_{dimer} (het) to the value predicted by modeling to test the accuracy of the mathematical model. We will also be able to plug the experimentally determined K_{dimer} (het) into the mathematical model to further reduce the degrees of freedom. This will allow us to more accurately predict the remaining kinetic constants in the model [K_S (m), k_{phos} (m), K_S (het), k_{phos} (het)].

4.4.2 Interaction between receiver and DNA-binding domains may affect K_{dimer} (het)

The potential to monitor $PhoB_N$ heterodimer formation and measure K_{dimer} (het) may lead to understanding of dimerization of other response regulators. We predict that there is a relationship between the extent of interdomain contacts between the receiver and DNA-binding domains of response regulators and the extent of heterodimer formation. Because crystallization of multi-domain proteins is difficult, we are aware of only four crystal structures of full-length, multi-domain response regulators. Three of the crystallized response regulators showed extensive interdomain contacts between the receiver domain and the DNA-binding domain: MtrA (101), PrrA (102), DrrB (103). In these response regulators, the α4-β5-α5 interface of the receiver domain makes the majority of the contacts with the DNA-binding domain. The interactions between the domains are thought to stabilize the inactive conformation because the physiologically relevant α4-β5-α5 interface is occluded. Furthermore, the interdomain contacts in DrrB (103) and MtrA (101) involve the conserved Tyr switch residue and this interaction must be broken for the response regulators to obtain the active conformation. Conformational rearrangements are thought to be the rate-limiting step of both autophosphorylation and

dimerization in response regulators with extensive interdomain contacts (78). Response regulators with extensive interactions between the receiver domain and the DNA-binding domain (MtrA, DrrB, PrrA) have slow rates of autophosphorylation and removal of the DNA-binding domain enhanced the rate of autophosphorylation at least nine-fold over full length protein (78).

In contrast to MtrA, DrrB, and PrrA, the crystal structure of full-length DrrD did not show extensive interdomain contacts between the receiver and DNA-binding domains (104). Full-length DrrD and the receiver domain alone had similar observed rates of autophosphorylation (78), suggesting that there are limited interdomain contacts in the protein in solution. Similarly, autophosphorylation of $PhoB_F$ and $PhoB_N$ had similar rates of autophosphorylation (78) (Chapter 2), also suggesting minimal interdomain contacts in PhoB.

We predict that the extent of interdomain contacts between the receiver domain and the DNA-binding domain of response regulators will affect the extent of heterodimer formation. Because there are limited interactions to disrupt, response regulators with few interdomain contacts will likely be able to readily form heterodimers. The lack of interdomain contacts to break will likely result in a lower activation energy for heterodimer formation, suggesting that K_{dimer} (het) will be similar to K_{dimer} (hom) as suggested in Chapter 2 for PhoB. In contrast, we predict response regulators with extensive interdomain contacts between the receiver and DNA-binding domains will not readily make heterodimers. The interdomain contacts must be broken prior to heterodimer formation, resulting in a high activation energy for heterodimer formation. Because it will be necessary to break these contacts, we predict K_{dimer} (het) will be much

larger than K_{dimer} (hom) for response regulators with extensive interactions. Therefore, in such response regulators homodimer formation is likely to proceed through interaction of two phosphorylated monomers (Figure 4.1 A).

4.4.3 DNA binding of heterodimers and homodimers

It is currently thought that two response regulator monomers phosphorylate and subsequently dimerize (Figure 4.1 A) allowing for interaction with symmetric DNA binding sites (95,96). A crystal structure of the PhoB DNA-binding domain in complex with the σ_4 domain of the σ^{70} transcription initiation complex and the DNA binding site (*pho* box) showed that two DNA-binding domains interact with one σ_4 domain (53), suggesting dimerization is important for transcription regulation. However, there is no evidence that the receiver domain interacts with the σ^{70} transcription initiation complex or the DNA binding site, suggesting that the phosphorylation state of the receiver domains should not affect DNA binding or transcription regulation. Because dimer 1 of PhoB orients the DNA-binding domains to interact with the symmetric DNA-binding sites (62), it is possible that a PhoB heterodimer would have similar affinity for DNA as a PhoB homodimer and thus could regulate transcription *in vivo*.

As discussed in Chapter 2, there is an apparent link between dimerization and autophosphorylation of PhoB; however, little is known about the link between dimerization and phosphorylation of response regulators in general. It is possible that all four mechanisms describing the relationship between phosphorylation and dimerization (Figure 4.1) are present in nature. Understanding the relationship between dimerization and phosphorylation of response regulators will require further investigation.

4.5 Figures

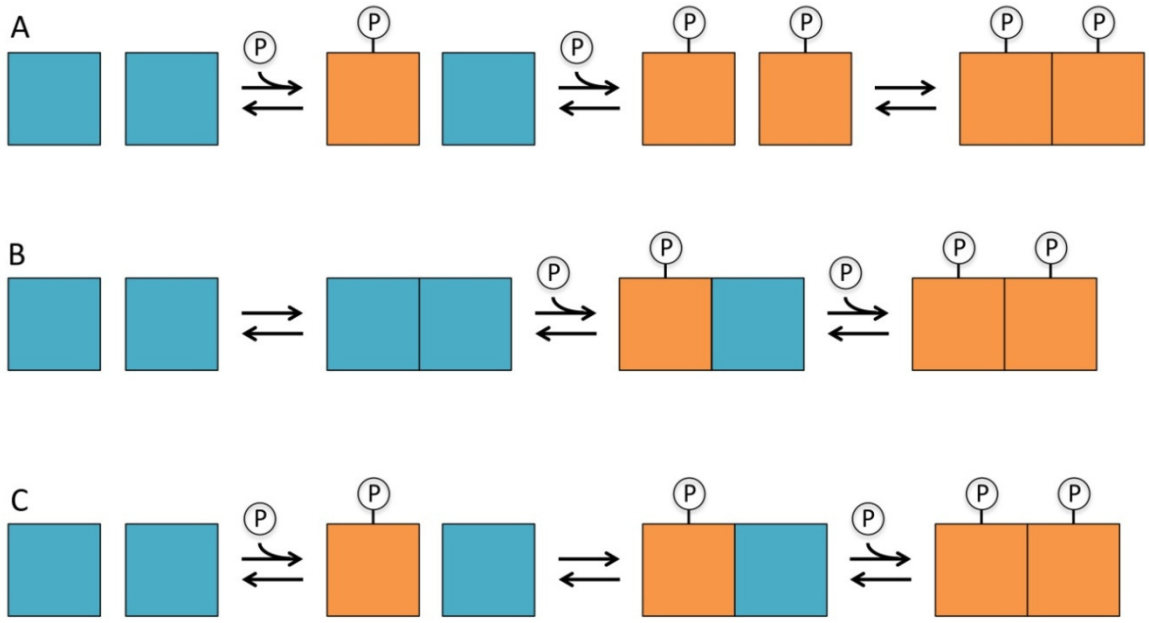

Figure 4.1. Sequential modes of response regulator phosphorylation and dimerization. There are at least three mechanisms describing the relationship between unphosphorylated monomers (blue) and phosphorylated monomers (orange). **(A)** Phosphorylation of both monomers precedes dimerization. **(B)** Dimerization precedes phosphorylation of both monomers. **(C)** A single monomer is phosphorylated and binds an unphosphorylated monomer. The unphosphorylated monomer is subsequently phosphorylated.

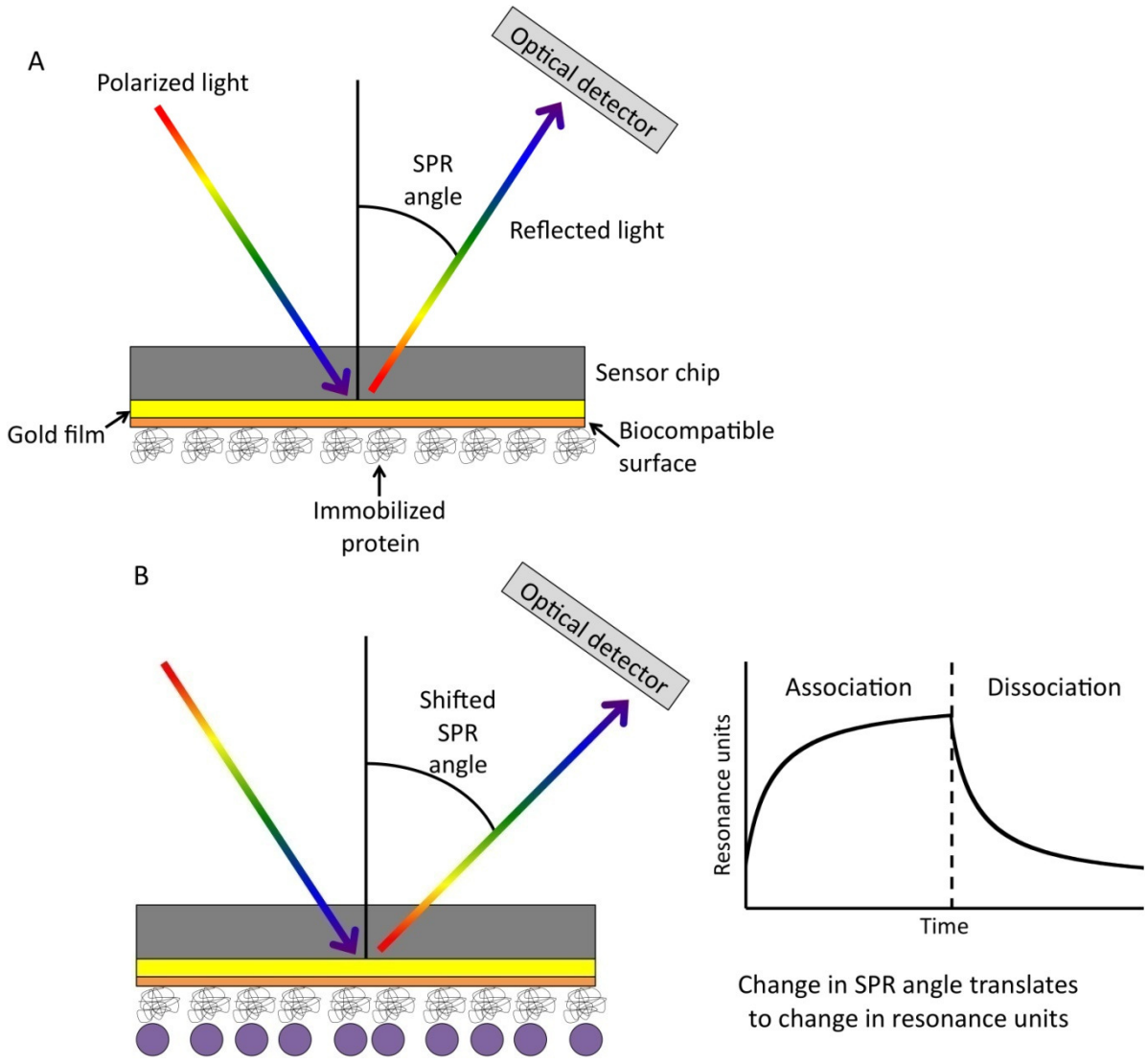

Figure 4.2. Surface plasmon resonance. Modified from (105). **(A)** A ligand is immobilized on a sensor chip containing a metal buffer interface and a baseline SPR angle is monitored. **(B)** Binding of an analyte to the immobilized ligand is monitored, causing a change in the SPR angle. After the association phase, the initial buffer is passed over the chip to allow for dissociation of the analyte from the ligand and the SPR angle to return to baseline values.

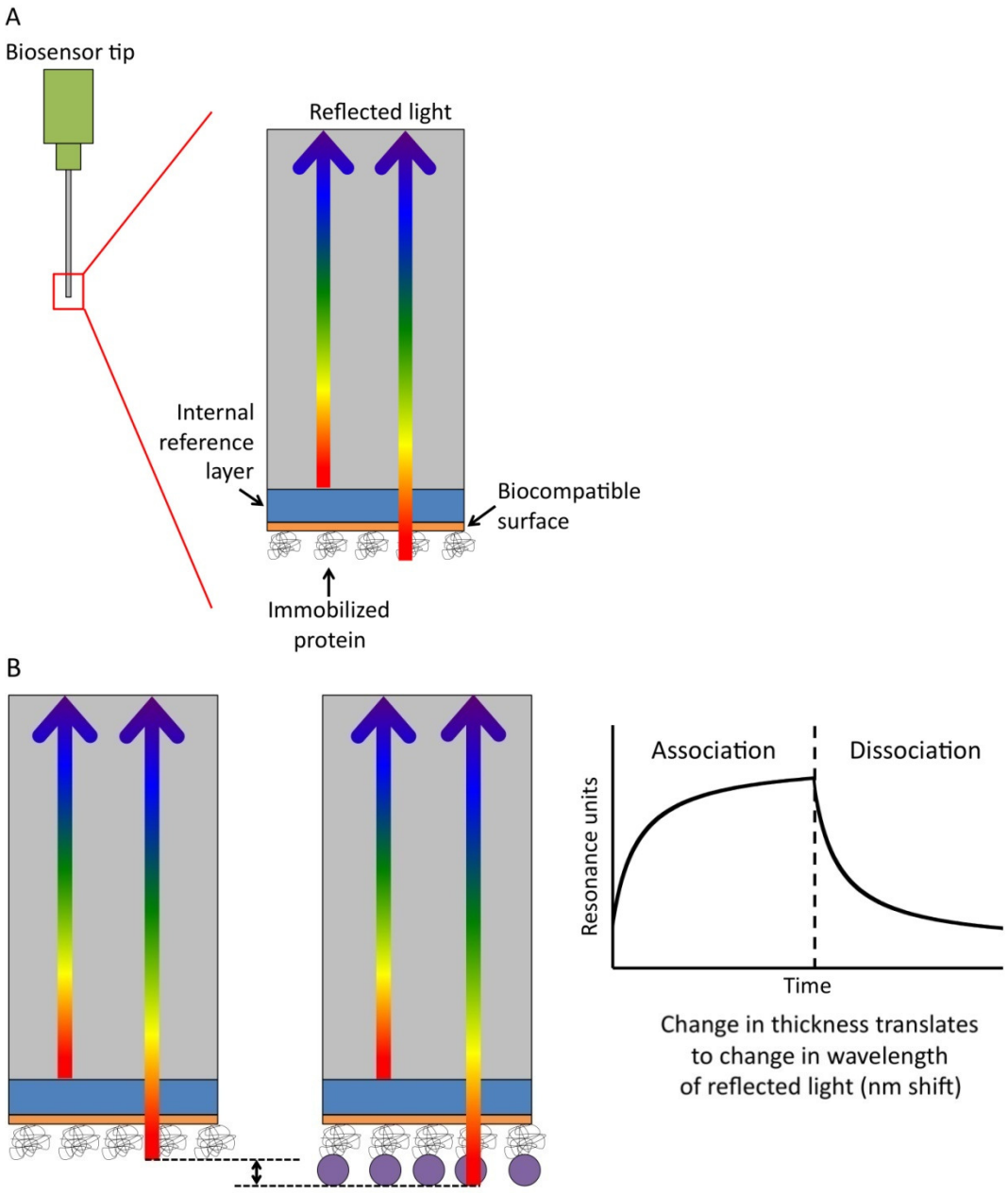

Figure 4.3. Biolayer interferometry. Modified from (106). **(A)** BLI measures the interference pattern of white light reflected from two surfaces: an internal reference layer and the end of the sensor tip (e.g. immobilized protein). **(B)** Binding of ligand to the immobilized protein changes the interference pattern due to an increase in optical thickness on the sensor tip and is reported in units of wavelength nm shift.

Chapter 5 – Conclusions and future directions

5.1 Expanded knowledge of response regulator autophosphorylation kinetics

Prior to the work presented in this dissertation, CheY was the only response regulator for which extensively characterized autophosphorylation kinetics had been published (40,42,44,46). With the work presented here on autophosphorylation of PhoB, the number of response regulators with extensively characterized autophosphorylation kinetics measured has doubled to two. Response regulators have a highly conserved tertiary structure and a high degree of amino acid sequence similarity, including the perfectly conserved quintet of active site residues (23,25). This suggested that the fundamental characteristics of autophosphorylation and autodephosphorylation are likely to be very similar for all response regulators. Therefore, going into this dissertation work, we hypothesized that all response regulators catalyze autophosphorylation in a fundamentally similar way. Based on this hypothesis, we predicted that the characteristics of autophosphorylation of PhoB would be similar to CheY; however, that prediction was proven false. Autophosphorylation of PhoB with PAM and MPI was much slower than autophosphorylation of CheY. Also, autophosphorylation of CheY is nonsaturable with respect to small molecule phosphodonor concentration (40,42,44,46), whereas autophosphorylation of PhoB appears to both saturate at high phosphodonor concentrations and to have cooperative autophosphorylation kinetics (see Chapter 2).

These results suggest that there may be a link between autophosphorylation kinetics and the wide variety of response regulator functions. Response regulator autodephosphorylation rate constants span many orders of magnitude (94), setting a precedent for a wide range in autophosphorylation kinetics depending on response regulator function

Though response regulators do not typically phosphorylate *in vivo* through autophosphorylation by small-molecule phosphodonors, are there any biological implications to different autophosphorylation kinetics for different response regulators? CheY is a response regulator in a chemotaxis-like signaling system whereas PhoB is a response regulator in a two-component system. Because chemotaxis is a very fast process that literally involves split second decisions (107), CheY may have evolved an active site that allows for very fast movement of phosphoryl groups (including by autophosphorylation) within the system. Chemotaxis evolved with monomeric response regulator and cannot introduce cooperativity to the chemotaxis system through dimerization of the response regulator. However, it is interesting to note that chemotaxis evolved cooperativity through another mechanism, e.g. the relationship between the input stimulus and the amount of CheY-P may be linear because the flagellar switch has a highly cooperative output response with respect to CheY-P concentration [Hill coefficient ≈ 11 (108)].

5.2 Speculation about range of response regulator autophosphorylation rate constants

Because phosphorylation and dephosphorylation of response regulators are catalyzed by the same set of conserved active site residues, it may be reasonable to speculate about trends in autophosphorylation and phosphotransfer from sensor kinases based on trends in autodephosphorylation and phosphatase activity. Response regulators perform the chemistry of autodephosphorylation, whereas auxiliary phophatases act to help orient a water molecule rather than dephosphorylate the response regulator (7,109-111). Two extremes in the range of possible relationships between autodephosphorylation rate constants and stimulatory effects of phosphatases are: i) all response regulators have the same autodephosphorylation rate constants and phosphotases stimulate dephosphorylation to the rate required for nature, ii) response regulators have greatly differing autodephosphorylation rate constants and phosphatases have mild stimulatory effects to fine-tune a system. Published response regulator autodephosphorylation rate constants span up to six orders of magnitude (66), which is much larger than the range of stimulatory effects of phophatases [often one to two orders of magnitude (7)], suggesting that response regulators have evolved autodephosphorylation rate constants that are near the timescale required for the biology of the system and that phosphatases fine-tune the dephosphorylation rate further.

It is known that response regulators can catalyze autophosphorylation, but little is still known about the role sensor kinases play in the phosphotransfer reaction. Sensor kinases, among other possibilities, may act as a passive phosphodonor substrate, may contribute catalytic residues to enhance phosphorylation, or may provide a high local

concentration of phosphodonor to properly orient the phosphoryl group for chemistry. Again there are two extremes in the possible relationship between autophosphorylation and phosphotransfer are: i) response regulator autophosphorylation rate constants are similar and phosphotransfer rate constants vary greatly between systems, ii) autophosphorylation rate constants differ greatly and phosphotransfer rate constants with sensor kinases are similar. Published bimolecular rate constants for phosphotransfer from sensor kinases to response regulators are all similar and fast [$>10^6$ M^{-1} s^{-1} (64,112-114)]. Until we can measure autophosphorylation kinetics for many response regulators, mutants of well-characterized response regulators may provide the best hint of what the range of autophosphorylation rate constants might be for response regulators. Analysis of autophosphorylation kinetics of mutants of CheY and PhoB [Table 3.2 and other work from our lab (46) (Immormino, R.M, Starbird, C., Silversmith, R.E., & Bourret, R.B., unpublished)] suggests an approximately three- to four-order of magnitude range in autophosphorylation rate constants.

The relationship between autophosphorylation rate constants and phosphotransfer rates suggests that, as opposed to the relationship between autodephosphorylation and phosphatase stimulation, autophosphorylation rate constants differ greatly between response regulators whereas phosphotransfer rates with sensor kinases are similar. For dephosphorylation, there is a large range of autodephosphorylation rates and a small range of phosphatase stimulation, but the overall effect is to have a wide range of dephosphorylation rates presumably matching biological timescales. However, for phosphorylation, there appears to be a large range of autophosphorylation rates and a very small range in the absolute rates of phosphotransfer. From the limited

phosphotransfer data currently available, it appears that phosphotransfer from the sensor kinase is rapid, allowing for response regulators in different two-component systems to instantly respond to changes in stimuli. Furthermore, it appears that the kinetic control of two-component systems is through dephosphorylation. In other words, the concentration of phosphorylated response regulator (and thus the output of the system) may be determined by the balance between the rates of formation and destruction. It appears that the rate of formation is binary (very fast or totally off), whereas the rate of destruction (the lifetime of the phosphorylated response regulator) varies between systems.

5.3 Mn^{2+} is able to support autophosphorylation of response regulators

A divalent cation bound in the receiver domain active site is required for catalysis of both response regulator phosphorylation and dephosphorylation (9,43). It was known that Mg^{2+}, Mn^{2+}, Zn^{2+}, Co^{2+}, and Cd^{2+} are able to support autodephosphorylation of CheY, but Ca^{2+} is not (9). However, prior to the work presented here, little was known about how different divalent cations are able to support response regulator phosphorylation reactions. Mn^{2+} supports autophosphorylation of the response regulator Spo0F with PAM (74), autophosphorylation of several sensor kinases, and phosphotransfer from a sensor kinase to a response regulator *in vitro* (75-77). Here we show that Mn^{2+} supports autophosphorylation of both CheY (Chapter 2) and $PhoB_N$ 55MD (Chapter 3) to approximately the same extent as Mg^{2+}. Although Mg^{2+} is most likely the divalent cation utilized by response regulators *in vivo*, Mg^{2+} and Mn^{2+} have similar size and preferred coordination number, geometry, and ligand type (73).

5.4 Apparent saturation of PhoB autophosphorylation may allow for differentiation between substrate binding and reaction chemistry

For CheY, the relationship between the observed rate of autophosphorylation and the concentration of small-molecule phosphodonor is linear up to the highest concentrations of phosphodonor tested, indicating very weak substrate binding (40,42,46). For PhoB, however, the relationship between the apparent rate of autophosphorylation and the concentration of small-molecule phosphodonor appears to saturate at high concentrations of phosphodonor, indicating measurable binding of small molecules to PhoB. Binding of a non-hydrolyzable substrate analog (H_3N^+–PSO_2^{2-}, SPAM) to $PhoB_N$ also suggested positive cooperativity of substrate binding (data not shown). Attempts were made to obtain co-crystals between SPAM and $PhoB_N$ to directly visualize small molecule binding to response regulators, but this strategy has not yet been successful.

The apparent saturability of PhoB autophosphorylation potentially offers an opportunity not available with CheY to gain a better understanding of the factors that determine the specificity and affinity of small molecule binding to response regulators. It may be possible to determine residues that interact with small molecule phosphodonors in the background of PhoB. However, none of the substitutions made in $PhoB_N$ tested here affected small molecule phosphodonor binding to $PhoB_N$ as assessed by analysis of autophosphorylation kinetics (see Chapter 3). As an alternate approach, it may be possible to monitor SPAM binding to $PhoB_N$ mutants to determine which residues, if any, affect small molecule binding to $PhoB_N$. Further experiments are needed to identify the determinants of small molecule phosphodonor binding to PhoB.

5.5 Heterodimer formation may play a role in response regulator phosphorylation

An exciting prediction from the kinetic modeling presented in Chapters 2 and 4 was that $PhoB_N$ dimerization occurs through multiple mechanisms that include a heterodimer (one unphosphorylated monomer and one phosphorylated monomer) and a homodimer (two phosphorylated monomers). The kinetics predicted for PhoB heterodimer formation were on the same order of magnitude as those measured for formation of a PhoB homodimer. Could this be a general mechanism for response regulator dimerization? As described in Chapter 4, we predict that there is a relationship between the extent of heterodimer formation and the extent of interdomain contacts between the receiver domain and the DNA-binding domain of response regulators. Response regulators with few interdomain contacts [e.g. DrrD (104)] will likely be able to readily form heterodimers because there are few interactions that need to be disrupted prior to heterodimer formation. In contrast, response regulators with extensive interdomain contacts [e.g. MtrA (101), PrrA (102), DrrB (103)] likely will not readily form heterodimers due to the large number of contacts that need to be broken. Further characterization of response regulator interdomain interactions and dimerization is required to better understand the relationship.

The current dogma of the field is that two phosphorylated monomers phosphorylate and subsequently dimerize allowing for interaction with symmetric DNA binding sites (95,96). However, dimer 1 of PhoB orients the DNA-binding domains to interact with the symmetric DNA-binding sites (62). Furthermore, a crystal structure of the PhoB DNA-binding domain in complex with the DNA binding site and a portion of the transcription initiation complex showed that, while dimerization is important for

transcription regulation, the receiver domain likely does not participate. Therefore, it is possible that a PhoB heterodimer would have similar affinity for DNA as a PhoB homodimer and thus could regulate transcription *in vivo*. Understanding the relationship between phosphorylation, dimerization, and DNA-binding of response regulators will require further investigation. An initial approach is described in Chapter 4.

References

1. Marijuan, P. C., Navarro, J., and del Moral, R. (2010) On prokaryotic intelligence: strategies for sensing the environment. *Biosystems* **99**, 94-103

2. Capra, E. J., and Laub, M. T. (2012) Evolution of two-component signal transduction systems. *Annu. Rev. Microbiol.* **66**, 325-347

3. Ulrich, L. E., Koonin, E. V., and Zhulin, I. B. (2005) One-component systems dominate signal transduction in prokaryotes. *Trends Microbiol.* **13**, 52-56

4. Galperin, M. Y., Higdon, R., and Kolker, E. (2010) Interplay of heritage and habitat in the distribution of bacterial signal transduction systems. *Mol. Biosyst.* **6**, 721-728

5. Hess, J. F., Bourret, R. B., Oosawa, K., Matsumura, P., and Simon, M. I. (1988) Protein phosphorylation and bacterial chemotaxis. *Cold Spring Harb. Symp. Quant. Biol.* **53 Pt 1**, 41-48

6. Silversmith, R. E. (2010) Auxiliary phosphatases in two-component signal transduction. *Curr. Opin. Microbiol.* **13**, 177-183

7. Huynh, T. N., and Stewart, V. (2011) Negative control in two-component signal transduction by transmitter phosphatase activity. *Mol. Microbiol.* **82**, 275-286

8. Georgellis, D., Kwon, O., De Wulf, P., and Lin, E. C. (1998) Signal decay through a reverse phosphorelay in the Arc two-component signal transduction system. *J. Biol. Chem.* **273**, 32864-32869

9. Lukat, G. S., Stock, A. M., and Stock, J. B. (1990) Divalent metal ion binding to the CheY protein and its significance to phosphotransfer in bacterial chemotaxis. *Biochemistry* **29**, 5436-5442

10. Gao, R., and Stock, A. M. (2009) Biological insights from structures of two-component proteins. *Annu. Rev. Microbiol.* **63**, 133-154

11. Kirby, J. R. (2009) Chemotaxis-like regulatory systems: unique roles in diverse bacteria. *Annu. Rev. Microbiol.* **63**, 45-59

12. Wuichet, K., and Zhulin, I. B. (2010) Origins and diversification of a complex signal transduction system in prokaryotes. *Sci. Signal* **3**, ra50

13. Sourjik, V., and Wingreen, N. S. (2012) Responding to chemical gradients: bacterial chemotaxis. *Curr. Opin. Cell Biol.* **24**, 262-268

14. Hazelbauer, G. L. (1992) Bacterial chemoreceptors. *Curr. Opin. Struc. Biol.* **2**, 505-510

15. Gao, R., Mack, T. R., and Stock, A. M. (2007) Bacterial response regulators: versatile regulatory strategies from common domains. *Trends Biochem. Sci.* **32**, 225-234

16. Gotoh, Y., Eguchi, Y., Watanabe, T., Okamoto, S., Doi, A., and Utsumi, R. (2010) Two-component signal transduction as potential drug targets in pathogenic bacteria. *Curr. Opin. Microbiol.* **13**, 232-239

17. McCubrey, J. A., Steelman, L. S., Chappell, W. H., Sun, L., Davis, N. M., Abrams, S. L., Franklin, R. A., Cocco, L., Evangelisti, C., Chiarini, F., Martelli, A. M., Libra, M., Candido, S., Ligresti, G., Malaponte, G., Mazzarino, M. C., Fagone, P., Donia, M., Nicoletti, F., Polesel, J., Talamini, R., Basecke, J., Mijatovic, S., Maksimovic-Ivanic, D., Michele, M., Tafuri, A., Dulinska-Litewka, J., Laidler, P., D'Assoro, A. B., Drobot, L., Umezawa, D., Montalto, G., Cervello, M., and Demidenko, Z. N. (2012) Advances in targeting signal transduction pathways. *Oncotarget* **3**, 1505-1521

18. Riggs, B. L., and Hartmann, L. C. (2003) Selective estrogen-receptor modulators — mechanisms of action and application to clinical practice. *New Engl. J. Med.* **348**, 618-629

19. Miller, S. I., Kukral, A. M., and Mekalanos, J. J. (1989) A two-component regulatory system (*phoP phoQ*) controls *Salmonella typhimurium* virulence. *Proc. Natl. Acad. Sci. U.S.A.* **86**, 5054-5058

20. Tang, Y. T., Gao, R., Havranek, J. J., Groisman, E. A., Stock, A. M., and Marshall, G. R. (2012) Inhibition of bacterial virulence: drug-like molecules targeting the *Salmonella enterica* PhoP response regulator. *Chem. Biol. Drug Des.* **79**, 1007-1017

21. Clarke, M. B., Hughes, D. T., Zhu, C., Boedeker, E. C., and Sperandio, V. (2006) The QseC sensor kinase: a bacterial adrenergic receptor. *Proc. Natl. Acad. Sci. U.S.A.* **103**, 10420-10425

22. Rasko, D. A., Moreira, C. G., Li de, R., Reading, N. C., Ritchie, J. M., Waldor, M. K., Williams, N., Taussig, R., Wei, S., Roth, M., Hughes, D. T., Huntley, J. F., Fina, M. W., Falck, J. R., and Sperandio, V. (2008) Targeting QseC signaling and virulence for antibiotic development. *Science* **321**, 1078-1080

23. Volz, K. (1993) Structural conservation in the CheY superfamily. *Biochemistry* **32**, 11741-11753

24. Gao, R., and Stock, A. M. (2010) Molecular strategies for phosphorylation-mediated regulation of response regulator activity. *Curr. Opin. Microbiol.* **13**, 160-167

25. Bourret, R. B. (2010) Receiver domain structure and function in response regulator proteins. *Curr. Opin. Microbiol.* **13**, 142-149

26. McDonald, L. R., Boyer, J. A., and Lee, A. L. (2012) Segmental motions, not a two-state concerted switch, underlie allostery in CheY. *Structure* **20**, 1363-1373

27. Volkman, B. F., Lipson, D., Wemmer, D. E., and Kern, D. (2001) Two-state allosteric behavior in a single-domain signaling protein. *Science* **291**, 2429-2433

28. Lee, S.-Y., Cho, H. S., Pelton, J. G., Yan, D., Berry, E. A., and Wemmer, D. E. (2001) Crystal structure of activated CheY: comparison with other activated receiver domains. *J. Biol. Chem.* **276**, 16425-16431

29. Dyer, C. M., and Dahlquist, F. W. (2006) Switched or not?: the structure of unphosphorylated CheY bound to the N terminus of FliM. *J. Bacteriol.* **188**, 7354-7363

30. Guhaniyogi, J., Robinson, V. L., and Stock, A. M. (2006) Crystal structures of beryllium fluoride-free and beryllium fluoride-bound CheY in complex with the conserved C-terminal peptide of CheZ reveal dual binding modes specific to CheY conformation. *J. Mol. Biol.* **359**, 624-645

31. Simonovic, M., and Volz, K. (2001) A distinct meta-active conformation in the 1.1-A resolution structure of wild-type ApoCheY. *J. Biol. Chem.* **276**, 28637-28640

32. Ma, L., and Cui, Q. (2007) Activation mechanism of a signaling protein at atomic resolution from advanced computations. *J. Am. Chem. Soc.* **129**, 10261-10268

33. Fiedler, U., and Weiss, V. (1995) A common switch in activation of the response regulators NtrC and PhoB: phosphorylation induces dimerization of the receiver modules. *EMBO J.* **14**, 3696-3705

34. Gao, R., Tao, Y., and Stock, A. M. (2008) System-level mapping of *Escherichia coli* response regulator dimerization with FRET hybrids. *Mol. Microbiol.* **69**, 1358-1372

35. McCleary, W. R. (1996) The activation of PhoB by acetyl phosphate. *Mol. Microbiol.* **20**, 1155-1163

36. Vogt, A. D., and Di Cera, E. (2012) Conformational selection or induced fit? A critical appraisal of the kinetic mechanism. *Biochemistry* **51**, 5894-5902

37. Barak, R., and Eisenbach, M. (1992) Correlation between phosphorylation of the chemotaxis protein CheY and its activity at the flagellar motor. *Biochemistry* **31**, 1821-1826

38. Makino, K., Shinagawa, H., Amemura, M., Kawamoto, T., Yamada, M., and Nakata, A. (1989) Signal transduction in the phosphate regulon of *Escherichia coli* involves phosphotransfer between PhoR and PhoB proteins. *J. Mol. Biol.* **210**, 551-559

39. Volz, K., and Matsumura, P. (1991) Crystal structure of *Escherichia coli* CheY refined at 1.7-A resolution. *J. Biol. Chem.* **266**, 15511-15519

40. Schuster, M., Silversmith, R. E., and Bourret, R. B. (2001) Conformational coupling in the chemotaxis response regulator CheY. *Proc. Natl. Acad. Sci. U.S.A.* **98**, 6003-6008

41. Ames, S. K., Frankema, N., and Kenney, L. J. (1999) C-terminal DNA binding stimulates N-terminal phosphorylation of the outer membrane protein regulator OmpR from *Escherichia coli*. *Proc. Natl. Acad. Sci. U.S.A.* **96**, 11792-11797

42. Da Re, S. S., Deville-Bonne, D., Tolstykh, T., Veron, M., and Stock, J. B. (1999) Kinetics of CheY phosphorylation by small molecule phosphodonors. *FEBS Lett.* **457**, 323-326

43. Lukat, G. S., McCleary, W. R., Stock, A. M., and Stock, J. B. (1992) Phosphorylation of bacterial response regulator proteins by low molecular weight phospho-donors. *Proc. Natl. Acad. Sci. U.S.A.* **89**, 718-722

44. Mayover, T. L., Halkides, C. J., and Stewart, R. C. (1999) Kinetic characterization of CheY phosphorylation reactions: comparison of P-CheA and small-molecule phosphodonors. *Biochemistry* **38**, 2259-2271

45. Silversmith, R. E., Appleby, J. L., and Bourret, R. B. (1997) Catalytic mechanism of phosphorylation and dephosphorylation of CheY: kinetic characterization of imidazole phosphates as phosphodonors and the role of acid catalysis. *Biochemistry* **36**, 14965-14974

46. Thomas, S. A., Immormino, R. M., Bourret, R. B., and Silversmith, R. E. (2013) Nonconserved active site residues modulate CheY autophosphorylation kinetics and phosphodonor preference. *Biochemistry* **52**, 2262-2273

47. Galperin, M. Y. (2010) Diversity of structure and function of response regulator output domains. *Curr. Opin. Microbiol.* **13**, 150-159

48. Hsieh, Y. J., and Wanner, B. L. (2010) Global regulation by the seven-component Pi signaling system. *Curr. Opin. Microbiol.* **13**, 198-203

49. Wanner, B. L. (1993) Gene regulation by phosphate in enteric bacteria. *J. Cell. Biochem.* **51**, 47-54

50. Lamarche, M. G., Wanner, B. L., Crepin, S., and Harel, J. (2008) The phosphate regulon and bacterial virulence: a regulatory network connecting phosphate homeostasis and pathogenesis. *FEMS Microbiol. Rev.* **32**, 461-473

51. Makino, K., Shinagawa, H., Amemura, M., Kimura, S., Nakata, A., and Ishihama, A. (1988) Regulation of the phosphate regulon of *Escherichia coli*. Activation of *pstS* transcription by PhoB protein in vitro. *J. Mol. Biol.* **203**, 85-95

52. Makino, K., Amemura, M., Kawamoto, T., Kimura, S., Shinagawa, H., Nakata, A., and Suzuki, M. (1996) DNA binding of PhoB and its interaction with RNA polymerase. *J. Mol. Biol.* **259**, 15-26

53. Blanco, A. G., Canals, A., Bernues, J., Sola, M., and Coll, M. (2011) The structure of a transcription activation subcomplex reveals how sigma(70) is recruited to PhoB promoters. *EMBO J.* **30**, 3776-3785

54. Wanner, B. L., and Chang, B. D. (1987) The *phoBR* operon in *Escherichia coli* K-12. *J. Bacteriol.* **169**, 5569-5574

55. Ulrich, L. E., and Zhulin, I. B. (2010) The MiST2 database: a comprehensive genomics resource on microbial signal transduction. *Nucleic Acids Res.* **38**, D401-407

56. Barbieri, C. M., and Stock, A. M. (2008) Universally applicable methods for monitoring response regulator aspartate phosphorylation both *in vitro* and *in vivo* using Phos-tag-based reagents. *Anal. Biochem.* **376**, 73-82

57. Hiratsu, K., Nakata, A., Shinagawa, H., and Makino, K. (1995) Autophosphorylation and activation of transcriptional activator PhoB of *Escherichia coli* by acetyl phosphate *in vitro*. *Gene* **161**, 7-10

58. McCleary, W. R., and Stock, J. B. (1994) Acetyl phosphate and the activation of two-component response regulators. *J. Biol. Chem.* **269**, 31567-31572

59. Sola, M., Gomis-Ruth, F. X., Serrano, L., Gonzalez, A., and Coll, M. (1999) Three-dimensional crystal structure of the transcription factor PhoB receiver domain. *J. Mol. Biol.* **285**, 675-687

60. Sola, M., Drew, D. L., Blanco, A. G., Gomis-Ruth, F. X., and Coll, M. (2006) The cofactor-induced pre-active conformation in PhoB. *Acta Crystallogr., Sect. D: Biol. Crystallogr.* **62**, 1046-1057

61. Mack, T. R., Gao, R., and Stock, A. M. (2009) Probing the roles of the two different dimers mediated by the receiver domain of the response regulator PhoB. *J. Mol. Biol.* **389**, 349-364

62. Bachhawat, P., Swapna, G. V., Montelione, G. T., and Stock, A. M. (2005) Mechanism of activation for transcription factor PhoB suggested by different modes of dimerization in the inactive and active states. *Structure* **13**, 1353-1363

63. Gao, R., and Stock, A. M. (2013) Probing kinase and phosphatase activities of two-component systems *in vivo* with concentration-dependent phosphorylation profiling. *Proc. Natl. Acad. Sci. U.S.A.* **110**, 672-677

64. Skerker, J. M., Prasol, M. S., Perchuk, B. S., Biondi, E. G., and Laub, M. T. (2005) Two-component signal transduction pathways regulating growth and cell cycle progression in a bacterium: a system-level analysis. *PLoS Biol.* **3**, e334

65. Silversmith, R. E. (2005) High mobility of carboxyl-terminal region of bacterial chemotaxis phosphatase CheZ is diminished upon binding divalent cation or CheY-P substrate. *Biochemistry* **44**, 7768-7776

66. Bourret, R. B., Thomas, S. A., Page, S. C., Creager-Allen, R. L., Moore, A. M., and Silversmith, R. E. (2010) Measurement of response regulator autodephosphorylation rates spanning six orders of magnitude. *Methods Enzymol.* **471**, 89-114

67. Sheridan, R. C., McCullough, J. F., Wakefield, Z. T., Allcock, H. R., and Walsh, E. J. (1971) Phosphoramidic acid and its salts. in *Inorg. Synth.*, John Wiley & Sons, Inc. pp 23-26

68. Zundel, C. J., Capener, D. C., and McCleary, W. R. (1998) Analysis of the conserved acidic residues in the regulatory domain of PhoB. *FEBS Lett.* **441**, 242-246

69. Martin, R. B. (1988) Ternary hydroxide complexes in neutral solutions of Al_3^+ and F. *Biochem. Biophys. Res. Commun.* **155**, 1194-1200

70. Kuzmic, P. (1996) Program DYNAFIT for the analysis of enzyme kinetic data: application to HIV proteinase. *Anal. Biochem.* **237**, 260-273

71. Janin, J., and Chothia, C. (1990) The structure of protein-protein recognition sites. *J. Biol. Chem.* **265**, 16027-16030

72. Fisher, S. L., Kim, S. K., Wanner, B. L., and Walsh, C. T. (1996) Kinetic comparison of the specificity of the vancomycin resistance VanS for two response regulators, VanR and PhoB. *Biochemistry* **35**, 4732-4740

73. da Silva, J. J. R. F., and Williams, R. J. P. (2001) *The Biological Chemistry of the Elements: The Inorganic Chemistry of Life*, Oxford University Press, U.S.A.

74. Zapf, J. W., Hoch, J. A., and Whiteley, J. M. (1996) A phosphotransferase activity of the *Bacillus subtilis* sporulation protein Spo0F that employs phosphoramidate substrates. *Biochemistry* **35**, 2926-2933

75. Psakis, G., Mailliet, J., Lang, C., Teufel, L., Essen, L. O., and Hughes, J. (2011) Signaling kinetics of cyanobacterial phytochrome Cph1, a light regulated histidine kinase. *Biochemistry* **50**, 6178-6188

76. Gilles-Gonzalez, M. A., and Gonzalez, G. (1993) Regulation of the kinase activity of heme protein FixL from the two-component system FixL/FixJ of *Rhizobium meliloti*. *J. Biol. Chem.* **268**, 16293-16297

77. McCleary, W. R., and Zusman, D. R. (1990) Purification and characterization of the *Myxococcus xanthus* FrzE protein shows that it has autophosphorylation activity. *J. Bacteriol.* **172**, 6661-6668

78. Barbieri, C. M., Mack, T. R., Robinson, V. L., Miller, M. T., and Stock, A. M. (2010) Regulation of response regulator autophosphorylation through interdomain contacts. *J. Biol. Chem.* **285**, 32325-32335

79. Yan, D., Cho, H. S., Hastings, C. A., Igo, M. M., Lee, S.-Y., Pelton, J. G., Stewart, V., Wemmer, D. E., and Kustu, S. (1999) Beryllofluoride mimics phosphorylation of NtrC and other bacterial response regulators. *Proc. Natl. Acad. Sci. U.S.A.* **96**, 14789-14794

80. Weber, G. (1972) Ligand binding and internal equilibria in proteins. *Biochemistry* **11**, 864-878

81. Hung, D. C., Downey, J. S., Kreth, J., Qi, F., Shi, W., Cvitkovitch, D. G., and Goodman, S. D. (2012) Oligomerization of the response regulator ComE from *Streptococcus mutans* is affected by phosphorylation. *J. Bacteriol.* **194**, 1127-1135

82. Kierzek, A. M., Zhou, L., and Wanner, B. L. (2010) Stochastic kinetic model of two component system signalling reveals all-or-none, graded and mixed mode stochastic switching responses. *Mol. Biosyst.* **6**, 531-542

83. Goulian, M. (2010) Two-component signaling circuit structure and properties. *Curr. Opin. Microbiol.* **13**, 184-189

84. Shinagawa, H., Makino, K., and Nakata, A. (1983) Regulation of the *pho* regulon in *Escherichia coli* K-12. Genetic and physiological regulation of the positive regulatory gene *phoB*. *J. Mol. Biol.* **168**, 477-488

85. Zhou, L., Grégori, G., Blackman, J. M., Robinson, J. P., and Wanner, B. L. (2005) Stochastic activation of the response regulator PhoB by noncognate histidine kinases. *J. Integr. Bioinform.* **2**

86. Head, C. G., Tardy, A., and Kenney, L. J. (1998) Relative binding affinities of OmpR and OmpR-phosphate at the *ompF* and *ompC* regulatory sites. *J. Mol. Biol.* **281**, 857-870

87. Decker, K. B., James, T. D., Stibitz, S., and Hinton, D. M. (2012) The *Bordetella pertussis* model of exquisite gene control by the global transcription factor BvgA. *Microbiology* **158**, 1665-1676

88. Magasanik, B. (1996) Regulation of nitrogen utilization. in *Escherichia coli and Salmonella: Cellular and molecular biology* (Neidhardt, F. C. ed.), 2nd Ed., ASM Press, Washington, D.C. pp 1344-1356

89. Stock, A. M., Martinez-Hackert, E., Rasmussen, B. F., West, A. H., Stock, J. B., Ringe, D., and Petsko, G. A. (1993) Structure of the Mg(2+)-bound form of CheY and mechanism of phosphoryl transfer in bacterial chemotaxis. *Biochemistry* **32**, 13375-13380

90. Baker, N. A., Sept, D., Joseph, S., Holst, M. J., and McCammon, J. A. (2001) Electrostatics of nanosystems: application to microtubules and the ribosome. *Proc. Natl. Acad. Sci. U.S.A.* **98**, 10037-10041

91. Word, J. M., Lovell, S. C., Richardson, J. S., and Richardson, D. C. (1999) Asparagine and glutamine: using hydrogen atom contacts in the choice of side-chain amide orientation. *J. Mol. Biol.* **285**, 1735-1747

92. Rathlev, T., and Rosenberg, T. (1956) Non-enzymic formation and rupture of phosphorus to nitrogen linkages in phosphoramido derivatives. *Arch. Biochem. Biophys.* **65**, 319-339

93. Kuznetsova, E., Proudfoot, M., Gonzalez, C. F., Brown, G., Omelchenko, M. V., Borozan, I., Carmel, L., Wolf, Y. I., Mori, H., Savchenko, A. V., Arrowsmith, C. H., Koonin, E. V., Edwards, A. M., and Yakunin, A. F. (2006) Genome-wide analysis of substrate specificities of the *Escherichia coli* haloacid dehalogenase-like phosphatase family. *J. Biol. Chem.* **281**, 36149-36161

94. Thomas, S. A., Brewster, J. A., and Bourret, R. B. (2008) Two variable active site residues modulate response regulator phosphoryl group stability. *Mol. Microbiol.* **69**, 453-465

95. Barbieri, C. M., Wu, T., and Stock, A. M. (2013) Comprehensive analysis of OmpR phosphorylation, dimerization, and DNA binding supports a canonical model for activation. *J. Mol. Biol.* **425**, 1612-1626

96. Singh, V., Ekka, M. K., and Kumaran, S. (2012) Second monomer binding is the rate-limiting step in the formation of the dimeric PhoP-DNA complex. *Biochemistry* **51**, 1346-1356

97. Bamdad, C. (2001) Surface plasmon resonance for measurements of biological interest. in *Current Protocols in Molecular Biology*, John Wiley & Sons, Inc. pp

98. Abdiche, Y., Malashock, D., Pinkerton, A., and Pons, J. (2008) Determining kinetics and affinities of protein interactions using a parallel real-time label-free biosensor, the Octet. *Anal. Biochem.* **377**, 209-217

99. McMurry, J. L., Chrestensen, C. A., Scott, I. M., Lee, E. W., Rahn, A. M., Johansen, A. M., Forsberg, B. J., Harris, K. D., and Salerno, J. C. (2011) Rate, affinity and calcium dependence of nitric oxide synthase isoform binding to the primary physiological regulator calmodulin. *FEBS J* **278**, 4943-4954

100. Morris, D. P., Roush, E. D., Thompson, J. W., Moseley, M. A., Murphy, J. W., and McMurry, J. L. (2010) Kinetic characterization of *Salmonella* FliK-FlhB interactions demonstrates complexity of the Type III secretion substrate-specificity switch. *Biochemistry* **49**, 6386-6393

101. Friedland, N., Mack, T. R., Yu, M., Hung, L.-W., Terwilliger, T. C., Waldo, G. S., and Stock, A. M. (2007) Domain orientation in the inactive response regulator *Mycobacterium tuberculosis* MtrA provides a barrier to activation. *Biochemistry* **46**, 6733-6743

102. Nowak, E., Panjikar, S., Konarev, P., Svergun, D. I., and Tucker, P. A. (2006) The structural basis of signal transduction for the response regulator PrrA from *Mycobacterium tuberculosis*. *J. Biol. Chem.* **281**, 9659-9666

103. Robinson, V. L., Wu, T., and Stock, A. M. (2003) Structural analysis of the domain interface in DrrB, a response regulator of the OmpR/PhoB subfamily. *J. Bacteriol.* **185**, 4186-4194

104. Buckler, D. R., Zhou, Y., and Stock, A. M. (2002) Evidence of intradomain and interdomain flexibility in an OmpR/PhoB homolog from *Thermotoga maritima*. *Structure* **10**, 153-164

105. Madeira, A., Ohman, E., Nilsson, A., Sjogren, B., Andren, P. E., and Svenningsson, P. (2009) Coupling surface plasmon resonance to mass spectrometry to discover novel protein-protein interactions. *Nat. Protoc.* **4**, 1023-1037

106. Dayne, D. (2012) Biolayer interferometry (BLI) - How does it work? *ForteBio Interactions* **5**

107. Segall, J. E., Manson, M. D., and Berg, H. C. (1982) Signal processing times in bacterial chemotaxis. *Nature* **296**, 855-857

108. Cluzel, P., Surette, M., and Leibler, S. (2000) An ultrasensitive bacterial motor revealed by monitoring signaling proteins in single cells. *Science* **287**, 1652-1655

109. Zhao, R., Collins, E. J., Bourret, R. B., and Silversmith, R. E. (2002) Structure and catalytic mechanism of the E. coli chemotaxis phosphatase CheZ. *Nat Struct Biol* **9**, 570-575

110. Pazy, Y., Motaleb, M. A., Guarnieri, M. T., Charon, N. W., Zhao, R., and Silversmith, R. E. (2010) Identical phosphatase mechanisms achieved through distinct modes of binding phosphoprotein substrate. *Proc. Natl. Acad. Sci. U.S.A.* **107**, 1924-1929

111. Huynh, T. N., Noriega, C. E., and Stewart, V. (2010) Conserved mechanism for sensor phosphatase control of two-component signaling revealed in the nitrate sensor NarX. *Proc Natl Acad Sci U S A* **107**, 21140-21145

112. Groban, E. S., Clarke, E. J., Salis, H. M., Miller, S. M., and Voigt, C. A. (2009) Kinetic buffering of cross talk between bacterial two-component sensors. *J Mol Biol* **390**, 380-393

113. Stewart, R. C., Jahreis, K., and Parkinson, J. S. (2000) Rapid phosphotransfer to CheY from a CheA protein lacking the CheY-binding domain. *Biochemistry* **39**, 13157-13165

114. Janiak-Spens, F., Cook, P. F., and West, A. H. (2005) Kinetic analysis of YPD1-dependent phosphotransfer reactions in the yeast osmoregulatory phosphorelay system. *Biochemistry* **44**, 377-386